

Information Leakage Detection through Approximate Bayes-optimal Prediction

Pritha Gupta^{a,*}, Marcel Wever^b, Eyke Hüllermeier^b

^a*Paderborn University, Paderborn, Germany*

^b*MCML, LMU Munich, Munich, Germany*

Abstract

In today's data-driven world, the proliferation of publicly available information raises security concerns due to the information leakage (IL) problem. IL involves unintentionally exposing sensitive information to unauthorized parties via observable system information. Conventional statistical approaches rely on estimating mutual information (MI) between observable and secret information for detecting ILs, face challenges of the curse of dimensionality, convergence, computational complexity, and MI misestimation. Though effective, emerging supervised machine learning based approaches to detect ILs are limited to binary system sensitive information and lack a comprehensive framework. To address these limitations, we establish a theoretical framework using statistical learning theory and information theory to quantify and detect IL accurately. Using automated machine learning, we demonstrate that MI can be accurately estimated by approximating the typically unknown Bayes predictor's log-loss and accuracy. Based on this, we show how MI can effectively be estimated to detect ILs. Our method performs superior to state-of-the-art baselines in an empirical study considering synthetic and real-world OpenSSL TLS server datasets.

Keywords: Information Leakage Detection, Mutual Information, Bayes-optimal Predictor, AutoML, Statistical Tests, Privacy

*Corresponding author

Email addresses: `prithag@mail.upb.de` (Pritha Gupta),
`marcel.wever@ifi.lmu.de` (Marcel Wever), `eyke@lmu.de` (Eyke Hüllermeier)

1. Introduction

The rapid proliferation of publicly available data, coupled with the increasing use of Internet of Things (IoT) technologies in today’s data-driven world, has magnified the challenge of information leakage (IL), posing substantial risks to system security and confidentiality [61, 37]. IL occurs when sensitive or confidential information is inadvertently exposed to unauthorized individuals through observable system information [34]. This problem can lead to severe consequences, ranging from potential electrical blackouts to the theft of critical information like medical records and military secrets, making the efficient detection and quantification of IL of paramount importance [34, 61].

According to information theory, quantifying IL typically involves estimating mutual information (MI) between observable and secret information [8]. Despite being a pivotal measure, MI is difficult to compute for high-dimensional data, facing challenges such as the *curse of dimensionality*, convergence, and computational complexity [26, 43]. Traditional statistical estimation methods often struggle with all of these challenges [26, 43], more recent robust non-parametric approaches with improved convergence rates still find high-dimensional scenarios challenging [47].

In recent years, machine learning (ML) techniques have gained popularity in information leakage detection (ILD), particularly for performing side-channel attacks (SCAs) on cryptographic systems [55]. These systems release the *observable information* via many modes called the side-channels, such as network messages, CPU caches, power consumption, or electromagnetic radiation, which are exploited by SCAs to reveal secret inputs (secret keys, plaintexts), potentially rendering cryptographic protections ineffective [48, 34]. Therefore, detecting the existence of a side-channel is equivalent to uncovering IL [34]. In this field, the most relevant literature uses ML to perform SCAs rather than preventing side-channels through early detection of ILs [34]. Current ML-based methods in this realm detect side-channels to prevent SCAs and protect the system on both algorithmic and hardware levels [49, 48]. These approaches leverage observable information to classify systems as vulnerable (with IL) or non-vulnerable (without IL) [53, 49]. They extract observable information from secure systems, categorizing them as non-vulnerable (labeled 0), then introduce known ILs to categorize them as vulnerable (labeled 1), creating a classification dataset for the learning model. However, this approach is limited to domain-specific scenarios and

cannot be easily transferred to detect other unknown leakages [53].

Recent promising ML-based methods proposed for estimating MI within classification datasets grapple with challenges related to convergence and computational complexity [11], and others may underestimate MI or miss specific subclasses of IL [59]. Recent advancements have demonstrated the effectiveness of ML-based techniques in directly detecting IL by analyzing the accuracy of the supervised learning models on extracted system data [48]. Yet, these methods exhibit limitations in handling imbalanced and noisy real-world datasets, commonly encountered in practical scenarios, and tend to miss ILs by producing false negatives [70, 54].

To address these limitations, in our prior work, we proposed utilizing binary classifiers integrated with Fisher’s exact test (FET) and paired t-test (PTT) statistical tests to account for imbalance [31]. To mitigate noise, an ensemble of binary classifiers, including a deep multi-layer perceptron (MLP), along with their derived results (p -values) from the statistical tests, are aggregated using Holm-Bonferroni correction to enhance ILD accuracy and confidence. Despite its merits, this approach is limited to binary classification tasks and needs a comprehensive theoretical framework.

Our Contributions.

- We establish a comprehensive theoretical framework leveraging the connection between MI and the performance of the Bayes predictor to quantify IL using leakage assessment score and formalize its existence conditions in a system.
- We propose two MI estimation approaches by approximating the Bayes predictor induced using automated machine learning (AutoML) and demonstrate its effectiveness through a rigorous empirical evaluation.
- Using a cut-off on estimated MI through a one-sample t-test (OTT), we devise a technique for ILD. Furthermore, we propose using the Holm-Bonferroni correction on multiple models’ estimates to enhance IL detection confidence by making it robust against noise and variations in AutoML pipelines’ quality.
- We conduct an extensive empirical study, comparing our ILD methods against state-of-the-art approaches for detecting timing side-channels to counter Bleichenbacher’s attacks.

2. Information Leakage Detection Problem

In this section, we formalize the information leakage detection (ILD) task of categorizing a system as vulnerable or non-vulnerable using the proposed generalized leakage assessment score (LAS) measure to quantify information leakage (IL), subsequently used to detect IL in the system. LAS is evaluated by comparing the (approximate) performance of the Bayes predictor and marginal Bayes predictor. When using log-loss, it reduces to mutual information (MI) commonly used for IL quantification. We also briefly introduce the concepts of Bayes predictor and MI, with details of statistical learning theory and notations used throughout the paper in Appendix A.1.

2.1. Formal Setting

ILD aims to identify unintended disclosure of *secret information* through *observable information* of the system. The ILD algorithm analyzes the system dataset $\mathcal{D} = \{(\mathbf{x}_i, y_i)\}_{i=1}^N \subset \mathcal{X} \times \mathcal{Y}, N \in \mathbb{N}$, where $\mathcal{X} = \mathbb{R}^d$ represents observable information and $\mathcal{Y} = [M]$ represents secret information as categorical classes. The goal is to label \mathcal{D} with 1 indicating IL and 0 its absence, represented by the mapping L as:

$$L : \bigcup_{N \in \mathbb{N}} (\mathcal{X} \times \mathcal{Y})^N \rightarrow \{0, 1\},$$

which takes a dataset \mathcal{D} of any size as input and outputs the decision on the presence of IL in the system. The ILD approach produces the mapping \hat{L} and predicts ILs in the given system.

Let $\mathcal{L} = \{(\mathcal{D}_i, z_i)\}_{i=1}^{N_L}$ be an **IL-Dataset**, such that $N_L \in \mathbb{N}, z_i \in \{0, 1\}$ and $\mathbf{z} = (z_1, \dots, z_{N_L})$ be the ground truth vector generated by L . The predicted ILs produced by \hat{L} are denoted as the vector $\hat{\mathbf{z}} = (\hat{z}_1, \dots, \hat{z}_{N_L})$, such that $\hat{z}_i = \hat{L}(\mathcal{D}_i)$. The performance of an ILD approach (\hat{L}) is measured using standard binary classification metrics ($m_{(\cdot)}(\mathbf{z}, \hat{\mathbf{z}})$), described in Appendix A.1.2.

2.2. Fundamentals

We briefly introduce the concepts of Bayes predictor and MI, with details of statistical learning theory in Appendix A.1.

2.2.1. Mutual Information

Mutual information (MI) measures the extent to which knowledge of one random variable informs about another, quantifying their dependence degree [10]. Consider a pair of random variables X and Y with joint distribution $p_{(X,Y)}(\cdot)$ on $\mathcal{X} \times \mathcal{Y}$. We assume that X is a continuous d -dimensional real-valued random variable ($\mathcal{X} = \mathbb{R}^d$), and Y is a discrete random variable with M possible values,— as in the IL scenario relevant to us [8]. Let the measure P induces a marginal probability density function (PDF) on \mathcal{X} and \mathcal{Y} denoted by $p_X(\cdot)$ and $p_Y(\cdot)$ of the joint distribution $p_{(X,Y)}(\cdot)$, which induces the conditional distributions $p_{Y|X}(\cdot)$ and $p_{X|Y}(\cdot)$.

The entropy of a discrete random variable Y is defined as

$$H(Y) = - \sum_{y \in \mathcal{Y}} p_Y(y) \lg(p_Y(y)), \quad (1)$$

where $0 \lg(0) = 0$ by definition. It reaches the maximum value of $\lg(M)$ when outcomes are equally likely ($p_Y(y) = 1/M, \forall y \in [M]$), indicating complete uncertainty of the outcome. The minimum value of 0 occurs in the case of a Dirac measure when only one outcome is certain, i.e., $p_Y(y) = 0, \forall y \in [M] \setminus m, p_Y(m) = 1$.

The conditional entropy of Y given X is defined as

$$H(Y | X) = - \int_{\mathbf{x} \in \mathcal{X}} p_X(\mathbf{x}) \sum_{y \in \mathcal{Y}} p_{Y|X}(y | \mathbf{x}) \lg(p_{Y|X}(y | \mathbf{x})) d\mathbf{x}.$$

Conditional entropy measures the residual uncertainty in one random variable Y given knowledge of the other X — more specifically, it measures the *expected* residual uncertainty, with the expectation taken with respect to the marginal distribution of Y . It reaches its maximum value of $H(Y)$, when X does not inform about Y , i.e., $H(Y | \mathbf{x}) = p_Y(\cdot), \forall \mathbf{x} \in \mathcal{X}$, and the minimum entropy of 0 occurs when X completely determines Y and again all conditionals $p_{Y|X}(\cdot | \mathbf{x})$ are Dirac distributions.

MI measures the reduction of uncertainty about variable Y by observing variable X :

$$I(X; Y) = H(Y) - H(Y | X). \quad (2)$$

Plugging in the expressions for (conditional) entropy and rearranging terms shows that MI equals the Kullback-Leibler (KL) divergence of the joint distribution $p_{(X,Y)}(\cdot)$ from the product of the marginals (i.e., the joint distribution

under the assumption of independence):

$$\begin{aligned} I(X; Y) &= H(Y) - H(Y | X) \\ &= \int_{\mathbf{x} \in \mathcal{X}} \sum_{y \in \mathcal{Y}} p_{(X,Y)}(\mathbf{x}, y) \lg \left(\frac{p_{(X,Y)}(\mathbf{x}, y)}{p_X(\mathbf{x}) \cdot p_Y(y)} \right) d\mathbf{x}. \end{aligned} \quad (3)$$

The MI is a symmetric measure and ranges from 0 to $\min(\{H(X), H(Y)\})$, where a value of 0 indicates complete independence between X and Y , while the maximum value signifies full dependence [10]. In our paper, MI is calculated using base-2 logarithms and measured in *bits*.

2.2.2. Bayes-optimal Predictor

In statistical learning theory, the *Bayes predictor* is the optimal classification function $g^b: \mathcal{X} \rightarrow \mathcal{Y}$, which minimizes expected risk (A.1) for a given loss function $\ell(\cdot): \mathcal{Y} \times \mathcal{Y} \rightarrow \mathbb{R}$:

$$g^b(\mathbf{x}) = \arg \min_{\hat{y} \in \mathcal{Y}} \sum_{y \in \mathcal{Y}} \ell(y, \hat{y}) \cdot p_{Y|X}(y | \mathbf{x}) = \arg \min_{\hat{y} \in \mathcal{Y}} \mathbb{E}_y[\ell(y, \hat{y}) | \mathbf{x}],$$

where $\mathbb{E}_y[\ell]$ is the expected loss of prediction \hat{y} for $y \in \mathcal{Y}$, and $p_{Y|X}(y | \mathbf{x})$ is the (conditional) class y probability for input \mathbf{x} [14]. For 0-1 loss, it simplifies to:

$$g^{bc}(\mathbf{x}) = \arg \max_{y \in \mathcal{Y}} p_{Y|X}(y | \mathbf{x}). \quad (4)$$

It produces the minimum expected loss, known as *Bayes error rate*, denoted by $m_{\text{ERR}}(g^{bc})$. When \mathcal{X} and \mathcal{Y} are independent of each other, i.e., $p_{Y|X}(y | \mathbf{x}) = p_Y(y), \forall \mathbf{x} \in \mathcal{X}$, it reduces to the marginal Bayes predictor:

$$g^{bc}(\mathbf{x}) \equiv g^{mc}(\mathbf{x}) \equiv \arg \max_{y \in \mathcal{Y}} p_Y(y). \quad (5)$$

It assigns to each input \mathbf{x} a class label from the set of labels with the highest marginal probability, as input features are completely uninformative. Strictly speaking, as the maximum in (5) is not necessarily unique, the marginal Bayes predictor may pick any label with the highest probability — in that case, we nevertheless assume that it picks the same label for every \mathbf{x} , so that it is a constant function.

2.3. Quantifying and Detecting Information Leakage

IL occurs when observable information ($\mathbf{x} \in \mathcal{X}$, represented by X) is correlated with secret information ($y \in \mathcal{Y}$, represented by Y), allowing inference of y from \mathbf{x} [37, 8]. To quantify IL, we introduce LAS $\delta(\cdot)$, evaluating the difference in average penalties of marginal Bayes predictor and Bayes predictor using loss functions ($\ell_{(\cdot)}$) or metrics ($\mathfrak{m}_{(\cdot)}$):

$$\delta(\mathfrak{m}_{(\cdot)}) = |\mathfrak{m}_{(\cdot)}(g^{mc}) - \mathfrak{m}_{(\cdot)}(g^{bc})|, \quad \delta(\ell_{(\cdot)}) = \ell_{(\cdot)}(g^{mc}) - \ell_{(\cdot)}(g^{bc}).$$

where $|\cdot|$ is used to avoid negative values for accuracy measures. For log-loss loss function, LAS is equal to **MI**, i.e., $\delta(\ell_u) = I(X; Y) = \mathbb{E}[\ell_u(g^{mc})] - \mathbb{E}[\ell_u(g^{bc})]$ and Bayes error rate ($\mathfrak{m}_{\text{ERR}}(g^{bc})$) bounds the MI, which serves as the foundation for our LOG-LOSS and MID-POINT estimation approaches, respectively, as discussed in Section 3.1.

In practice, since $p_{(X,Y)}(\cdot)$ is seldom observed, we approximate LAS using empirical risk minimizers (g_p or g) as proxies for Bayes predictor and g_p^{mc} for marginal Bayes predictor:

$$\delta(\mathfrak{m}_{(\cdot)}) \cong |\mathfrak{m}_{(\cdot)}(g_p^{mc}) - \mathfrak{m}_{(\cdot)}(g)|, \quad \delta(\ell_{(\cdot)}) \cong \ell_{(\cdot)}(g_p^{mc}) - \ell_{(\cdot)}(g_p).$$

For losses evaluated using (conditional) class probabilities, g_p minimizing (A.3) is used as a proxy for the Bayes predictor. However, for classification decision-based losses, g minimizing (A.2) or the decision rule of g_p is used, with g being a better proxy for error rate or accuracy measure.

IL Detection. IL occurs if LAS is significantly greater than 0, i.e., $\delta(\mathfrak{m}_{(\cdot)}) \gg 0$ or $\delta(\ell_{(\cdot)}) \gg 0$. Thus, ILD involves analyzing the learnability of empirical risk minimizers (g_p or g) on the system dataset \mathcal{D} . Our prior work [31] introduced classification-based ILD approaches using an average error rate (0-1 loss) to quantify and detect IL by analyzing $\delta(\mathfrak{m}_{\text{ERR}})$ and $\delta(\mathfrak{m}_{\text{CM}})$ using paired t-test (PTT) and Fisher’s exact test (FET), respectively. We also propose MI-based ILD approaches using the one-sample t-test (OTT) on multiple MI estimates, with LOG-LOSS effectively detecting IL in OpenSSL TLS servers, discussed in Section 4.3.

3. Mutual Information Estimation

This section introduces two techniques for estimating mutual information (MI) in classification datasets, including their performance in comparison to the state-of-the-art methods: Gaussian mixture model (GMM), mutual information neural estimation (MINE) and PC-SOFTMAX described in

Appendix A.2. We describe the experimental setup with the configuration of datasets generated by simulated systems and evaluation metrics and summarize the results with Appendix C.2 providing a detailed analysis of the generalization performance. Our results demonstrate the superior performance of our proposed methods for estimating MI.

3.1. Our Approaches

We introduce two techniques for estimating MI in classification datasets, the MID-POINT and LOG-LOSS, using statistical learning theory rather than relying solely on standard statistical methods.

3.1.1. Mid-point Estimation

The MID-POINT approach estimates MI by leveraging the relationship between Bayes error rate $m_{\text{ERR}}(g^{bc})$ and the conditional entropy $H(Y|X)$ for a classification task [64]. The MI is estimated using the empirical risk minimizer g of (A.2) to approximate the Bayes error rate.

The conditional entropy $H(Y|X)$ is bounded as

$$\begin{aligned} H_l(m_{\text{ERR}}(g^{bc}), M) &\leq H(Y|X) \leq H_u(m_{\text{ERR}}(g^{bc}), M) \\ H_l(m_{\text{ERR}}(g^{bc}), M) &= \lg(m) + m(m+1) \left(\lg\left(\frac{m+1}{m}\right) \right) \left(m_{\text{ERR}}(g^{bc}) - \frac{m-1}{m} \right) \\ H_u(m_{\text{ERR}}(g^{bc}), M) &= H_2(m_{\text{ERR}}(g^{bc})) + m_{\text{ERR}}(g^{bc}) \lg(M-1), \end{aligned}$$

where $H_l(\cdot)$ derived by Hellman and Raviv [33] is valid for $\frac{1}{m+1} \leq 1 - m_{\text{ERR}}(g^{bc}) \leq \frac{1}{m}$, $m = 1, \dots, M-1$ and $H_u(\cdot)$ derived by Fano [20] uses the binary cross-entropy function, $H_2(a) = -a \lg(a) - (1-a) \lg(1-a)$.

Plugging in $H_l(\cdot)$ and $H_u(\cdot)$ in (2), the bounds on MI are derived as

$$\begin{aligned} H(Y) - H_u(m_{\text{ERR}}(g^{bc}), M) &\leq I(X; Y) \leq H(Y) - H_l(m_{\text{ERR}}(g^{bc}), M) \\ F_l(m_{\text{ERR}}(g^{bc}), M) &\leq I(X; Y) \leq F_u(m_{\text{ERR}}(g^{bc}), M) \\ H(Y) - H_2(m_{\text{ERR}}(g^{bc})) &\leq I(X; Y) \leq H(Y) - 2 m_{\text{ERR}}(g^{bc}), \quad M = 2. \end{aligned}$$

MI is estimated as

$$\hat{I}(X; Y) \cong \frac{F_u(m_{\text{ERR}}(g), M) + F_l(m_{\text{ERR}}(g), M)}{2}, \quad (6)$$

where g is the *empirical risk minimizer* of (A.2) and serves as a proxy of the Bayes predictor, as $m_{\text{ERR}}(g^{bc}) \cong m_{\text{ERR}}(g)$.

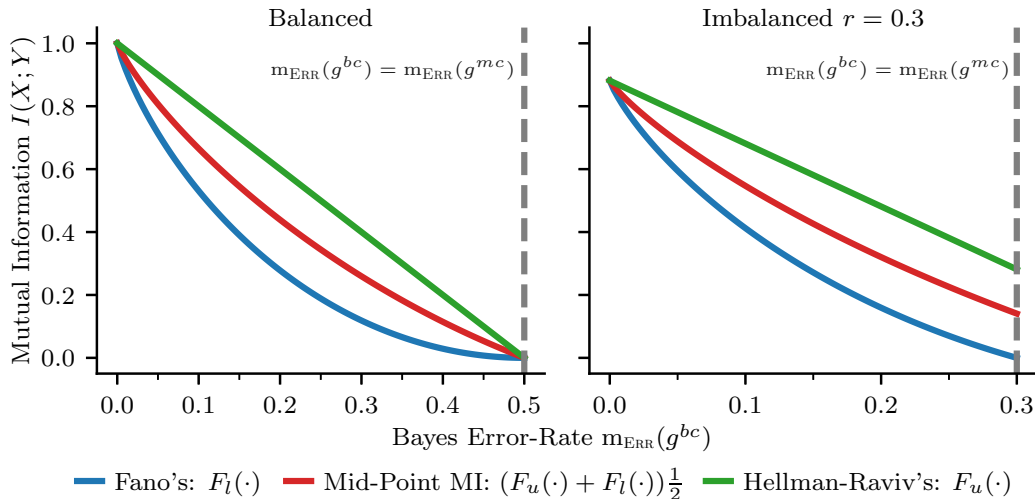


Figure 1: MID-POINT approach: Bayes error rate versus MI for $M = 2$

Limitations in Imbalanced Data. In imbalanced data, the MID-POINT approach can overestimate MI, leading to false positives in information leakage (IL) detection, as illustrated in Figure 1, where MI is greater than 0 despite no IL as per the condition discussed in Section 2.3. For instance, in (7), the ground truth MI is 0.0519 *bits*, while the MID-POINT MI estimate is approximately 0.0932 *bits*. This overestimation occurs because error rates capture deterministic rather than probabilistic relationships and are inadequate for imbalanced datasets, leading to false positives in IL detection. Zhao et al. [71] relate other appropriate metrics like balanced error rate (BER) with conditional entropy $H(Y | X)$ for binary classification, but this does not extend to multi-class cases.

Joint $p_{(X,Y)}(x, y)$				Conditionals $p_{Y X}(\cdot)$			
$p_{(X,Y)}(x, y)$	$y = 0$	$y = 1$	$p_X(x)$	$p_{Y X}(y x)$	$y = 0$	$y = 1$	$p_X(x)$
$x = 0$	0.5	0	0.5	$x = 0$	1	0	0.5
$x = 1$	0.45	0.05	0.5	$x = 1$	0.9	0.1	0.5
$p_Y(y)$	0.95	0.05	—	$p_Y(y)$	0.95	0.05	—

(7)

The two baseline information leakage detection (ILD) methods proposed in our prior work [31] fail to detect IL for the example defined in (7). The PTT-MAJORITY baseline compares error rates between the Bayes predictor and marginal Bayes predictor to detect IL since both predictors always choose

class 0, causing IL to go undetected. Similarly, FET-based approaches fail and produce a p -value of 1 for the confusion matrix by Bayes predictor $\begin{pmatrix} 95 & 00 \\ 05 & 00 \end{pmatrix}$. When Bayes error rate is close to the marginal Bayes predictor’s error rate, these baselines miss IL, resulting in false negatives.

3.1.2. LOG-LOSS Estimation

We propose the LOG-LOSS approach for MI estimation to address the overestimation and false positives of the MID-POINT approach and the false negatives of baseline ILD approaches. This approach uses the empirical risk minimizer g_p minimizing (A.3) to approximate the log-loss of the Bayes predictor.

The MI between X and Y in (2) is defined as

$$\begin{aligned} I(X; Y) &= -H(Y | X) + H(Y) \\ &= \int_{\mathbf{x} \in \mathcal{X}} p_X(\mathbf{x}) \sum_{y \in \mathcal{Y}} p_{Y|X}(y | \mathbf{x}) \lg(p_{Y|X}(y | \mathbf{x})) d\mathbf{x} - \sum_{y \in \mathcal{Y}} p_Y(y) \lg(p_Y(y)) \\ &= -\mathbb{E}[\ell_u(g^{bc})] + \mathbb{E}[\ell_u(g^{mc})] \cong -\mathbb{E}[\ell_u(g_p)] + \mathbb{E}[\ell_u(g_p^{mc})], \end{aligned}$$

where $\mathbb{E}[\ell_u(\cdot)]$ represents the expected log-loss. The conditional entropy $H(Y | X)$ equals the expected log-loss of the Bayes predictor g^{bc} , and the entropy of Y is the expected log-loss of the marginal Bayes predictor g^{mc} , making it a special case of leakage assessment score (LAS), as discussed in Section 2.3.

Log-loss. For probabilistic classifiers g_p , categorical cross-entropy (CCE) is used to obtain estimated conditional class probabilities, forming a vector $\hat{\mathbf{p}} = (\hat{p}_1, \dots, \hat{p}_M)$ for each input \mathbf{x} . The log-loss for g_p is defined in Bishop [5, chap. 4] as

$$\ell_u(y, \hat{\mathbf{p}}) = -\sum_{m=1}^M \hat{p}_m \lg(\hat{p}_m) = -\sum_{m=1}^M g_p(\mathbf{x})[m] \lg(g_p(\mathbf{x})[m]).$$

It reaches its minimum value of 0 when the class probability is high for one class m , i.e., $\hat{p}_m \cong 1$ and low for remaining, i.e., $\hat{p}_j \cong 0, \forall j \in [M] \setminus \{m\}$, and its maximum value $\lg(M)$ when probabilities are uniformly distributed, i.e., $\hat{p}_m = 1/M, \forall m \in [M]$, implying that high uncertainty in the classification also increases the log-loss, making it suitable to estimate the conditional entropy $H(Y | X)$.

Marginal Bayes predictor. The marginal Bayes predictor, denoted by g_p^{mc} , is estimated from the class distribution in the dataset $\mathcal{D} = \{(\mathbf{x}_i, y_i)\}_{i=1}^N$ using (A.3). The class probabilities for each input \mathbf{x} are $g_p^{mc}(\mathbf{x}) = \hat{\mathbf{p}}_{mc} = (\hat{p}_1, \dots, \hat{p}_M)$, where $\hat{p}_m = \frac{|\{(\mathbf{x}_i, y_i) \in \mathcal{D} \mid y_i = m\}|}{|\mathcal{D}|}$ is the fraction of instances for class m . The log-loss of the marginal Bayes predictor suitably estimates entropy of Y ($H(Y)$), i.e., $H(Y) \approx \ell_u(y, \hat{\mathbf{p}}_{mc})$, ranging from 0 and $\lg(M)$, attaining the maximum value for a balanced dataset.

MI estimation. We approximate the expected log-loss of the Bayes predictor and marginal Bayes predictor by evaluating the log-loss of g_p and g_p^{mc} for the dataset $\mathcal{D} = \{(\mathbf{x}_i, y_i)\}_{i=1}^N$ as

$$\begin{aligned} \mathbb{E}[\ell_u(g_p)] &= \frac{1}{N} \sum_{i=1}^N \ell_u(y_i, g_p(\mathbf{x}_i)) = -\frac{1}{N} \sum_{i=1}^N \sum_{m=1}^M g_p(\mathbf{x}_i)[m] \lg(g_p(\mathbf{x}_i)[m]) \\ \mathbb{E}[\ell_u(g_p^{mc})] &= \frac{1}{N} \sum_{i=1}^N \ell_u(y_i, g_p^{mc}(\mathbf{x}_i)) = -\sum_{m=1}^M \hat{p}_{mc}[m] \lg(\hat{p}_{mc}[m]). \end{aligned}$$

The MI is then estimated as

$$\hat{I}(X; Y) \cong \sum_{m=1}^M \left(\frac{1}{N} \sum_{i=1}^N g_p(\mathbf{x}_i)[m] \lg(g_p(\mathbf{x}_i)[m]) - \hat{p}_{mc}[m] \lg(\hat{p}_{mc}[m]) \right). \quad (8)$$

Classifier Calibration. To enhance LOG-LOSS estimation accuracy, we employ calibration techniques like Isotonic Regression (IR CAL LOG-LOSS), Platt’s Scaling (PS CAL LOG-LOSS), Beta Calibration (BETA CAL LOG-LOSS), Temperature Scaling (TS CAL LOG-LOSS), and Histogram Binning (HB CAL LOG-LOSS), referred to collectively as CAL LOG-LOSS, described in Appendix A.1.1. These techniques improve the precision of LOG-LOSS, estimating MI as 0.052 **bits** exactly for (7), avoiding false positives seen with the MID-POINT approach.

3.2. Empirical Evaluation

This section outlines the evaluation process for our MI estimation approaches compared to baselines, as illustrated in Figure 4. Our goal is to assess the generalization capabilities of these approaches under various conditions, including the number of classes (M), input dimensions (d), class imbalance (r), and noise level (ϵ), using datasets generated by systems with

different configurations $(\mathbf{g}_r, M, d, r, \epsilon)$ outlined in Table 1. Overall and generalization performance results are discussed in Section 3.3, with detailed analysis in Appendix C.2.

Table 1: Overview of the synthetic datasets for MI estimation experiments

Multivariate normal (MVN) Perturbation & MVN Proximity Synthetic Datasets					
Data set Type	Generation Method (\mathbf{g}_r)	Input Dimensions (d)	Classes (M)	Noise Level/Flip Percentage (ϵ)	Class Imbalance (r)
Balanced	NA	{2, 4, ..., 20}	{2, 4, ..., 10}	{0.0, 0.1, ..., 1.0}	NA
Binary-class Imbalanced	Minority	5	2	{0.0, 0.1, ..., 1.0}	{0.05, 0.1, ..., 0.5}
Multi-class Imbalanced	Minority, Majority	5	5	{0.0, 0.1, ..., 1.0}	{0.02, 0.04, ..., 0.2}

3.2.1. Synthetic Datasets

To evaluate our MI estimation approaches, we generated synthetic datasets by simulating real-world systems using the MVN distribution, allowing for straightforward calculation of ground truth MI, discussed in Appendix B.2.1. MVN perturbation and proximity techniques were used to introduce noise and simulate systems with varying levels of vulnerability, as detailed in Appendix B.2.2. The perturbation technique introduces noise by flipping a percentage of class labels, and the proximity technique reduces the distance between the mean vectors of the MVN for each class, causing the generated Gaussians to overlap. Figure 2 illustrates examples of two-dimensional data points with class imbalance $r = 0.1$, generated by vulnerable systems with noise levels 0 and 0.5 and a non-vulnerable system with noise level 1.0, using both techniques.

We also introduce imbalance in the datasets using *Minority* and *Majority* approaches to define the marginal distribution on Y ($p_Y(\cdot)$), as detailed in Appendix B.2.1, with an example class frequency for each case of binary-class and multi-class imbalanced datasets shown in Figure 3. The datasets are categorized into balanced, binary-class imbalanced, and multi-class imbalanced, with configurations based on input dimensions (d), number of classes (M), class imbalance (r), and noise level (ϵ) outlined in Table 1.

3.2.2. Experimental Setup

We evaluate each MI estimation approach on synthetic datasets generated for configurations outlined in Table 1, as shown in Figure 4. For each configuration $(\mathbf{g}_r, M, d, r, \epsilon)$, we generate 10 datasets (\mathcal{D}_j) using different seeds $j \in [10]$ and evaluate the performance using normalized mean absolute error (NMAE). Using nested cross-validation with hyperparameter optimiza-

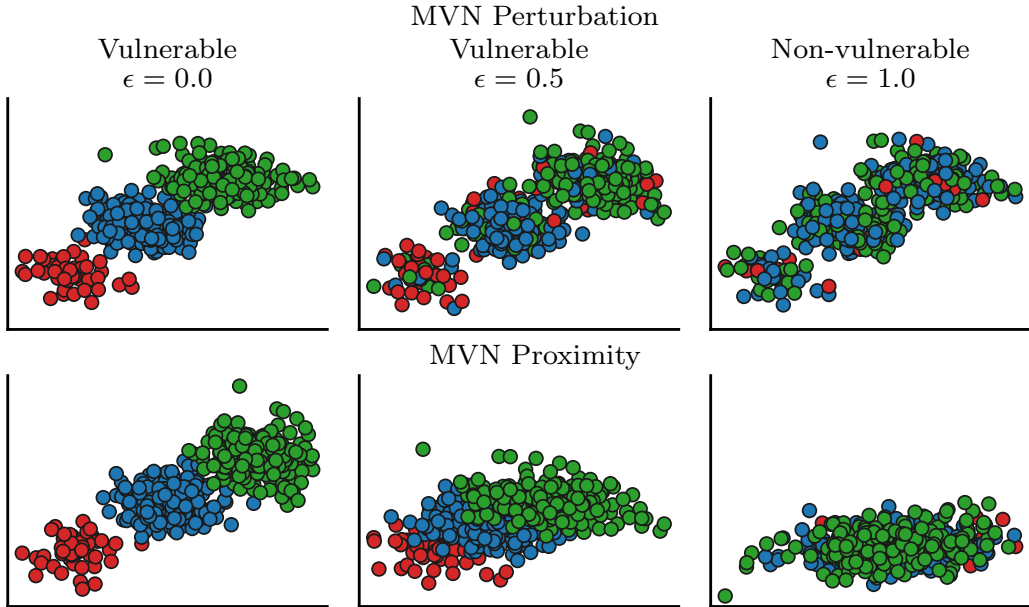


Figure 2: Generated synthetic datasets using MVN perturbation and proximity techniques

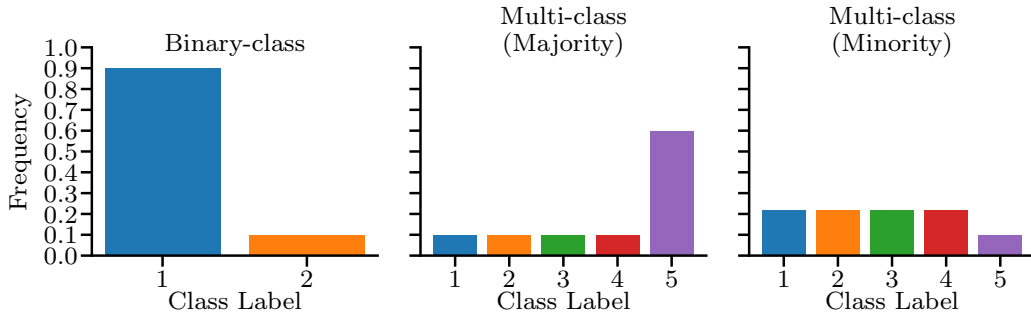


Figure 3: Class frequencies in the imbalanced datasets $r = 0.1$

tion (HPO), we split \mathcal{D}_j into 70% training and 30% test datasets. HPO involves 100 function evaluations using Monte Carlo cross-validation (MCCV) with 3 splits on the training set, reserving 30% for validation, denoted as “NIS-3SCV”, as shown in Figure 4. Objective functions for HPO include BER for PC-SOFTMAX, AutoGluon, and TabPFN, Akaike information criterion (AIC) for GMM, and mean squared error (MSE) for MINE with parameter ranges provided in Table B.4. We identify the best-performing pipeline from running AutoGluon for 1800 seconds and model using HPO on GMM,

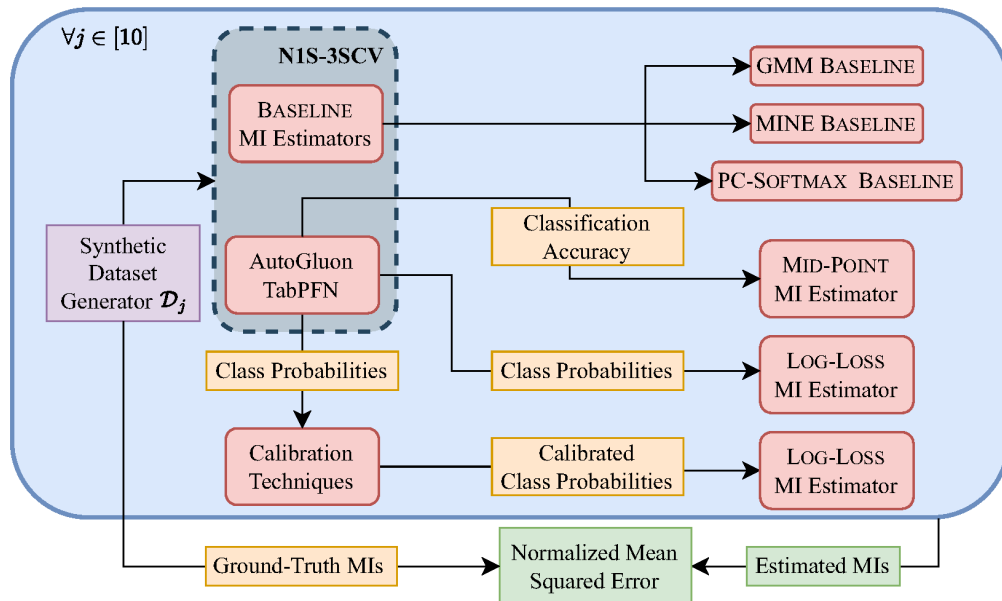


Figure 4: Experimental setup for evaluating MI estimation approaches

MINE PC-SOFTMAX, and TabPFN using validation loss or accuracy. The estimated MI of this model on the dataset \mathcal{D}_j , is compared with respect to the ground truth MI in (B.9), denoted by \hat{I}_j and I_j , using the NMAE evaluation metric defined in (9).

3.2.3. Evaluation Metric

We assess generalization performance using normalized mean absolute error (MAE) (NMAE), as MI values range from 0 to $\lg(M)$. The MAE is normalized using the entropy of Y : $H_Y(\mathbf{g}_r, M, r) = -\sum_{m=1}^M p_Y(m) \lg(p_Y(m))$. For each approach and dataset configuration $(\mathbf{g}_r, d, M, r, \epsilon)$, we obtain 10 ground truth using (B.9) and estimated MI values, denoted by vectors $\mathbf{I} = (I_1, \dots, I_{10})$ and $\hat{\mathbf{I}} = (\hat{I}_1, \dots, \hat{I}_{10})$, respectively. The performance is evaluated using the NMAE metric as

$$m_{\text{NMAE}}(\mathbf{I}, \hat{\mathbf{I}}) = \frac{1}{10} \sum_{j=1}^{10} \frac{|\mathbf{I}[j] - \hat{\mathbf{I}}[j]|}{H_Y(\mathbf{g}_r, M, r)} = \sum_{j=1}^{10} \frac{|I_j - \hat{I}_j|}{10 \cdot H_Y(\mathbf{g}_r, M, r)}. \quad (9)$$

3.3. Results

This section discusses the overall performance of various MI estimation approaches on systems simulated using perturbation and proximity techniques.

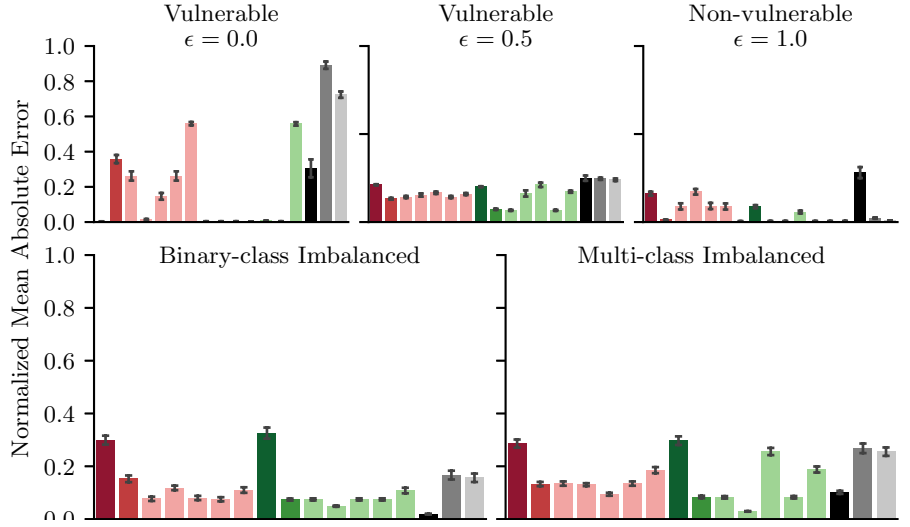
We also assess the generalization capabilities of selected approaches across various factors, including the number of classes (M), input dimensions (d), class imbalance (r), and noise levels (ϵ), detailed analysis in Appendix C.2.

3.3.1. Overall Performance

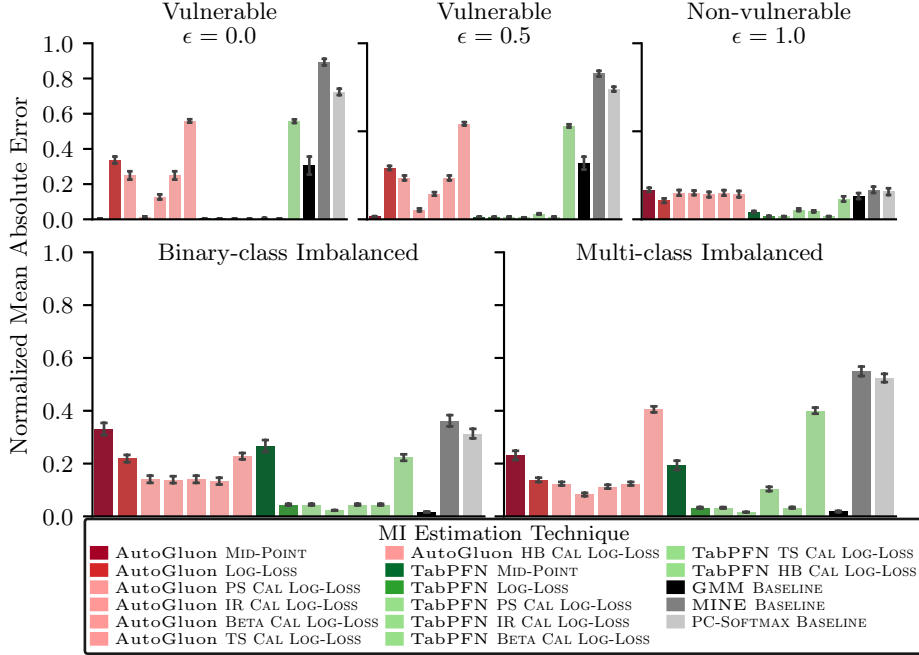
We present the performance of various MI estimation approaches using bar charts of mean and standard error (SE) of NMAE on systems simulated by MVN perturbation and proximity techniques, as shown in Figures 5a and 5b, respectively. Our analysis covers balanced, binary-class, and multi-class imbalanced datasets, as detailed in Table 1. We examine scenarios with no noise and 50% noise for balanced datasets, including non-vulnerable systems, to emphasize the importance of accurate MI estimation for ILD.

MVN Perturbation. The results depicted in Figure 5a indicate that TabPFN IR CAL LOG-LOSS consistently excels in estimating MI, and approaches using AutoGluon significantly underperform compared to those using TabPFN. For systems generating *balanced* datasets, TabPFN IR CAL LOG-LOSS shows exceptional performance (≈ 0.0026 for $\epsilon = 0.0$, ≈ 0.0056 for $\epsilon = 1.0$) and low SE of 0.0013. For more vulnerable systems with noise ($\epsilon = 5.0$), TabPFN IR CAL LOG-LOSS performs less effectively ($\approx 0.2115 \pm 0.0124$), while TabPFN PS CAL LOG-LOSS and BETA CAL LOG-LOSS perform better ($\approx 0.067 \pm 0.0032$). The HB CAL LOG-LOSS method does not enhance the LOG-LOSS estimation for both automated machine learning (AutoML) tools. For systems generating *binary-class imbalanced* datasets, the GMM shows exceptional performance ($\approx 0.019 \pm 0.0017$), with TabPFN LOG-LOSS and TabPFN IR CAL LOG-LOSS also performing well (≈ 0.05). For *multi-class imbalanced* datasets, TabPFN IR CAL LOG-LOSS leads ($\approx 0.0293 \pm 0.0013$), with the GMM also performing well ($\approx 0.10 \pm 0.002$), demonstrating strong adaptability for imbalanced datasets.

MVN Proximity. Overall, MI estimation is more straightforward on datasets generated using proximity than on ones using the perturbation technique, as it introduces more complexity (Appendix B.2). However, performance trends are similar to MVN perturbation datasets: TabPFN IR CAL LOG-LOSS outperforms, while AutoGluon performs worse. For systems generating *balanced* datasets, TabPFN IR CAL LOG-LOSS performs exceptionally well for vulnerable systems (≈ 0.003 for $\epsilon = 0.0$ and ≈ 0.010 for $\epsilon = 0.5$) with low variance. For non-vulnerable systems, TabPFN PS CAL LOG-LOSS and TS CAL LOG-LOSS perform best (≈ 0.016). For systems generating *binary-class*



(a) Performance on systems simulated using MVN perturbation technique



(b) Performance on systems simulated using MVN proximity technique

Figure 5: Overall NMAE of MI estimation approaches on synthetic datasets

imbalanced datasets, the GMM and TabPFN IR CAL LOG-LOSS are top performers ($\approx 0.017 \pm 0.001$). In *multi-class imbalanced* datasets, TabPFN

IR CAL LOG-LOSS maintains superior performance (≈ 0.016), while the GMM also performs well (≈ 0.017).

Summary. The TabPFN approaches, particularly IR CAL LOG-LOSS, consistently excel in MI estimation across various systems simulated using MVN perturbation and proximity techniques, with AutoGluon models significantly underperforming compared to those using TabPFN. However, the GMM accurately estimates MI in imbalanced datasets. Calibration techniques (CAL LOG-LOSS) generally do not significantly impact TabPFN LOG-LOSS’s performance for balanced datasets but enhance AutoGluon LOG-LOSS’s performance in vulnerable datasets, indicating AutoGluon’s poor calibration and TabPFN’s well-calibrated class probabilities, as observed in Appendix C.2. However, these techniques can sometimes worsen AutoGluon LOG-LOSS’s performance in non-vulnerable systems, leading to MI overestimation and potential false positives in ILD, as shown in Appendix C.1.2.

3.3.2. Generalization Performance

This section examines the generalization capabilities of different MI estimation approaches relative to baselines, identifying the best-performing methods using AutoGluon and TabPFN on balanced (non-vulnerable, vulnerable with noise levels 0.0 and 0.5), binary-class, and multi-class imbalanced datasets using NMAE, as detailed in Section 3.3.1.

We assess generalization based on the number of classes (M) and input dimensions (d) by aggregating NMAE across dimensions for each class ($M \in 2, 4, \dots, 10$) and classes for each dimension ($d \in 2, 4, \dots, 20$). For class imbalances, we aggregate NMAE across noise levels for each imbalance parameter ($r \in 0.05, 0.1, \dots, 0.5$ for binary-class and $r \in 0.02, 0.04, \dots, 0.2$ for multi-class datasets). Similarly, we assess generalization for noise levels ($\epsilon \in 0.0, 0.1, \dots, 1.0$) by aggregating NMAE across class imbalances. Figures 6 and 7 visualize these results with line plots, showing NMAE on systems simulated using MVN perturbation and proximity techniques, respectively. These plots assess the generalization capabilities of MI estimation approaches across various factors: number of classes (M), input dimensions (d), class imbalance (r), and noise level (ϵ).

Number of Classes (M). The top row of Figures 6 and 7 shows MI estimation methods’ generalization across datasets with varying numbers of classes ($M \in [2, 10]$) on the X-axis in systems simulated using MVN perturbation and proximity techniques, respectively. In *vulnerable* and *non-vulnerable*

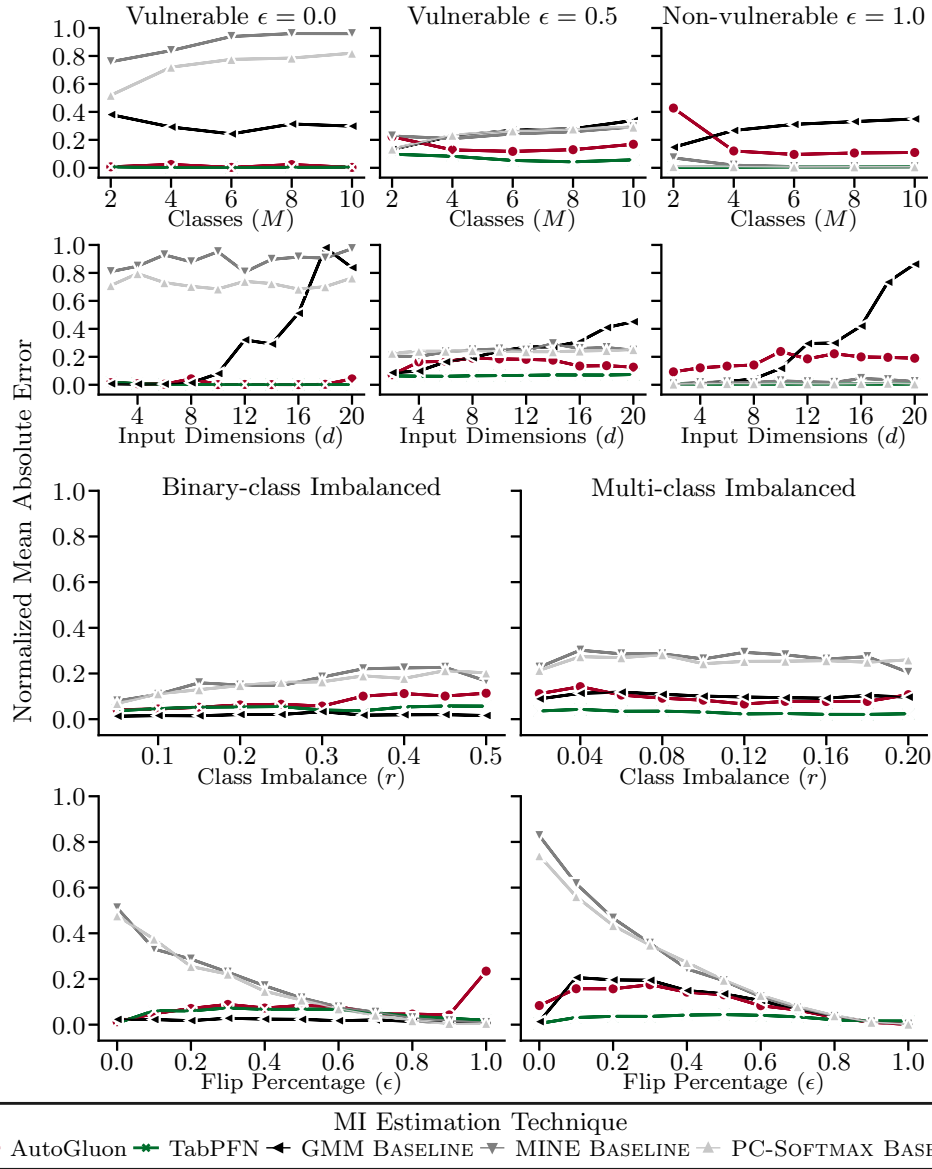


Figure 6: Generalizability of MI estimation approaches on MVN perturbation systems

systems, AutoGluon and TabPFN show high accuracy (lower NMAE) with increasing classes, with TabPFN outperforming AutoGluon, especially at 50% noise ($\epsilon = 0.5$). Baselines degrade (NMAE increases) with increasing classes. In the *vulnerable* system, MINE is the least accurate, as illustrated in Fig-

ures C.12 and C.13. For *non-vulnerable* systems, MINE and PC-SOFTMAX perform better than GMM in systems simulated using the perturbation technique.

Input Dimensions (d). The second row of Figures 6 and 7 shows MI estimation methods’ generalization across datasets with varying input dimensions ($d \in [2, 20]$) on the X-axis in systems simulated MVN perturbation and MVN proximity techniques, respectively. In *vulnerable* and *non-vulnerable* systems, AutoGluon and TabPFN improve notably with more dimensions, with TabPFN leading, specifically in systems with 50% noise. Baselines, especially GMM, deteriorate significantly with more dimensions, as also discussed in Appendix C.2.2, indicating that even deep multi-layer perceptrons (MLPs) struggle with high-dimensional datasets. MINE and PC-SOFTMAX perform well in *non-vulnerable* systems simulated using perturbation but deteriorate in ones using the proximity technique.

Class Imbalance (r). In the third row of Figures 6 and 7 shows MI estimation methods’ generalization across datasets with varying class imbalances ($r \in [0.05, 0.5]$ for binary-class and $r \in [0.02, 0.2]$ for multi-class) on X-axis, in imbalanced datasets generated using MVN perturbation and MVN proximity technique, respectively. In systems generating imbalanced datasets, TabPFN and GMM show high accuracy and stay unaffected, especially in systems generated using perturbation techniques. AutoGluon, MINE, and PC-SOFTMAX are deteriorating, notably beyond 0.25 imbalance level for systems generating *binary class imbalanced* datasets using perturbation techniques. While for systems generating *multi-class imbalanced* datasets, AutoGluon improve as class imbalance decreases, MINE and PC-SOFTMAX remain relatively constant with a notable drop at 0.04 imbalance level.

Noise Level (ϵ). The last row of Figures 6 and 7 shows MI estimation methods’ generalization across datasets with varying noise levels ($\epsilon \in [0.0, 1.0]$) on the X-axis, in imbalanced datasets generated using MVN perturbation and MVN proximity techniques, respectively. In systems generating imbalanced datasets, TabPFN and GMM show high accuracy on all noise levels, especially in systems generated using the perturbation technique. AutoGluon deteriorates with increasing noise, while MINE and PC-SOFTMAX improve significantly.

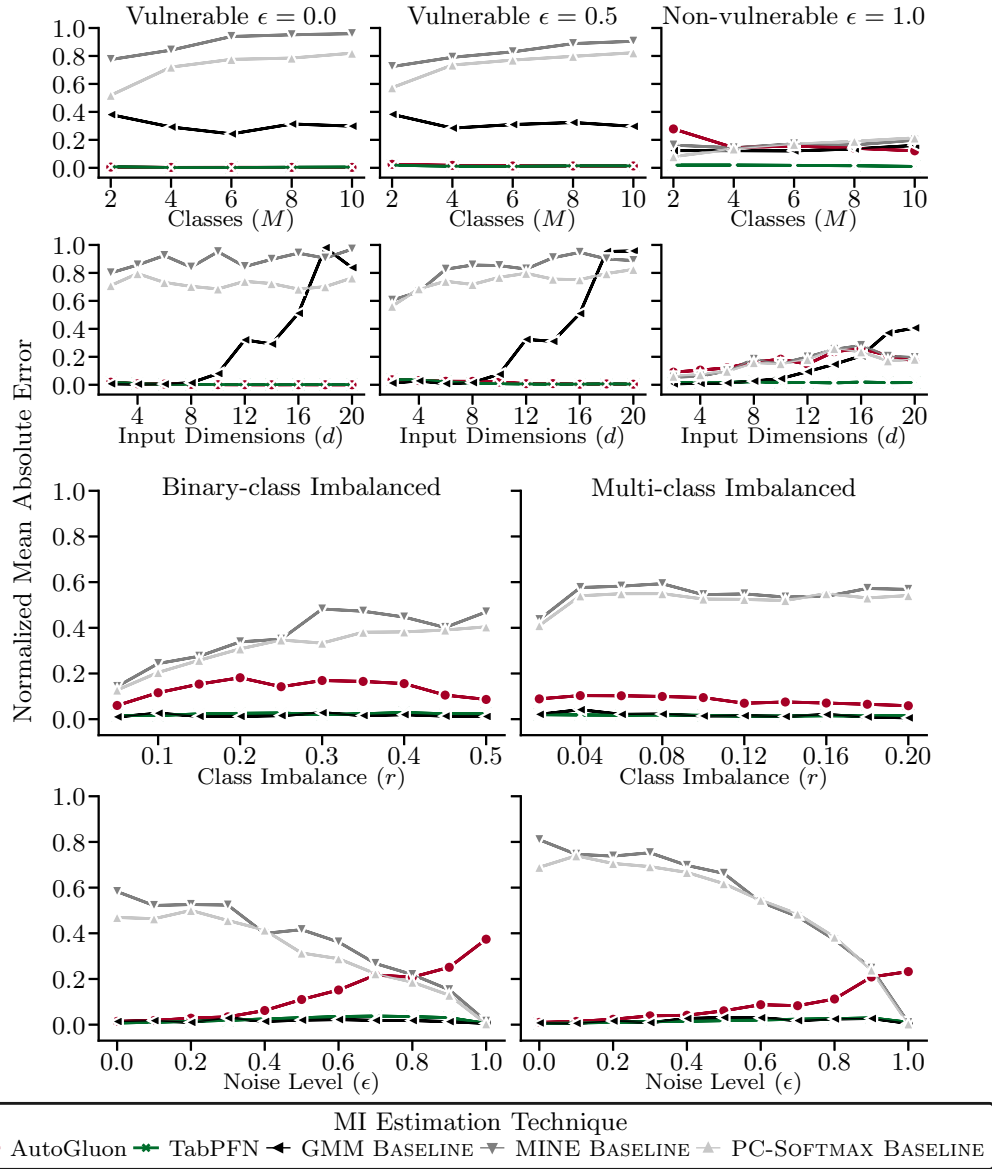


Figure 7: Generalizability of MI estimation approaches on MVN proximity systems

Summary. TabPFN, particularly IR CAL LOG-LOSS, consistently demonstrates remarkable generalization in MI estimation across various factors for systems simulated using both MVN perturbation and proximity techniques. TabPFN and AutoGluon show strong generalization performance

across different *numbers of classes (M) and input dimensions (d)*, with baselines performing worse as they increase. GMM struggles with high-dimensional datasets. MINE shows the lowest generalization capability, suggesting its unsuitability for estimating MI in classification datasets, as confirmed in Appendix C.2.1. TabPFN and GMM exhibit robust generalization across various *class imbalances (r) and noise levels (ϵ)*. GMM handles noise and imbalance well in low-dimensional datasets ($d = 5$) but struggles with high-dimensional ones. Conversely, AutoGluon, MINE, and PC-SOFTMAX show weaker generalization with respect to class imbalances (r) and noise levels (ϵ), as confirmed in Appendix C.2.2.

4. Information Leakage Detection

This section introduces the information leakage detection (ILD) process and various mutual information (MI)-based and classification-based ILD approaches. We describe the experimental setup and IL-Datasets descriptions used to evaluate information leakage detection approaches for detecting side-channel leaks (information leakages (ILs)) through time delays, countering Bleichenbacher’s attacks on OpenSSL TLS servers, and summarize the results with Appendix C.1 providing a detailed analysis. Our results conclude that our MI-based ILD approach estimating MI using calibrated log-loss (CAL LOG-LOSS) outperforms state-of-the-art methods.

4.1. ILD Methodology

The process of detecting IL in a system generating classification dataset by various ILD approaches is depicted in Figure 8. To enhance IL detection confidence, we apply Holm-Bonferroni correction on p -values by using statistical tests (details in Appendix A.3) on performance estimates of the top-10 automated machine learning (AutoML) models or pipelines from AutoGluon and TabPFN obtained through hyperparameter optimization (HPO).

4.1.1. ILD Approaches

We divide the ILD approaches based on using MI and classification metrics to detect IL in a system into MI-based and classification-based methods. We propose to use the AutoML tools, AutoGluon and TabPFN, described in Appendix B.1, for an accurate estimation of empirical risk minimizers (g or g_p) to serve as an appropriate proxy for Bayes predictor. We propose to apply statistical tests on the leakage assessment score (LAS), calculated using

LOG-LOSS, accuracy, and confusion matrix of the top-performing AutoML models or pipelines (g or g_p), to obtain a p -value with a predefined significance level of $\alpha = 0.01$. If the p -value is below α , we reject H_0 , indicating the presence of IL; otherwise, we fail to reject H_0 .

MI-based Approach. The MI-based ILD approach is based on the condition that IL occurs in the system if MI or LAS with log-loss must be significantly greater than 0, i.e., $\delta(\ell_u) \gg 0$, as per Section 2.3. To archive this, we propose to apply the one-sample t-test (OTT) on 10 MI estimates obtained using K -fold cross-validation (KFCV) on the LOG-LOSS and MID-POINT techniques on top- j th performing pipeline, as well as baseline methods, denoted by vector $\hat{\mathbf{I}}_j$. The OTT, provides a p -value representing the probability of observing the sample mean to be around the actual mean (0 in our case), defined by the null hypothesis $H_0(\hat{\mathbf{I}}_j \sim 0)$ implying absence of IL in a system, as detailed in Appendix A.3.1.

Classification-based Approaches. Our prior work Gupta et al. [31] proposes classification-based ILD approaches based on the condition that IL occurs if the Bayes predictor accuracy significantly surpasses that of a marginal Bayes predictor, i.e., LAS is significantly greater than 0, as per Section 2.3.

PTT-based Approach The PTT-MAJORITY approach applies paired t-test (PTT) between the 10 accuracy estimates from KFCV for the j -th best performing AutoML pipeline and of g_p^{mc} , denoted by \mathbf{a}_j and \mathbf{a}_{mc} , respectively, to obtain a p -value. The p -value represents the probability of obtaining our observed mean accuracy difference, assuming the null hypothesis $H_0(\cdot)$ holds, implying that accuracies are drawn from the same distribution or have nearly zero average difference [13]. This approach is based on the condition that $\delta(m_{ACC}) \gg 0$ for IL to exist in a system, as detailed in Appendix A.3.2. However, PTT assumes asymptotic behavior and normal distribution of accuracy differences, which can lead to optimistic p -values, and using accuracy can misestimate results on imbalanced datasets [58, 54].

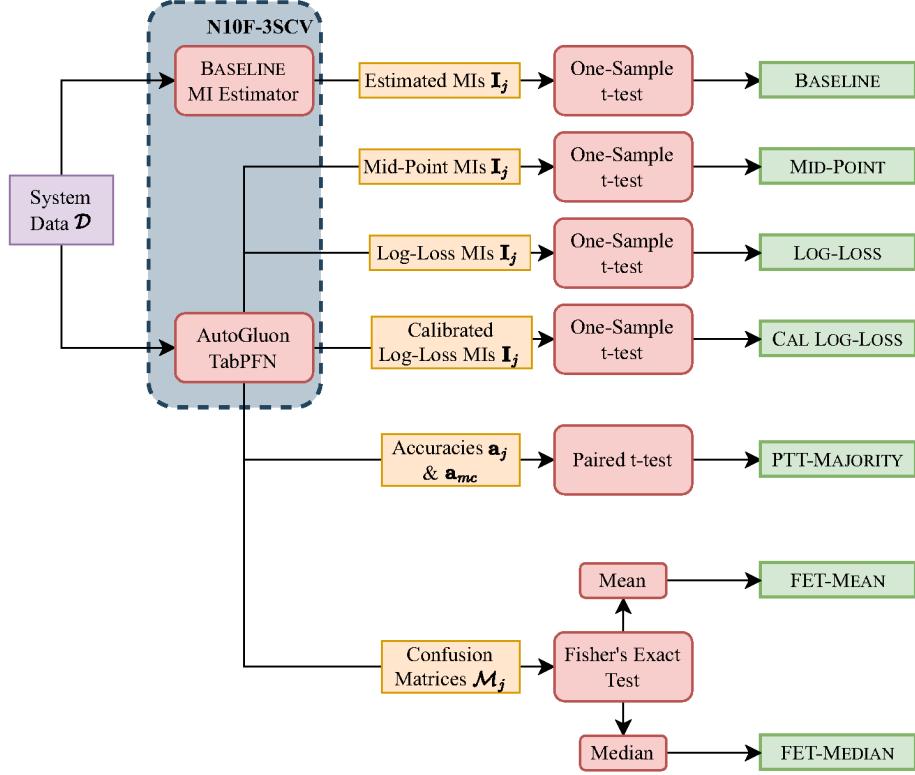
FET-based Approach To address the class imbalance and improve p -value estimation, we use Fisher’s exact test (FET) on K confusion matrices from KFCV to detect IL. If a strong correlation exists between inputs \mathbf{x} and outputs y in \mathcal{D} , the AutoML pipeline’s prediction $\hat{y} = g(\mathbf{x})$ encapsulates

input information, and FET can assess IL using the confusion matrix (analyzing LAS $\delta(m_{\text{CM}})$), which contains relevant information for predicting correct outputs ($m_{\text{TP}}, m_{\text{TN}}$). The p -value represents the probability of independence between the ground truth and predictions defined by the null hypothesis $H_0(\cdot)$, as detailed in Appendix A.3.3. We aggregate 10 p -values obtained using FET on confusion matrices $\mathcal{M}_j = \{\mathbf{M}_j^k\}_{k=1}^K$, through *median* and *mean*, referred to as FET-MEDIAN and FET-MEAN approaches.

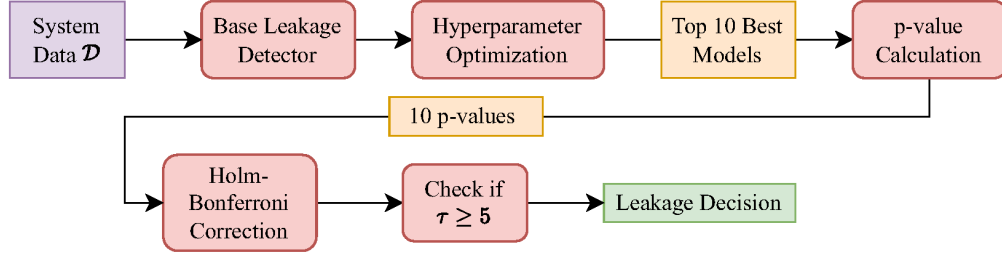
4.1.2. Detection Process

The ILD process involves rigorous estimation, statistical assessment, and correction techniques to confidently detect IL in a system. The process starts with obtaining accurate MI or Bayes predictor performance estimates using nested K -fold cross-validation (KFCV) with HPO and specific parameter ranges provided in Table B.4. The dataset \mathcal{D} is split into 90 % training and 10 % test sets using KFCV (10), conducting HPO with 100 evaluations using Monte Carlo cross-validation (MCCV) with 3 splits, reserving 30 % of training data for validation, denoted as “N10F-3SCV”, as depicted in Figure 8a. Objective functions for HPO include balanced error rate (BER) for PC-SOFTMAX, AutoGluon, and TabPFN, Akaike information criterion (AIC) for Gaussian mixture model (GMM), and mean squared error (MSE) for mutual information neural estimation (MINE) with parameter ranges provided in Table B.4. We identify top-10 best-performing pipelines from running AutoGluon for 1800 seconds and top-performing models using HPO on GMM, MINE PC-SOFTMAX and TabPFN, using validation loss or accuracy. KFCV is applied to the top-10 models or pipelines, generating 10 estimates from the entire dataset \mathcal{D} , which statistical tests use to produce p -values, which are assessed to detect IL. We obtain 10 MI estimates, accuracies, and confusion matrices for each of the j -th best-performing model/AutoML pipeline, denoted by $\hat{\mathbf{I}}_j$, \mathbf{a}_j and $\mathcal{M}_j = \{\mathbf{M}_j^k\}_{k=1}^K$, respectively. The OTT is used on MI estimates ($\hat{\mathbf{I}}_j$), PTT compares the accuracies (\mathbf{a}_j) with that of g_p^{mc} (\mathbf{a}_{mc}), and FET is applied to confusion matrices ($\mathcal{M}_j = \{\mathbf{M}_j^k\}_{k=1}^K$), producing 10 p -values which are aggregated using *mean* and *median* operators.

To enhance **robustness and reliability** in ILD, we use the Holm-Bonferroni correction to ensure accuracy and reliability in our ILD framework, which mitigates the influence of overfitting and noisy estimates that can arise when using just one pipeline (model) [36]. After obtaining 10 p -values from top-10 models/pipelines, we apply the correction to acquire the number of rejected hypotheses or the cut-off parameter $\tau = |\mathcal{F}_r|$, quantifying IL detection confi-



(a) Calculation of p -value by different ILD approaches



(b) Information leakage (IL) detection process

Figure 8: Procedure of using ILD approaches to detect ILs in a system generating \mathcal{D}

dence. To detect IL efficiently, it is imperative to set an appropriate *rejection threshold* on the cut-off parameter τ , as a higher threshold avoids false positives and a lower value reduces false negatives, as detailed in Appendix A.3.4.

Based on prior work [31], setting the rejection threshold to $\lfloor J/2 \rfloor$ on the cut-off parameter τ ensures robust and accurate IL detection, which we also use for this study, i.e., $\tau \geq 5$.

4.2. Empirical Evaluation

This section outlines the evaluation process for our ILD approaches compared to baselines in detecting timing side-channel leaks in OpenSSL TLS servers, as illustrated in Figure 8. Our main objective is to assess the generalization capability of various ILD approaches with respect to the LAS of systems, generating both balanced and imbalanced datasets, as outlined in Table 2. The overall performance results for selected approaches are discussed in Section 4.3, with detailed analysis in Appendix C.1.

4.2.1. OpenSSL Timing Datasets

We target side-channel vulnerabilities in cryptographic software to validate our approaches using network traffic generated by a modified OpenSSL TLS server. Bleichenbacher’s attack exploits server behavior to differentiate correctly formatted decrypted messages from incorrect ones [6]. A secure OpenSSL TLS server exhibits no time difference in processing correctly and incorrectly formatted messages, but a vulnerable server does, exposing IL through processing time differences. For our experiments, the timing side-channel or time delay, i.e., observable differences in server computation times when processing messages with correct and manipulated padding, was introduced as per the Java TLS implementation vulnerability CVE-2014-0411¹ [44]. Datasets were provided by Funke [25] from the vulnerable (DamnVulnerableOpenSSL²) OpenSSL TLS server, which exhibits longer computation times for incorrectly formatted messages with manipulated padding, and the non-vulnerable (OpenSSL 1.0.2³), which shows no time delay (no IL). There are 10 padding manipulations: five cause longer processing times (simulating IL, $z = 1$), and five do not (no IL, $z = 0$). Each IL-Dataset \mathcal{L} contains 10 binary-class datasets corresponding to 10 padding manipulations \mathcal{D} , with label 0 instances corresponding to correctly formatted messages and positive label ($y = 1$) instances to incorrectly formatted messages. Table 2 details the IL-Datasets generated for time delays

¹<https://cve.mitre.org/cgi-bin/cvename.cgi?name=CVE-2014-0411>

²<https://github.com/tls-attacker/DamnVulnerableOpenSSL>

³<https://www.openssl.org/source/old/1.0.2/>

of $t \in \{2^0, 2^1, \dots, 2^8\} \cup \{5, 10, \dots, 35\}$ (in μ seconds) serving as the system’s LAS, and class imbalances of $r \in \{0.1, 0.3, 0.5\}$ uploaded on OpenML⁶.

Table 2: Overview of the OpenSSL timing IL-Datasets used for the ILD experiments

Time Delay (in μ seconds)	# Folds	Imbalance r	IL-Dataset \mathcal{L} configuration			Dataset \mathcal{D} configuration			
			# Systems $ \mathcal{L} $	# $z=0$	# $z=1$	$ \mathcal{D} $	# $y=0$	# $y=1$	# Features
$\{2^0, 2^1, \dots, 2^8\}$	3	0.1	10	5	5	[943, 1064]	[849, 958]	[94, 106]	124
$\{2^0, 2^1, \dots, 2^8\}$	3	0.3	10	5	5	[1212, 1368]	[849, 958]	[363, 410]	124
$\{2^0, 2^1, \dots, 2^8\}$	3	0.5	10	5	5	[1725, 1929]	[849, 958]	[829, 989]	124
$\{10, 15, \dots, 35\}$	10	0.1	10	5	5	[962, 2263]	[866, 2037]	[96, 226]	[124, 154]
$\{10, 15, \dots, 35\}$	10	0.3	10	5	5	[1237, 2910]	[866, 2037]	[371, 873]	[124, 154]
$\{10, 15, \dots, 35\}$	10	0.5	10	5	5	[1721, 4084]	[866, 2037]	[826, 2104]	[124, 154]

4.2.2. Experimental Setup

We apply each ILD approach depicted in Figure 8a to a set of IL-Datasets detailed in Table 2. Each IL-Dataset ($\mathcal{L} = \{(\mathcal{D}_i, z_i)\}_{i=1}^{10}$) consists of 10 system datasets corresponding to 10 messages with manipulated padding ($y_i = 1$), with five systems containing IL ($z = 1$) and five not ($z = 0$), as discussed in Section 4.2.1. We evaluate each ILD approach using standard binary classification metrics: Accuracy, FPR, and FNR, as defined in Appendix A.1.2, on the predicted IL decisions ($\hat{\mathbf{z}} = (\hat{z}_1, \dots, \hat{z}_{10})$) and the ground truth vector ($\mathbf{z} = (z_1, \dots, z_{10})$).

4.3. Results: Detection Accuracy

We analyze the performance of various ILD approaches based on class imbalance and time delay factors. We consider OpenSSL systems with short time delays ($\leq 25 \mu$ -seconds) with complex IL and larger time delays ($\geq 25 \mu$ -seconds), where detection is more straightforward. Additionally, we consider the class imbalance in the system dataset ($r \in \{0.1, 0.3, 0.5\}$). We present the mean detection accuracy with standard error (SE) for each method across different IL-Datasets, using a rejection threshold 5 on τ , as shown in Figure 9. For a detailed analysis of ILD approaches’ generalization capability with respect to LAS or time delay, see Appendix C.1.

Selected ILD Approaches. To identify the best-performing calibration approach for both TabPFN and AutoGluon using LOG-LOSS estimation, we assessed their normalized mean absolute error (NMAE) from experiments detailed in Section 3.2.2. This process determined the optimal calibration

approach for each AutoML tool separately for balanced ($r = 0.5$) and imbalanced ($r \in 0.1, 0.3$) datasets. AutoGluon TS CAL LOG-LOSS was most effective for both scenarios, while TabPFN IR CAL LOG-LOSS performed best on imbalanced datasets and TabPFN PS CAL LOG-LOSS for balanced ones. We focus on FET-MEDIAN’s performance, as Bhattacharya and Habtzghi [3] highlighted its robustness, and Gupta et al. [31] concluded that FET-MEDIAN and FET-MEAN perform similarly for $\tau = 5$.

4.3.1. Short Time Delay

Our first set of experiments focuses on systems with short time delays ($\leq 25 \mu$ -seconds) with complex IL.

Imbalanced. Detecting ILs with short time delays or LAS is challenging. Notably, the TabPFN CAL LOG-LOSS approach consistently exhibits high detection accuracy, with AutoGluon FET-MEDIAN also performing well. For $r = 0.1$, TabPFN CAL LOG-LOSS achieves 69% accuracy and 58% for $r = 0.3$, while AutoGluon FET-MEDIAN detects 54% and 58% of ILs, respectively. However, detecting ILs in these scenarios remains challenging due to missed IL and high false positive rates, as detailed in Appendix C.1.

Balanced. Detecting ILs in systems generating balanced datasets with short time delays remains challenging but more manageable than generating imbalanced ones. AutoGluon LOG-LOSS and CAL LOG-LOSS approaches outperform, detecting a significant proportion of ILs (approximately 68%). IR CAL LOG-LOSS enhances TabPFN LOG-LOSS detection accuracy to 67%, making it a competent approach, while PS CAL LOG-LOSS does not improve its detection performance. Overall, AutoGluon outperforms TabPFN, with PTT-MAJORITY detecting over 61% of ILs.

4.3.2. Long Time Delay

Our first set of experiments focuses on systems with long time delay ($\geq 25 \mu$ -seconds) with simpler IL.

Imbalanced. Detecting ILs in systems with larger time delays or LAS is more straightforward, with all approaches consistently performing well, detecting more than 50% of ILs. In particular, the TabPFN CAL LOG-LOSS approach detects approximately 94% of ILs, while AutoGluon FET-MEDIAN excels, detecting over 92% of ILs for $r = 0.3$ and approximately 72% for $r = 0.1$. FET based approaches perform better than PTT-MAJORITY in detecting ILs in imbalanced systems’ datasets, also confirmed in [31].

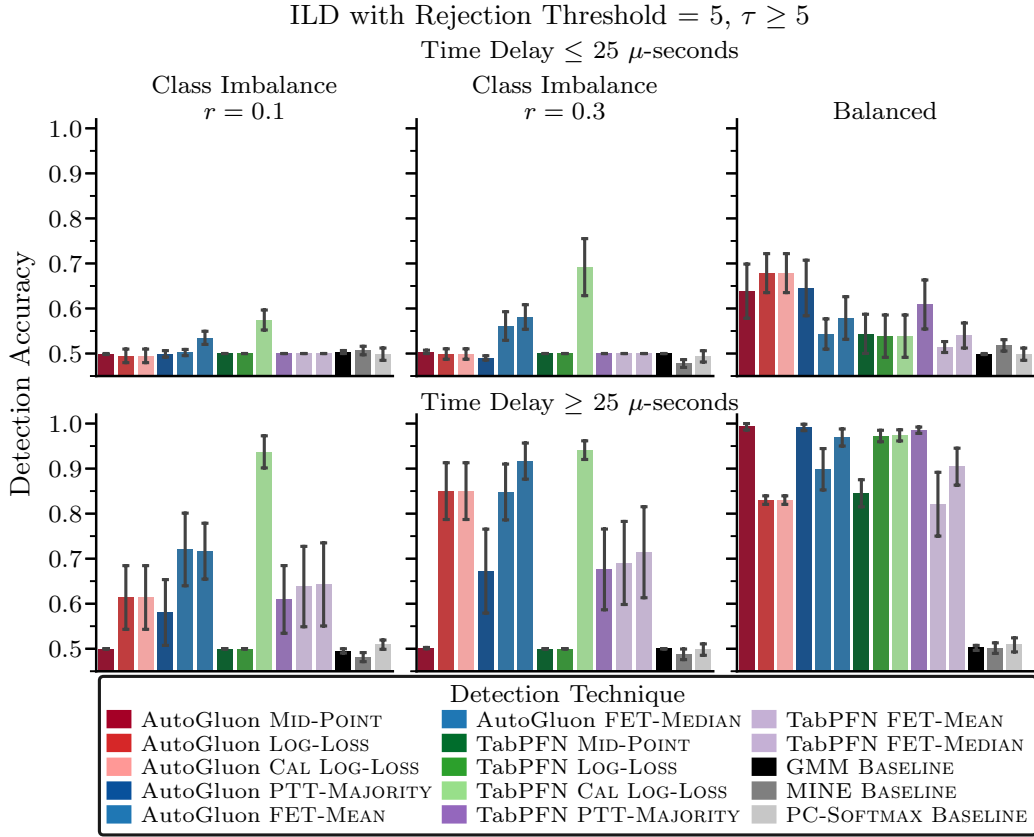


Figure 9: ILD performance in detecting OpenSSL TLS timing side-channels

Balanced. In systems with balanced datasets and longer time delays, detecting ILs becomes straightforward. AutoGluon MID-POINT and TabPFN IR CAL LOG-LOSS consistently detect the majority (around 99%) of ILs, confirming IR CAL LOG-LOSS’s offering an alternative calibration technique to improve the efficacy for TabPFN LOG-LOSS approach. TabPFN PS CAL LOG-LOSS and LOG-LOSS approaches detect 97%, showing no improvement with the selected calibration technique, while TabPFN MID-POINT detects 85%. Among classification-based approaches, PTT-MAJORITY consistently outperforms detecting 99% of ILs, contrary to findings in [31].

4.3.3. Summary

Detecting IL is easier in systems generating balanced datasets, where TabPFN IR CAL LOG-LOSS, MID-POINT, and PTT-MAJORITY using Au-

toGluon show robust performance. Contrary to Gupta et al. [31], PTT-MAJORITY outperforms FET-based approaches in balanced datasets, indicating that ILD performance varies with IL patterns. Baseline methods detect only 50% of ILs, reflecting random detection decisions, as discussed in Appendix C.1. TabPFN CAL LOG-LOSS consistently outperforms other approaches, highlighting the need for calibrating TabPFN LOG-LOSS for precise MI estimation. The MID-POINT approach is unable to detect ILs in systems generating imbalanced datasets, as expected. For balanced datasets, IR CAL LOG-LOSS significantly improves detection accuracy compared to PS CAL LOG-LOSS, as shown in Appendix C.1, indicating that calibration choice is complex based on synthetic dataset results in Section 3.3.1. Calibration of LOG-LOSS using AutoGluon often leads to overfitting and overestimating MI, resulting in false positives as shown in Section 3.3.1. This discrepancy may result from feature reduction (from 150 to [20, 50]) for TabPFN and the scarcity of positive instances in imbalanced datasets, implying that the choice and necessity of calibration techniques depend on the underlying datasets.

5. Conclusion

This paper presents a comprehensive framework for information leakage detection (ILD), leveraging information theory and statistical learning theory concepts to enhance cybersecurity by identifying vulnerabilities. We introduced two techniques for quantifying and detecting information leakage (IL) by estimating mutual information (MI) between a system’s observable and secret information, using the Bayes predictor’s LOG-LOSS and accuracy. Our methods employ two powerful automated machine learning (AutoML) tools, TabPFN and AutoGluon, for efficient MI estimation, offering an automated alternative to traditional statistical techniques or deep multi-layer perceptrons (MLPs). We propose applying the one-sample t-test (OTT) on the estimated MIs, enhancing robustness with Holm-Bonferroni correction and boosting confidence in IL decisions, as established in our prior work [31].

Our empirical results show that our approach, mainly using TabPFN for calibrated LOG-LOSS approximation, effectively estimates MI and detects timing side-channel leaks in OpenSSL TLS servers, outperforming state-of-the-art methods. The key contributions of our work include a comprehensive ILD framework, addressing imbalance with minimal false positives, robustness to noise in generated system datasets, and an adaptable, scalable IL detection solution for real-world scenarios. Furthermore, our work concludes

that the choice and requirement of calibration techniques for LOG-LOSS estimation depend on the characteristics of the system datasets.

Future work will focus on providing an automated solution for high-dimensional datasets with many classes, mitigating current limitations using TabPFN [35]. We aim to develop an end-to-end AutoML tool that integrates dimensionality reduction and calibration methods to estimate MI and detect IL accurately. Improving the MID-POINT approach to account for dataset imbalance and extending the balanced error rate (BER) and MI relationship by Zhao et al. [71] for multiple classes is essential. Additionally, we will explore detecting leaks through CPU caches, power consumption, and electromagnetic radiation [49, 55]. We intend to examine adaptive techniques for adjusting and refining IL detection based on evolving attack strategies or changing environments, considering methods like reinforcement learning [18].

Acknowledgment

We are grateful to Dennis Funke, Jan Peter Drees, Karlson Pfannschmidt, Arunselvan Ramaswamy, Björn Haddenhorst, and Stefan Heid for their valuable suggestions. We acknowledge computing time on the high-performance computers Noctua2 at the NHR Center PC² for performing the simulations, granted under the project “hpc-prf-aiafs” (AProSys) project funded by Bundesministerium für Wirtschaft und Klimaschutz (BMWK), Förderkennzeichen: 03EI6090E under Abrechnungsobjekt: 3130500154.

Appendix A. Fundamentals

This section recalls some fundamental classification problem concepts with the relevant metric from statistical learning theory, with notations listed in Table A.3. Building upon this, we define the concept of Bayes predictor and the classification problem by estimating (class) conditional probabilities in Section 2.2.2, which are necessary to formalize the conditions for IL occurrence in a system, as discussed in Section 2.3. Additionally, we also describe the state-of-the-art techniques Gaussian mixture model (GMM), mutual information neural estimation (MINE) and PC-SOFTMAX proposed for estimating MI and the statistical tests used to detect IL in a system.

Table A.3: Notation used throughout the paper

Symbol	Meaning
$[n]$	Set of integers $\{1, 2, \dots, n\}, n \in \mathbb{N}$
$\mathbb{I}[A]$	Indicator function which is 1 if statement A is true and 0 otherwise
$p_{(X,Y)}(\cdot), \hat{p}_{(X,Y)}(\cdot)$	Actual and predicted joint probability density function (PDF) between (X, Y)
$p_{(X,Y)}(\mathbf{x}, y) = p_{(X,Y)}(\mathbf{x}, y)$	Joint PDF of X and Y , at point (\mathbf{x}, y)
$p_X(\cdot), \hat{p}_X(\cdot)$	Actual and predicted marginal PDF of X
$p_X(\mathbf{x}) = p_X(\mathbf{x})$	Probability mass of input \mathbf{x}
$p_Y(\cdot), \hat{p}_Y(\cdot)$	Actual and predicted marginal probability mass function (PMF) of Y
$p_Y(y) = p_Y(y)$	Probability of class label y
$p_{Y X}(\cdot), \hat{p}_{Y X}(\cdot)$	Actual and predicted conditional PDF of Y given X
$p_{Y X}(y \mathbf{x}) = p_{Y X}(y \mathbf{x})$	Probability of y given \mathbf{x}
$p_{X Y}(\cdot), \hat{p}_{X Y}(\cdot)$	Actual and predicted conditional PDF of Y given X
$p_{X Y}(\mathbf{x} y) = p_{X Y}(\mathbf{x} y)$	Probability of \mathbf{x} given y
X	Input ($\mathbf{x} \in \mathbb{R}^d$) random variable (d-dimensional continuous)
Y	Output ($y \in [M]$) random variable (discrete)
$\mathcal{X} \in \mathbb{R}^d$	Input Space, set of \mathbf{x} sampled from X
$\mathcal{Y} \in [M]$	Output Space, set of y sampled from Y
$\mathcal{D} = \{(\mathbf{x}_i, y_i)\}_{i=1}^N$	Classification dataset
r	Imbalance in a dataset \mathcal{D}
ϵ	Noise in a dataset \mathcal{D}
$I(X; Y)$	MI between X and Y
$H(Y X)$	Conditional entropy for Y given X
$H(X), H(Y)$	Entropy for random variable X and Y
$H_2(a) = -(a) \lg(a) - (1-a) \lg(1-a)$	Binary cross-entropy function for $a \in (0, 1)$
$\lg(a), \log(a), \ln(a), a \in \mathbb{R}^+$	Binary (base 2), Decimal (base 10) and Natural (base e) of a
$m_{\text{ERR}}(g^{bc}), m_{\text{ERR}}(g^{mc})$	The Bayes error rate and error rate of marginal Bayes predictor
$\delta(\ell_{(\cdot)}) = \ell_{(\cdot)}(g^{mc}) - \ell_{(\cdot)}(g^{bc})$	Leakage assessment score (LAS) is the difference in performance of g^{bc} and g^{mc} quantifying IL
$\delta(m_{(\cdot)}) = m_{(\cdot)}(g^{mc}) - m_{(\cdot)}(g^{bc}) $	
L, \mathcal{L}	ILD function and IL-Dataset
$H_0(\text{condition}), H_1(\text{condition})$	Null and Alternate hypothesis for statistical tests
$\tau \in [J], J \in \mathbb{N}$	Cut-off parameter on J hypothesis for Holm-Bonferroni correction
$\alpha = 0.01$	Rejection threshold on H_0 (accept H_1) for statistical tests

Appendix A.1. Classification Problem

In the realm of classification, the learning algorithm (learner) is provided with a training dataset $\mathcal{D} = \{(\mathbf{x}_i, y_i)\}_{i=1}^N \subset \mathcal{X} \times \mathcal{Y}$ of size $N \in \mathbb{N}$, where $\mathcal{X} = \mathbb{R}^d$ is the input (instance) space and $\mathcal{Y} = \{1, 2, \dots, M\} = [M]$, $M \in \mathbb{N}$ the output (categorical classes) space [67], and the (\mathbf{x}_i, y_i) are assumed to be independent and identically distributed (i.i.d.) according to $p_{(X,Y)}(\cdot)$. According to statistical learning theory, the primary goal of the learner in standard classification is to induce a hypothesis $h: \mathcal{X} \rightarrow \mathcal{Y}$, $h \in \mathcal{H}$, with low generalization error (risk)

$$R(h) = \mathbb{E}[\ell(y, h(\mathbf{x}))] = \int_{\mathcal{X} \times \mathcal{Y}} \ell(y, h(\mathbf{x})) d p_{(X,Y)}(\mathbf{x}, y), \quad (\text{A.1})$$

where \mathcal{H} is the underlying hypothesis space (set of candidate functions the learner can choose from), $\ell: \mathcal{Y} \times \mathcal{Y} \rightarrow \mathbb{R}$ a loss function, and $p_{(X,Y)}(\cdot)$ is the joint probability measure modeling the underlying data-generating process. A loss function commonly used in standard classification is the 0-1 loss $\ell_{01}(y, \hat{y}) := \mathbb{I}[\hat{y} \neq y]$, where $\hat{y} = h(\mathbf{x})$ and $\mathbb{I}[\cdot]$ is the indicator function as defined in Table A.3. The risk minimizer (denoted by h^*) achieves the minimum expected loss $\mathbb{E}[\ell(\cdot)]$ in terms of the loss function ℓ across the entire joint distribution $p_{(X,Y)}(\cdot)$ and is defined as $h^* = \arg \min_{h \in \mathcal{H}} R(h)$. The measure $p_{(X,Y)}(\cdot)$ in (A.1) induces marginal probability (density or mass) functions on \mathcal{X} and \mathcal{Y} as well as a conditional probability of the class Y given an input instance \mathbf{x} , i.e., $p_{(X,Y)}(\mathbf{x}, y) = p_{Y|X}(y | \mathbf{x}) \times p_X(\mathbf{x})$. In practice, these probabilities are not observed by the learner, so directly minimizing the risk (A.1) is not feasible. Instead, learning in a standard classification setting is commonly accomplished by minimizing (a regularized version of) *empirical risk* for h :

$$R_{\text{emp}}(h) = \frac{1}{N} \sum_{i=1}^N \ell(y_i, h(\mathbf{x}_i)). \quad (\text{A.2})$$

In the subsequent discussions, we denote by $g = \arg \min_{h \in \mathcal{H}} R_{\text{emp}}(h)$ the (learned) hypothesis that minimizes (A.2), i.e., the empirical risk minimizer [67]. In practice, for the available finite sampled dataset \mathcal{D} , g is the best possible approximation (empirical estimation) of the true risk minimizer h^* and is an appropriation thereof.

Appendix A.1.1. Probabilistic Classification

Distinct from standard classifiers, probabilistic classifiers focus on estimating the (conditional) class probabilities $p_{Y|X}(y | \mathbf{x})$ for each class y in \mathcal{Y} , given an input instance $\mathbf{x} \in \mathcal{X}$. We denote predictions of that kind by $\hat{p}_{Y|X}(y | \mathbf{x})$. As before, training data comes in the form $\mathcal{D} = \{(\mathbf{x}_i, y_i)\}_{i=1}^N \subset \mathcal{X} \times \mathcal{Y}$, where the (\mathbf{x}_i, y_i) are i.i.d. according to $p_{(X,Y)}(\cdot)$, and the goal to induce a hypothesis $h_p: \mathcal{X} \rightarrow \mathbb{P}(\mathcal{Y})$ with low generalization error (risk)

$$R_p(h_p) = \mathbb{E}[\ell_p(y, h_p(\mathbf{x}))] = \int_{\mathcal{X} \times \mathcal{Y}} \ell_p(y, h_p(\mathbf{x})) d p_{(X,Y)}(\mathbf{x}, y).$$

Now, however, instead of comparing a predicted class \hat{y} with a true class y , the loss ℓ_p compares a predicted probability distribution with y —thus, the loss is a mapping $\ell_p: \mathcal{Y} \times \mathbb{P}(\mathcal{Y}) \rightarrow \overline{\mathbb{R}}$, where $\mathbb{P}(\mathcal{Y})$ denotes the set of PMFs on \mathcal{Y} .

Since \mathcal{Y} is finite and consists of M classes, $\mathbb{P}(\mathcal{Y})$ can be represented by the $(M - 1)$ -simplex, i.e., predictions can be represented as probability vectors $h_p(\mathbf{x}) = \hat{\mathbf{p}} = (\hat{p}_1, \dots, \hat{p}_M)$, where $\hat{p}_m = \hat{\mathbf{p}}[m] = \hat{p}_{Y|X}(m | \mathbf{x})$ is the probability assigned to class m . Typically, learning predictors of that kind involve minimizing the *empirical risk*

$$R_{\text{emp}|p}(h_p) = \frac{1}{N} \sum_{i=1}^N \ell_p(y_i, h_p(\mathbf{x}_i)). \quad (\text{A.3})$$

In the subsequent discussions, we denote the empirical risk minimizer by $g_p = \arg \min_{h_p \in \mathcal{H}_p} R_{\text{emp}|p}(h_p)$ [67, 5, chap. 4]. In the case where Y is independent of X , the marginal Bayes predictor or marginal classifier (denoted by g_p^{mc}) is again the best constant probability predictor, i.e., the one with the lowest risk (A.3) among all constant predictors.

Proper Scoring Rules. So-called (strictly) *proper scoring rules* constitute an important class of loss functions in probabilistic classification [28]. Roughly speaking, such losses incentivize the learner to predict accurate probabilities. Formally, a loss $\ell_p(\cdot)$ is a proper scoring rule if

$$\mathbb{E}_{Y \sim \mathbf{p}} \ell_p(Y, \mathbf{p}) \leq \mathbb{E}_{Y \sim \mathbf{p}} \ell_p(Y, \hat{\mathbf{p}})$$

for all distributions $\mathbf{p}, \hat{\mathbf{p}}$, and a *strictly* proper scoring rule is the above inequality is strict whenever $\mathbf{p} \neq \hat{\mathbf{p}}$. Thus, by predicting the true distribution

\mathbf{p} of the (categorical) random variable Y , the learner minimizes its loss in expectation. Important examples of strictly proper scoring rules include the Brier score and the categorical cross-entropy (CCE). The latter is defined as $\ell_{\text{CCE}}(y, \hat{\mathbf{p}}) := -\ln(\hat{p}_y)$ [5, chap. 4]. The CCE loss (logarithmic scoring rule) is widely recognized for its information-theoretic interpretations and practical effectiveness [29, 60, 12]. It can also be motivated in Neyman–Pearson theory [21].

Probability Calibration. Despite its sound theoretical grounding, the (empirical) minimization of a proper scoring rule is not guaranteed to produce accurate probability estimates in practice. Instead, predictions are often noisy or systematically biased — neural networks, for instance, tend to be over-confident and predict probabilities that are biased toward the extremes, especially in the case of imbalanced datasets [63]. So-called *calibration* methods seek to improve probability estimates through suitable post-hoc adjustments. Such methods leverage validation data to learn calibration functions from (monotone) mappings from predicted probabilities to improved probabilities [62]. This study uses five multi-class calibration methods to improve MI estimation accuracy with the LOG-LOSS approach:

Isotonic Regression (IR CAL LOG-LOSS): Fits a monotonic function to transform original scores using ground truth labels, minimizing mean squared error (MSE) and ensuring improved calibration without overfitting [1].

Platt’s Scaling (PS CAL LOG-LOSS): Trains a logistic regression model on the classifier’s outputs and accurate labels to induce calibrated class probabilities [56].

Beta Calibration (BETA CAL LOG-LOSS): Uses a parametric transformation with a beta distribution with adjustable hyperparameters, offering flexible calibration for different datasets [39].

Temperature Scaling (TS CAL LOG-LOSS): Scales the logits of predicted probabilities with a “temperature” parameter, calibrates the entire distribution, while maintaining the rank order of classes [30].

Histogram Binning (HB CAL LOG-LOSS): Predicted probabilities are discretized into bins. The actual class frequency in each bin is used to adjust predicted class probabilities and achieve calibration [69].

These calibration techniques are pivotal in refining predicted class probabilities and ensuring accurate MI estimation through the LOG-LOSS approach. When using these techniques to estimate MI and perform ILD using LOG-LOSS, we refer to them collectively as CAL LOG-LOSS.

Deterministic Prediction. Obviously, a probabilistic prediction may also serve as a basis for a deterministic prediction if needed. Typically, the class label with the highest (predicted) probability is adopted in that case, i.e., $\hat{y} = \arg \max_{y \in \mathcal{Y}} \hat{p}_{Y|X}(y | \mathbf{x})$. As readily seen, this prediction minimizes the standard 0-1 loss in expectation. The other way around, this also shows that to perform well in terms of standard 0-1 loss, the learner merely needs to identify the most probable class, or, stated differently, strong performance can even be achieved with relatively inaccurate estimates, provided the highest predicted probability is still assigned to the indeed most probable class label [15].

Appendix A.1.2. Performance Evaluation Metrics

Koyejo et al. [38] and Powers [58] define evaluation measures used for evaluating the performance of classifiers, using the ground truth labels denoted by $\mathbf{y} = (y_1, \dots, y_N)$ for a given $\mathcal{D} = \{(\mathbf{x}_i, y_i)\}_{i=1}^N$ and the predictions denoted by the vector $\hat{\mathbf{y}} = (\hat{y}_1, \dots, \hat{y}_N)$. The predictions could be obtained by the empirical risk minimizer g derived using (A.2) for a standard classification, such that $\hat{y}_i = g(\mathbf{x}_i), \forall i \in [N]$ or by the deterministic predictions produced by a probabilistic classifier g_p derived using (A.3), such that $\hat{y}_i = \arg \max_{m \in M} g_p(\mathbf{x}_i)[m], \forall i \in [N]$.

Accuracy is defined as the proportion of correct predictions

$$m_{\text{ACC}}(\mathbf{y}, \hat{\mathbf{y}}) := \frac{1}{N} \sum_{i=1}^N \mathbb{I}[y_i = \hat{y}_i].$$

Error-rate is defined as the proportion of incorrect predictions

$$m_{\text{ERR}}(\mathbf{y}, \hat{\mathbf{y}}) := \frac{1}{N} \sum_{i=1}^N \mathbb{I}[y_i \neq \hat{y}_i].$$

Confusion matrix (CM) Many evaluation metrics are based on the concepts, *true positive* (m_{TP}), *true negative* (m_{TN}), *false positive* (m_{FP}), and *false negative* (m_{FN}), which are defined as

$$\begin{aligned} m_{\text{TN}}(\mathbf{y}, \hat{\mathbf{y}}) &= \sum_{i=1}^N \llbracket y_i = 0, \hat{y}_i = 0 \rrbracket, & m_{\text{TP}}(\mathbf{y}, \hat{\mathbf{y}}) &= \sum_{i=1}^N \llbracket y_i = 1, \hat{y}_i = 1 \rrbracket, \\ m_{\text{FP}}(\mathbf{y}, \hat{\mathbf{y}}) &= \sum_{i=1}^N \llbracket y_i = 0, \hat{y}_i = 1 \rrbracket, & m_{\text{FN}}(\mathbf{y}, \hat{\mathbf{y}}) &= \sum_{i=1}^N \llbracket y_i = 1, \hat{y}_i = 0 \rrbracket. \end{aligned}$$

The confusion matrix is defined using these metrics as

$$\mathbf{m}_{\text{CM}}(\mathbf{y}, \hat{\mathbf{y}}) = \begin{pmatrix} m_{\text{TN}}(\mathbf{y}, \hat{\mathbf{y}}) & m_{\text{FP}}(\mathbf{y}, \hat{\mathbf{y}}) \\ m_{\text{FN}}(\mathbf{y}, \hat{\mathbf{y}}) & m_{\text{TP}}(\mathbf{y}, \hat{\mathbf{y}}) \end{pmatrix}.$$

False negative rate (FNR) is defined as the ratio of *false negatives* to the number of positive instances

$$m_{\text{FNR}}(\mathbf{y}, \hat{\mathbf{y}}) = \frac{m_{\text{FN}}(\mathbf{y}, \hat{\mathbf{y}})}{m_{\text{FN}}(\mathbf{y}, \hat{\mathbf{y}}) + m_{\text{TP}}(\mathbf{y}, \hat{\mathbf{y}})}.$$

False positive rate (FPR) is defined as the ratio of *false positives* to the number of negative instances

$$m_{\text{FPR}}(\mathbf{y}, \hat{\mathbf{y}}) = \frac{m_{\text{FP}}(\mathbf{y}, \hat{\mathbf{y}})}{m_{\text{FP}}(\mathbf{y}, \hat{\mathbf{y}}) + m_{\text{TN}}(\mathbf{y}, \hat{\mathbf{y}})}.$$

Matthews correlation coefficient (MCC) is another balanced measure that considers true and false positives, including true and false negatives. It produces a value between -1 and $+1$, where $+1$ represents a perfect prediction, 0 is random, and -1 indicates total disagreement between the predictions and ground truths. It is formally defined as

$$\begin{aligned} m_{\text{MCC}}(\mathbf{y}, \hat{\mathbf{y}}) &= \left(\frac{(m_{\text{TP}}(\mathbf{y}, \hat{\mathbf{y}}) \times m_{\text{TN}}(\mathbf{y}, \hat{\mathbf{y}}) - m_{\text{FP}}(\mathbf{y}, \hat{\mathbf{y}}) \times m_{\text{FN}}(\mathbf{y}, \hat{\mathbf{y}}))}{\sqrt{(m_{\text{TP}}(\mathbf{y}, \hat{\mathbf{y}}) + m_{\text{FP}}(\mathbf{y}, \hat{\mathbf{y}}))(m_{\text{TP}}(\mathbf{y}, \hat{\mathbf{y}}) + m_{\text{FN}}(\mathbf{y}, \hat{\mathbf{y}}))}} \right) \\ &\quad \times \left(\frac{1}{(m_{\text{TN}}(\mathbf{y}, \hat{\mathbf{y}}) + m_{\text{FP}}(\mathbf{y}, \hat{\mathbf{y}}))(m_{\text{TN}}(\mathbf{y}, \hat{\mathbf{y}}) + m_{\text{FN}}(\mathbf{y}, \hat{\mathbf{y}}))} \right). \end{aligned}$$

BER is the average of both FPR and FNR, offering a balanced evaluation metric for a given classification model as

$$\begin{aligned} m_{\text{BER}}(\mathbf{y}, \hat{\mathbf{y}}) &= \frac{1}{2} \left(\frac{m_{\text{FP}}(\mathbf{y}, \hat{\mathbf{y}})}{m_{\text{TN}}(\mathbf{y}, \hat{\mathbf{y}}) + m_{\text{FP}}(\mathbf{y}, \hat{\mathbf{y}})} + \frac{m_{\text{FN}}(\mathbf{y}, \hat{\mathbf{y}})}{m_{\text{TP}}(\mathbf{y}, \hat{\mathbf{y}}) + m_{\text{FN}}(\mathbf{y}, \hat{\mathbf{y}})} \right) \\ &= \frac{m_{\text{FNR}}(\mathbf{y}, \hat{\mathbf{y}}) + m_{\text{FPR}}(\mathbf{y}, \hat{\mathbf{y}})}{2}. \end{aligned}$$

Appendix A.2. MI Estimation Baseline Approaches

This section describes three baseline MI estimation approaches: GMM, MINE, and PC-SOFTMAX [43, 2, 59].

Appendix A.2.1. Gaussian Mixture Model

GMM robustly approximates unknown PDFs ($p_{(X,Y)}$, p_X , p_Y) to estimate MI via (3) for classification datasets \mathcal{D} [43]. The process starts by fitting a GMM to the joint space $\mathcal{X} \times \mathcal{Y}$, estimating the joint PDF $\hat{p}_{(X,Y)}(\cdot)$, which is in turn used to derive the marginal PDFs on X ($\hat{p}_X(\cdot)$) and Y ($\hat{p}_Y(\cdot)$). The MI is approximated on the provided dataset $\mathcal{D} = \{\mathbf{x}_i, \mathbf{y}_i\}_{i=1}^N$:

$$\hat{I}(X; Y) = \frac{1}{N} \sum_{i=1}^N (\lg(\hat{p}_{(X,Y)}(\mathbf{x}_i, \mathbf{y}_i)) - \lg(\hat{p}_X(\mathbf{x}_i)) - \lg(\hat{p}_Y(\mathbf{y}_i))).$$

While robust, GMM faces overfitting in high-dimensional data regimes, as model parameters grow quadratically with the dimensionality (d) of the dataset [43]. The high-dimensional data clustering (HDCC) variant restricts covariance matrices to reduce parameters, allowing efficient estimation and compatibility with the expectation-maximization (EM) algorithm to address the curse of dimensionality [43]. GMM is particularly suited for data that follows a multivariate normal (MVN) distribution.

Estimation Process. A GMM with K components in $\mathcal{X} \times \mathcal{Y}$ has parameters: mixing coefficients (π_k), means (μ_k), and covariance matrices (Σ_k) [43]. These mixing coefficients satisfy $0 < \pi_k < 1$ and $\sum_{k=1}^K \pi_k = 1$, with:

$$\mu_k = \begin{bmatrix} \mu_{X_k} \\ \mu_{Y_k} \end{bmatrix}, \quad \Sigma_k = \begin{bmatrix} \Sigma_{XX_k} & \Sigma_{XY_k} \\ \Sigma_{YX_k} & \Sigma_{YY_k} \end{bmatrix}.$$

The marginal PDF $\hat{p}_X(\cdot)$ for X is a GMM with the same mixing coefficients but only μ_{X_k} and Σ_{XX_k} associated with X and similarly, marginal PDF for Y

are determined. [43]. The value of K is essential since insufficient components can overlook data properties, while too many may lead to overfitting. The Akaike information criterion (AIC) assists in this decision, considering both the log-likelihood $\ell(\theta)$ of the fitted model and the number of free parameters F , defined as $\text{AIC} = -2 \log \ell(\theta) + 2F$ [43]. Hyperparameter optimization (HPO) uses the Akaike information criterion (AIC) as an objective function to ensure robustness and fair comparison with our approaches.

Appendix A.2.2. Mutual Information Neural Estimation

MINE estimates MI between two variables (X, Y) by training a neural network to optimize a specific objective function for a dataset $\mathcal{D} = \{\mathbf{x}_i, y\}_{i=1}^N$:

$$\ell_{\text{MINE}}(\mathbf{x}, y) = \sup_{\theta} \left(\mathbb{E}_{(\mathbf{x}, y) \sim p_{(X, Y)}(\mathbf{x}, y)} [T_{\theta}(\mathbf{x}, y)] - \log(\mathbb{E}_{(\mathbf{x}, y) \sim p_X(\mathbf{x})p_Y(y)} [\mathbf{e}^{(T_{\theta}(\mathbf{x}, y))}] \right),$$

where $T_{\theta}(\mathbf{x}, y) : \mathbb{R}^{d+M} \rightarrow \mathbb{R}$ represents the neural network with parameters θ [2]. The input \mathbf{x} is concatenated with one-hot-encoded y to form a vector of size $d + M$, and the network uses ReLU activation in hidden layers and a Linear output to quantify the dependency between \mathbf{x} and y . MINE maximizes the discrepancy between expectations over the joint $(p_{(X, Y)})$ and product of marginals (p_X, p_Y) distributions, serving as an *upper-bound* estimator for MI [2]. Through iterative training, MINE efficiently estimates MI, especially for high-dimensional data with unobserved PDFs, as outlined in Algorithm 1.

HPO for MINE. The main challenge for training MINE using Algorithm 1 lies in determining the suitable neural network architecture for estimating MI. Discrepancy-based objective functions like MINE and Kullback-Leibler (KL) divergence can lead to overfitting and biased MI estimates. To tackle this, we propose combining HPO with ensemble methods, aggregating the outputs of the top-performing architecture identified through HPO with MSE as the objective function. We created an ensemble of the 10 trained models with the same architecture trained with a different random seed to get a precise estimate. This approach enhances MI estimation precision and yields more reliable and robust estimates, demonstrating strong generalization across diverse datasets.

Appendix A.2.3. PC-Softmax

PC-SOFTMAX offers an alternative approach to estimating MI in classification datasets using a modified *softmax* function [59]. This approach com-

Algorithm 1 Training algorithm: MINE

Require: Dataset $\mathcal{D} = \{(\mathbf{x}_i, y_i)\}_{i=1}^N$, Neural Network T_θ

Ensure: Estimated MI: \hat{I}_θ

- 1: Initialize network parameters θ and hyperparameters
 - 2: Set $N_{epochs} = 10000$, Set B such that $N \bmod B = 0$
 - 3: **for** $n \in [N_{epochs}]$ **do**
 - 4: Define a random permutation π on set of indices $[N]$
 - 5: **for** $b \in [B]$ **do**
 - 6: Define batch start and end: $b_s = (b - 1) \frac{N}{B} + 1$, $b_e = b \cdot \frac{N}{B}$
 - 7: Evaluate the lower-bound:
 - 8: $V(\theta) \leftarrow \frac{1}{B} \sum_{i=b_s}^{b_e} T_\theta(\mathbf{x}_i, y_i) - \log \left(\frac{1}{B} \sum_{i=b_s}^{b_e} (\exp(T_\theta(\mathbf{x}_i, y_{\pi(i)}))) \right)$
 - 9: Correct gradient bias using exponential moving average:
 - 10: $G_b(\theta) \leftarrow \nabla_\theta V(\theta)$
 - 11: Update the statistics network parameters: $\theta \leftarrow \theta + G_b(\theta)$
 - 12: **end for**
 - 13: **end for**
 - 14: Compute $\hat{I}_\theta = \frac{1}{N} \sum_{i=1}^N T_\theta(\mathbf{x}_i, y_i) - \log \left(\frac{1}{N} \sum_{i=1}^N (\exp(T_\theta(\mathbf{x}_i, y_{\pi(i)}))) \right)$
 - 15: **return** Estimated MI: $\lg(e) \cdot \hat{I}_\theta$
-

bines probability-corrected softmax (PC-softmax) with the CCE loss function to acquire an empirical risk minimizer g_p for classification datasets \mathcal{D} , minimizing (A.3) and (conditional) class probabilities predicted by g_p are then used to estimate MI. This approach provides several advantages over MINE— it is straightforward and easy to implement, and the network architecture can be optimized using classification evaluation metrics or loss functions. It approximates the lower bound of KL divergence between the joint $(p_{(X,Y)}(\cdot))$ and the product of marginals $(p_X(\cdot), p_Y(\cdot))$ for variables X and Y to estimate a lower bound on the MI [59].

Estimation Process. Accurately estimating class probabilities by the empirical risk minimizer g_p is challenging. Typically, g_p is obtained by learning a scoring function $h_{s|\theta}(\mathbf{x}): \mathcal{X} \rightarrow \mathbb{R}^M$, assigning unnormalized scores to each class, parameterized by $\theta \in \mathbb{R}^n$ and a MLP with M linear nodes in the penultimate layer estimate these n trainable parameters, such that $h_{s|\theta}(\mathbf{x}) = \mathbf{s} = (s_1, \dots, s_M)$ for a given instance \mathbf{x} , where $s_m = h_{s|\theta}(\mathbf{x})[m] = \mathbf{s}[m]$ is the score assigned to class m [5, Chap. 4].

The *softmax* function, $S(\mathbf{x}): \mathbb{R}^M \rightarrow [0, 1]^M$ in the output layer with M nodes of the MLP converts scores into (conditional) class probabilities

$$\hat{\mathbf{p}}[y] = S(\mathbf{x})[y] = \frac{\exp(\mathbf{s}[y])}{\sum_{m=1}^M \exp(\mathbf{s}[m])}.$$

The empirical risk minimizer g_p is obtained using the CCE loss, defined as $\ell_{CCE}(\mathbf{x}, y) := -\ln(S(\mathbf{x})[y])$. Qin and Kim [59] shows that the expected CCE is equivalent to MI between input \mathcal{X} and output Y up to a constant $\lg(M)$ under a uniform label distribution, i.e., $I(X; Y) \geq \hat{I}(X; Y) \approx -\sum_{(\mathbf{x}, y) \in \mathcal{D}} \log(S(\mathbf{x})[y])$. PC-softmax extends traditional *softmax* for better MI estimation particularly effective for unbalanced datasets:

$$S_{pc}(\mathbf{x})[y] = \frac{\exp(\mathbf{s}[y])}{\sum_{m=1}^M \exp(p_Y(m) \cdot \mathbf{s}[m])}.$$

The PC-softmax function reduces to *softmax* when $p_Y(y) = \frac{1}{M}$, $\forall y \in [M]$ and the CCE loss for PC-softmax is defined as $\ell_{PCC}(\mathbf{x}, y) := -\ln(S_{pc}(\mathbf{x})[y])$, which maximizes the lower bound on the MI. The loss is evaluated by estimating the marginal using the dataset, such that $\hat{p}_Y(y = m) = |\{(\mathbf{x}_i, y_i) \in \mathcal{D} \mid y_i = m\}|/|\mathcal{D}|$, since $p_Y(\cdot)$ is seldom observed. MI is estimated as

$$I(X; Y) \geq \hat{I}(X; Y) \approx \frac{1}{N} \sum_{(\mathbf{x}, y) \in \mathcal{D}} \ell_{PCC}(\mathbf{x}, y) \times \lg(e) = -\frac{1}{N} \sum_{(\mathbf{x}, y) \in \mathcal{D}} \lg(S_{pc}(\mathbf{x})[y]).$$

This approach provides a *lower bound* on MI, similar to LOG-LOSS, but LOG-LOSS is more straightforward and potentially more accurate, and unlike MINE, MLP architecture for this approach can be optimized using standard objective functions for classification tasks.

Appendix A.3. Statistical Tests

This section explains the statistical tests used for our proposed ILD approaches in Section 4.1.1.

Appendix A.3.1. One-sample *t*-test (OTT)

The OTT is used to determine if the mean of a sample differs significantly from a known expected or hypothesized population mean [13]. In the context of ILD, this test evaluates whether MI values significantly deviate from zero, i.e., $I(X, Y) \gg 0$ or $\delta(\ell_U) \gg 0$. We collect 10 MI estimates using

K -fold cross-validation (KFCV), treated as sample data points, denoted by vector $\hat{\mathbf{I}}_j = (\hat{I}_{j1}, \dots, \hat{I}_{j10})$. Using the computed sample mean ($\mu_{\hat{\mathbf{I}}_j}$) and standard deviation ($\sigma_{\hat{\mathbf{I}}_j}$), the t -statistic representing the standard error from the expected mean under the null hypothesis is defined as

$$t = \frac{(\mu_{\hat{\mathbf{I}}_j} - \mu_0)}{\sigma_{\hat{\mathbf{I}}_j}/\sqrt{K}}, \quad (\text{A.4})$$

where $\mu_0 = 0.0$ under $H_0(\cdot)$ and $K = 10$ is the sample size. We consult the t -distribution with $K - 1$ degrees of freedom and calculate the p -value, representing the probability of observing our sample mean if the null hypothesis is true. The null hypothesis $H_0(\hat{\mathbf{I}}_j \sim 0)$ implies no IL, and the alternative hypothesis $H_1(\hat{\mathbf{I}}_j \gg 0)$ indicate presence of IL in the system. If the p -value is below a predefined significance level (e.g., $\alpha = 0.01$), we reject H_0 , indicating the presence of IL; otherwise, we fail to reject H_0 .

Appendix A.3.2. Paired t-test (PTT)

PTT is used to compare two samples (generated from an underlying population) where the observations in one sample can be paired with observations in the other sample [13]. For our ILD approach, we compare the 10 paired accuracy estimates of g_p^{mc} described in Section 3.1.2 (proxy of marginal Bayes predictor) and g (minimizing (A.2), proxy of Bayes predictor) from KFCV, denoted by vectors \mathbf{a}_{mc} and \mathbf{a}_j , respectively. The null hypothesis is $H_0(\mathbf{a}_j = \mathbf{a}_{mc})$, which implies no IL and the alternate hypothesis $H_1(\mathbf{a}_j \neq \mathbf{a}_{mc})$ implies presence of IL in the system.. The p -value represents the probability of obtaining our observed mean accuracy difference, assuming the null hypothesis $H_0(\cdot)$ holds, implying that accuracies are drawn from the same distribution or have nearly zero average difference [13]. The t -statistic is evaluated as

$$t = \frac{\mu}{\sigma/\sqrt{K}},$$

where $\mu = \frac{1}{K} \sum_{k=1}^K d_i$, $d_i = a_{jk} - a_{mck}$ and $\sigma^2 = \sum_{k=1}^K \frac{(\mu - d_k)^2}{K - 1}$. Nadeau [50] proposed to adjust the variance to consider the dependency in estimates due to KFCV, defined as:

$$\sigma_{Cor}^2 = \sigma^2 \left(\frac{1}{K} + \frac{1}{K - 1} \right),$$

which is used to calculate the value of the t -statistic as $t = \frac{\mu}{\sigma_{Cor}}$. The p -value is evaluated by determining the area under the Student’s t -distribution curve at value t as $1 - \text{cdf}(t)$, representing the probability of accepting H_0 . If the p -value is below a predefined significance level (e.g., $\alpha = 0.01$), we reject H_0 , indicating the presence of IL; otherwise, we fail to reject H_0 . However, PTT assumes asymptotic behavior and normal distribution of accuracy differences, which can lead to optimistic p -values. Additionally, using accuracy can misestimate results on imbalanced datasets [58, 54]. PTT requires a large number of estimates (large K) to produce a precise p -value, which diminishes the effect of the correction term $\frac{1}{(K-1)}$ for σ_{Cor}^2 and produces imprecise accuracy estimates as the test set size reduces.

Appendix A.3.3. Fisher’s exact test (FET)

FET is a non-parametric test that determines the probability of independence between two classification methods by analyzing the contingency table, in this case, classifying instances based on ground truths \mathbf{y} and AutoML predictions $\hat{\mathbf{y}}$ represented in a confusion matrix [23]. Unlike tests relying on approximations, the p -value is computed using the hypergeometric distribution as

$$Pr(p(\mathbf{y}, \hat{\mathbf{y}} | \mathbf{M})) = \frac{C_{(m_{TN})}^{(R)} \times C_{(r-m_{TN})}^{(N-R)}}{C_{(r)}^{(N)}} = \frac{C_{(m_{FN} + m_{TN})}^{(m_{FN} + m_{TN})} \times C_{(m_{FP})}^{(m_{FP} + m_{TP})}}{C_{(m_{TP} + m_{TN} + m_{FP} + m_{FN})}^{(m_{TP} + m_{TN} + m_{FP} + m_{FN})}}$$

where $r = m_{TN} + m_{FP}$, $N = m_{FP} + m_{TP} + m_{FN} + m_{TN}$, $R = m_{TN} + m_{FN}$ and $C_{(r)}^{(n)}$ represents the combinations of choosing r items from n items. The p -value is calculated by summing up the probabilities $Pr(\mathbf{M})$ for all tables having a probability equal to or smaller than the observed \mathbf{M} . This test considers all possible tables with the observed marginal counts for m_{TN} of the matrix \mathbf{M} to calculate the chance of getting a table at least as “extreme”. The null hypothesis $H_0(p(\mathbf{y}, \hat{\mathbf{y}} | \mathbf{M}) = p(\mathbf{y} | \mathbf{M})p(\hat{\mathbf{y}} | \mathbf{M}))$ posits that \mathbf{y} and $\hat{\mathbf{y}}$ are independent, indicating no IL, while the alternative hypothesis $H_1(p(\mathbf{y}, \hat{\mathbf{y}} | \mathbf{M}) \neq p(\mathbf{y} | \mathbf{M})p(\hat{\mathbf{y}} | \mathbf{M}))$ suggests significant dependence, implying IL. Note that, p -value for marginal Bayes predictor using above equation is $Pr(\mathbf{M}) = 1.0$, as if the predicted class is 0 ($\hat{\mathbf{y}} = \mathbf{0}$), then $m_{FP} = 0, m_{TP} = 0$ and if it is 1 ($\hat{\mathbf{y}} = \mathbf{1}$), then $m_{FN} = 0, m_{TN} = 0$. This approach directly tests the learnability of empirical risk minimizer g (proxy of Bayes predictor), independent of marginal Bayes predictor, and relates to the MCC, which accounts for

class imbalance [7, 9]. Using KFCV, we obtain $K = 10$ confusion matrices $\mathcal{M}_j = \{\mathbf{M}_j^k\}_{k=1}^K$ from the j -th best performing pipeline, yielding 10 p -values after applying FET. Bhattacharya and Habtzghi [3] showed that the *median* of multiple p -values provides the best estimate. Thus, we aggregate these p -values using *median* and *mean*, referred to as FET-MEDIAN and FET-MEAN ILD approaches, respectively. If the p -value is below a predefined significance level (e.g., $\alpha = 0.01$), we reject H_0 , indicating the presence of IL; otherwise, we fail to reject H_0 .

MCC (m_{MCC}) is a balanced accuracy evaluation measure that penalizes m_{FP} and m_{FN} equally and accounts for imbalance in the dataset [9]. Camilli [7] showed that m_{MCC} is directly proportional to the square root of the χ^2 statistic, i.e., $|m_{\text{MCC}}| = \sqrt{\chi^2/N}$. Since the χ^2 statistical test is asymptotically equivalent to FET, this makes FET an appropriate statistical test for testing the learnability of a g (proxy of Bayes predictor) using the confusion matrix while accounting for imbalance in the dataset.

Appendix A.3.4. Holm-Bonferroni Correction

The Holm-Bonferroni method controls the family-wise error rate, minimizing false positives (type-1 errors) by adjusting the rejection criteria α for each hypothesis within our family of null hypotheses, $\mathcal{F} = \{H_1, \dots, H_J\}$, ensuring that the significance level of \mathcal{F} not exceeding predefined threshold of $\alpha = 0.01$ [36]. Our process begins by independently testing each of the J models or pipelines, resulting in J p -values (p_1, \dots, p_J), sorted in ascending order, and making an aggregated decision. For each hypothesis $H_j \in \mathcal{F}$, if its associated p -value p_j is less than $\alpha/J+1-j$, we reject that null hypothesis. This continues until $p_{\tau+1} > \alpha/J-\tau$, with rejected hypotheses represented by $\mathcal{F}_r = \{H_1, \dots, H_\tau\}$, and the remaining hypothesis (non-rejected) by $\mathcal{F}_a = \{H_{\tau+1}, \dots, H_J\}$. Here, we define the number of rejected hypotheses $\tau = |\mathcal{F}_r|$ as the cut-off parameter, which also provides confidence in IL detection decision, i.e., a higher number signifies more confidence in the decision. To detect IL, we set a *rejection threshold* on the cut-off parameter τ quantifying IL detection confidence, corresponding to the number of rejected hypotheses, $|\mathcal{F}_r|$. A higher rejection threshold would help avoid false positives and prevent the detection of non-existent IL while decreasing it would avoid missing ILs occurrences and reduce false negatives. This systematic and rigorous approach empowers us to detect and characterize IL with a high degree of confidence, ensuring the robustness of our ILD framework.

Appendix B. Additional Experimental Details

This section will list all experimental details excluded from the main paper for conciseness. First, we explain the automated machine learning (AutoML) tools, AutoGluon, and the TabPFN in detail, and then we describe the detailed algorithms to generate synthetic system datasets, different hyperparameters tuned for other models and which parameters were kept fixed, including the implementation details of the python package⁴.

Appendix B.1. AutoML tools

In the last decade, the field of AutoML has emerged as a response to the high and unmet demand for engineering machine learning applications experts. While AutoML envisions the automation of the entire data science process, the arguably most studied problem is that of the combined algorithm selection and hyperparameter optimization (CASH), which was first formally specified by Thornton et al. [65].

Since then, various systems have been devised [65, 22, 51, 46], demonstrating promising performances for tailoring the choice of machine learning (ML) algorithms and the setting of their hyperparameters to a given task, typically comprising a dataset and a loss function. A more thorough overview of AutoML methods can be found in [72]. While various AutoML systems with complementary strengths have been proposed in the literature, a recent benchmark study [27] suggests AutoGluon [16, 17] as the AutoML system with the best performance across datasets and different tasks.

In Hollmann et al. [35], instead of tackling the CASH problem, a general predictor called TabPFN is fitted across various datasets and can immediately return highly accurate predictions. Yielding competitive performance to AutoGluon, TabPFN suggests itself as a state-of-the-art AutoML tool that returns results substantially faster than other AutoML systems.

Due to their strong performance, we selected AutoGluon and TabPFN to approximate the Bayes predictor in our method, and below, we describe the concepts on which they are based.

Appendix B.1.1. AutoGluon

In contrast to other AutoML systems that aim to select feature preprocessing algorithms and a learning algorithm and tune their respective hyperpa-

⁴<https://github.com/LeakDetectAI/AutoMLQuantILDetect>

Table B.4: Hyperparameter ranges for AutoML tools: AutoGluon models and TabPFN including the mutual information (MI) estimation baseline approaches (Gaussian mixture model (GMM), Mutual information neural estimation (MINE), and PC-SOFTMAX)

AutoGluon								
Tree-based Ensemble Models								
Learner	Learning Rate	# Estimators	Max Depth	# Leaves	Feature Fraction	Bagging Fraction	Min Data in Leaf	Lambda L1 / Lambda L2
Light gradient boosting machine (LightGBM)	[0.01, 0.5]	[20, 300]	[3, 20]	[20, 300]	[0.2, 0.95]	[0.2, 0.95]	[20, 5000]	[1e-6, 1e-2]
Categorical boosting machine (CatBoost)	[0.01, 0.5]	NA	[4, 10]	NA	NA	NA	NA	[0.1, 10]
EXtreme gradient boosting machine (XGBoost)	[0.01, 0.5]	[20, 300]	[3, 10]	NA	NA	NA	NA	NA
Random forest classifier (RF)	NA	[20, 300]	[6, 20]	NA	NA	NA	NA	NA
Extra trees classifier (XT)	NA	[20, 300]	[6, 20]	NA	NA	NA	NA	NA
Neural Networks (Multi-layer perceptrons (MLPs))								
Learner	Learning Rate	Dropout Prob	# Layers	# Units	Other Parameters			
FASTAI	[1e-5, 1e-1]	[0.0, 0.5]	NA	NA	NA	NA	NA	NA
NN_TORCH	[1e-5, 1e-1]	[0.0, 0.5]	[2, 20]	[8, 256]	NA	NA	NA	NA
TabPFN								
Learner	Reduction Technique	# Reduced Features	# Ensembles	Other Parameters				
TabPFN	RF , XT	[10, 50]	[32, 200]	NA	NA	NA	NA	NA
Baselines								
Learner	Reduction Technique	# Reduced Features	Covariance Matrix Type	Regularization Strength	Other Parameters			
GMM	RF , XT	[10, 50]	{Full, Diagonal, Tied, Spherical}	[1e-10, 1e-1]	NA	NA	NA	NA
Learner	Learning Rate	Optimizer Type	# Layers	# Units	Regularization Strength	Early Stopping	Batch Normalization	Other Parameters
MINE	[1e-5, 1e-1]	{RMSProp, SGD, Adam}	[1, 50]	[2, 256]	[1e-10, 0.2]	{True, False}	{True, False}	NA
PC-SOFTMAX	[1e-5, 1e-1]	{RMSProp, SGD, Adam}	[1, 50]	[2, 256]	[1e-10, 0.2]	{True, False}	{True, False}	NA

rameters, AutoGluon [16, 17] follows a different approach. More specifically, AutoGluon focuses on building a stacking ensemble, greedily adding more models as long as they are beneficial for the overall performance of the ensemble. To this end, AutoGluon searches over a wide range of different ML algorithms and pre-fitted models, including deep learning, gradient boosting, and linear models. Simultaneously, AutoGluon tunes hyperparameters for each model to optimize their performance. For performing hyperparameter optimization (HPO), different standard techniques can be used such as ASHA [42], Hyperband (HB) [41], Bayesian optimization (BO) [24], or Bayesian optimization and Hyperband (BOHB) [19].

A recent benchmark study found AutoGluon to perform superior to other AutoML systems in predictive performance and robustness. The only drawback noted by Gijbbers et al. [27] is the prediction time, as it will grow with the number of models included in the returned stacking ensemble.

Moreover, AutoGluon allows the customization of the set of considered ML algorithms and models, including gradient boosting machine (GBM) tree-based models and deep neural networks (NNs). For our study, we limited the search space of AutoGluon to consistent classifiers [45, 4]. In Table B.4, we present the models and learning algorithms with corresponding hyperparameters, including their range values available to AutoGluon in our experimental evaluation in Sections 3 and 4.2.

Appendix B.1.2. TabPFN

TabPFN [35] is an approach to AutoML that solves classification tasks in a transductive way. Instead of fitting a model specifically to a dataset and returning this model to the user, TabPFN is a transformer-based neural network architecture trained on the vast number of different probability distributions of tabular data. Instead of searching for a proper learning algorithm and its hyperparameter setting in the first place, TabPFN can be used to instantaneously make predictions as it is already fitted on prior data.

Due to this, predictions can be obtained faster by orders of magnitude compared to classical AutoML estimation baseline tools. Moreover, the predictions are highly accurate and excel, particularly on small tabular datasets. However, TabPFN was only considered for datasets consisting of up to 1000 training data points, 100 numeric features, and 10 classes. Hence, in practical applications with more data points, TabPFN is currently not reliably applicable.

Due to its highly accurate predictions, which appear to come with well-

calibrated probability estimates for the classes, TabPFN is an interesting pick for our approach to approximate the Bayes predictor. Since TabPFN is limited to handling datasets with up to 100 numeric features, our real-world IL-Datasets obtained from OpenSSL TLS server implementations contain more than 100 features. To address this, we recommend applying dimensionality reduction techniques, specifically RF and XT (only when $d > 100$). We perform fine-tuning on TabPFN, adjusting parameters such as the number of reduced features, the reduction model, and the number of prior-fitted models using HPO. Table B.4 lists the specific parameter ranges used for conducting our experiments detailed in Sections 3.2 and 4.2.

Appendix B.2. Simulating Synthetic Systems

We use the multivariate normal (MVN) distribution, which is ideal for simulating real-world vulnerable and non-vulnerable systems generating classification datasets, providing a straightforward means of obtaining ground truth MI, as described in Appendix B.2.3. The MVN distribution is a natural choice due to its simplicity, well-established statistical properties, and ability to model complex inter-variable correlations in real-world data effectively, and it is widely employed for benchmarking classifiers [5, chap. 2]. The central limit theorem further justifies this choice, stating that the cumulative sum of many independent random variables often conforms to a normal distribution [5, chap. 4]. We also simulate systems to generate both balanced and imbalanced datasets with varying leakage assessment score (LAS) or MI levels using the MVN perturbation and proximity techniques.

Appendix B.2.1. Generation Method

Synthetic datasets are generated using MVN to define the joint probability density function (PDF) ($p_{(X,Y)}$) between X and Y , inducing their marginals on X and Y . The dataset \mathcal{D} is created by sampling instances from $p_{X|Y}(\cdot)$ with class distribution $p_Y(y)$, as illustrated in Figure 2.

Formal Definition of PDFs. We define the joint distribution $p_{(X,Y)}(\cdot)$ and marginal on Y $p_X(\cdot)$, required to generate the dataset \mathcal{D} by sampling $(\mathbf{x}_i, y_i) \sim p_{X|Y}(\mathbf{x}_i | y_i), \forall i \in [N]$ with class distribution defined by $p_Y(y)$. These PDFs are used to define the conditionals $p_{Y|X}(\cdot)$ and $p_{X|Y}(\cdot)$ and induce the marginal on \mathcal{X} , denoted by $p_X(\cdot)$. The conditional PDF on X given Y is defined for class m as

$$p_{X|Y}(\mathbf{x} | m) = \text{MVN}(\boldsymbol{\mu}_m, \Sigma). \quad (\text{B.1})$$

where Σ is the covariance matrix and $\boldsymbol{\mu}_m$ is the mean vector for class m .

Generating Imbalanced Datasets: Marginal on Y The parameter r is the minimum proportion of instances for any class $m \in [M]$, defined as $r = \min_{m \in [M]} \frac{|\{(\mathbf{x}_i, y_i) \in \mathcal{D} \mid y_i = m\}|}{|\mathcal{D}|}$. For balanced datasets, $r = 1/M$, and for imbalanced ones, $r < 1/M$, i.e., $r \in (0, 1/M]$. To generate multi-class imbalanced datasets ($M > 2$), we introduce two methods: *Minority* and *Majority*, with an example class frequency in each case shown in Figure 3. In the *Minority* method, the **minority class** is assigned r fraction of total data points, and remaining samples are uniformly distributed among other classes ($> \frac{N}{M}$). While in the *Majority* method, all classes apart from the selected **majority class** is assigned r fraction of total data points ($< \frac{N}{M}$), and the **majority class** gets the remaining data points, To generate imbalanced datasets using MVN, we define the vector $\mathbf{n}_M^{\mathbf{g}_r} = (n_1, \dots, n_M)$, where n_m denotes the sample counts for each class $m \in [M]$, defined for each generation method as

$$\begin{aligned} \mathbf{n}_M^{\text{Majority}} &= (\lceil N \cdot r \rceil, \dots, \lceil N \cdot r \rceil, N - (M - 1)\lceil N \cdot r \rceil) \\ \mathbf{n}_M^{\text{Minority}} &= (\lceil \frac{N - \lceil N \cdot r \rceil}{(M - 1)} \rceil, \dots, \lceil \frac{N - \lceil N \cdot r \rceil}{(M - 1)} \rceil, \lceil N \cdot r \rceil). \end{aligned} \quad (\text{B.2})$$

The marginal on Y for a balanced dataset with $r = 1/M$ is defined as $p_Y(m) = 1/M$ and for imbalanced datasets using *Minority* or *Majority* generation methods is defined as

$$\mathbf{g}_r = \begin{cases} \text{Majority} & \begin{cases} p_Y(m) = r, & \text{if } m \in [M] \setminus M \\ p_Y(m) = 1 - r \cdot (M - 1), & \text{if } m = M \end{cases} \\ \text{Minority} & \begin{cases} p_Y(m) = \frac{1-r}{M-1}, & \text{if } m \in [M] \setminus M \\ p_Y(m) = r, & \text{if } m = M \end{cases} \end{cases} \quad (\text{B.3})$$

Using these, the joint distribution $p_{(X,Y)}(\mathbf{x}, m)$ for class m is defined as $p_{(X,Y)}(\mathbf{x}, m) = p_Y(m) \cdot p_{X|Y}(\mathbf{x} \mid m)$, which induces a marginal on X as

$$p_X(\mathbf{x}) = \sum_{m=1}^M p_Y(m) \cdot p_{X|Y}(\mathbf{x} \mid m) = \sum_{m=1}^M p_Y(m) \cdot \text{MVN}(\boldsymbol{\mu}_m, \Sigma) \quad (\text{B.4})$$

Conditional on Y given X The conditional $p_{Y|X}(\cdot)$ on Y given X for instance (\mathbf{x}, m) is defined as

$$p_{Y|X}(m | \mathbf{x}) = \frac{p_Y(m) \cdot p_{X|Y}(\mathbf{x} | m)}{\sum_{m=1}^M p_Y(m) \cdot p_{X|Y}(\mathbf{x} | m)} = \frac{p_{(X,Y)}(\mathbf{x}, m)}{p_X(\mathbf{x})}. \quad (\text{B.5})$$

Appendix B.2.2. Introducing Noise (ϵ)

To simulate real-world information leakage (IL) scenarios in cryptographic systems, we introduce noise, which decreases the certainty about output $y_i \in \mathcal{Y}$ with more observed inputs $\mathbf{x}_i \in \mathcal{X}$, resulting in $H(Y|X) > 0$ and $I(X;Y) < H(Y)$. We propose two methods: the MVN perturbation and proximity techniques. The perturbation technique introduces noise by flipping a percentage of outputs or classes in the dataset. In contrast, the proximity technique reduces the distance between mean vectors ($\boldsymbol{\mu}_m$) of each class, leading to overlap between the Gaussians $\text{MVN}(\boldsymbol{\mu}_m, \Sigma)$, outlined in Algorithms 2 and 3, respectively. These methods simulate scenarios where cryptographic systems leak no information (non-vulnerable) with $I(X;Y) = 0$.

MVN Perturbation Technique. This approach introduces noise by flipping a percentage of class labels in the dataset, simulating perturbed systems to generate classification datasets with specified configurations, including the generation method (\mathbf{g}_r), number of classes (M), input dimensions (d), noise (ϵ), and class imbalance (r), as outlined in Algorithm 2. Flipping ϵ percentage of class labels ($y \sim \mathcal{Y}$) modifies the original conditional PDFs $p_{Y|X}(\cdot)$ and $p_{X|Y}(\cdot)$, defined in B.5 and B.1, respectively.

Modified Output Variable Y_ϵ Let random variables $B \sim \text{Bernoulli}(p = \epsilon, q = 1 - \epsilon)$ and $\tilde{Y} \sim \text{Categorical}(p_Y(1), \dots, p_Y(M))$ are independent of $\{X, Y\}$, for a fixed ϵ . The modified output random variable Y_ϵ is defined as $Y_\epsilon = Y \cdot \mathbb{I}[B = 0] + \mathbb{I}[B = 1] \cdot \tilde{Y}$. The marginal distributions on X remain unchanged because only the class labels are flipped. Accordingly, the modified marginal on Y_ϵ is derived as $p_{Y_\epsilon}(Y_\epsilon = y) = \epsilon \cdot p_Y(Y = y) + (1 - \epsilon) \cdot p_Y(Y = y) = p_Y(Y = y)$. So, the marginal on Y_ϵ is the same as that of Y .

Modified Conditional on Y_ϵ given X The conditional on the modified output variable Y_ϵ given X is

$$p_{Y_\epsilon|X}(Y_\epsilon = m | \mathbf{x}) = p_B(B = 0) \cdot p_{Y|X}(m | \mathbf{x}) + p_B(B = 1) \cdot p_{\tilde{Y}}(\tilde{Y} = m) \quad (\text{B.6})$$

$$= (1 - \epsilon) \cdot p_{Y|X}(m | \mathbf{x}) + \epsilon \cdot p_Y(m). \quad (\text{B.7})$$

Modified Conditional on X given Y_ϵ The conditional on X given the modified output variable Y_ϵ is

$$p_{X|Y_\epsilon}(\mathbf{x} | Y_\epsilon = m) = \frac{p_{Y_\epsilon|X}(Y_\epsilon = m | \mathbf{x}) \cdot p_X(\mathbf{x})}{p_Y(m)}.$$

The altered conditional distribution $p_{X|Y_\epsilon}(\mathbf{x} | Y_\epsilon = m)$ becomes a combination of multiple MVN distributions, increasing complexity and making MI estimation more challenging.

MVN Proximity Technique. Our second approach introduces noise in the simulated systems by reducing the distance between the Gaussians generated by MVN distributions. This is achieved by moving the mean vectors $\boldsymbol{\mu}'_m, \forall m \in [M]_0$ corresponding to MVN distribution representing each class closer to each other. The updated MVNs for each class m is defined by $\text{MVN}(\boldsymbol{\mu}'_m, \Sigma)$, which in turn represents the conditional PDF $p_{X|Y}(\cdot)$ for the underlying generated system dataset. The process for simulating systems using the proximity technique to generate classification datasets for a unique configuration of the generation method (\mathbf{g}_r), number of classes (M), input dimensions (d), noise (ϵ), and class imbalance (r), is outlined in Algorithm 3. Notably, when introducing proximity, only the original MVN is modified, which only modifies the conditional on X given Y , i.e., $p'_{X|Y}(\mathbf{x} | m) = \text{MVN}(\boldsymbol{\mu}'_m, \Sigma)$. Consequently, the conditional probability $p_{Y|X}(\cdot)$ and the marginal on X can be computed using Equations (B.4) and (B.5) as

$$p'_{Y|X}(m | \mathbf{x}) = \frac{p_Y(m) \cdot p'_{X|Y}(\mathbf{x} | m)}{\sum_{m=1}^M p_Y(m) \cdot p'_{X|Y}(\mathbf{x} | m)} = \frac{p'_{(X,Y)}(\mathbf{x}, m)}{p_X(\mathbf{x})}. \quad (\text{B.8})$$

Therefore, the underlying distribution for synthetic datasets generated through the introduction of noise using the proximity approach remains the same as for the datasets using the MVN distribution with updated means.

Algorithm 2 Generate Perturbation MVN \mathcal{D} for given $\mathbf{g}_r, M, d, \epsilon$ and r

```

1: Define  $\mathcal{D} = \{\}$ ,  $N = 1000 \cdot M$ 
2: Calculate  $\mathbf{n}_M^{\mathbf{g}_r} = (n_1, \dots, n_M)$  using (B.2)
3: Sample positive semi-definite matrix for the MVN distribution

 $\mathbf{Q} \sim \text{OrthogonalMatrix}_{d \times d} = \begin{pmatrix} q_{1,1} & \dots & q_{1,d} \\ \vdots & \ddots & \vdots \\ q_{d,1} & \dots & q_{d,d} \end{pmatrix}$ ,  $q_{i,j} \in [-1, 1)$ ,  $\forall (i, j) \in [d] \times [d]$ 

 $\mathbf{S} \sim \text{Diagonal}(\text{RandomMatrix}_{d \times d}) = \begin{pmatrix} s_{1,1} & \dots & 0 \\ 0 & \dots & 0 \\ 0 & \dots & s_{d,d} \end{pmatrix}$ ,  $s_{i,i} \in [0, 1)$ ,  $\forall i \in [d]$ 

 $\Sigma = (\mathbf{Q} \cdot \mathbf{S}) \cdot \mathbf{Q}^T$ 

4: for  $m \in [M]$  do
5:   Define  $\boldsymbol{\mu}_m = (1.5m, \dots, 1.5m) \in \mathbb{R}^d$ 
6:   for  $i \in [n_m]$  do
7:     Sample  $\mathbf{x}_i \sim \text{MVN}(\boldsymbol{\mu}_m, \Sigma)$ 
8:     Assign label  $y_i$  using  $B \sim \text{Bernoulli}(p = \epsilon, q = 1 - \epsilon)$   $\triangleright$  Flip  $\epsilon$  %
labels
9:      $\begin{cases} y_i = m, & B = 0 \\ y_i \sim \text{Categorical}(p_Y(1), \dots, p_Y(M)), & B = 1 \end{cases}$ 
10:
11:      $\mathcal{D} = \mathcal{D} \cup \{(\mathbf{x}_i, y_i)\}$   $\triangleright$  Add instances
12:   end for
13: end for
14: return  $\mathcal{D}$ 

```

Appendix B.2.3. Ground truth MI

By plugging in the conditional $p_{Y|X}(\cdot)$ and the marginal $p_Y(\cdot)$ defined above in (2), the ground truth MI for the generated system dataset $\mathcal{D} = \{\mathbf{x}_i, y_i\}$ is approximated as

$$GI(\mathcal{D}) \cong \frac{1}{N} \sum_{i=1}^N p_{Y|X}(y_i | \mathbf{x}_i) \lg(p_{Y|X}(y_i | \mathbf{x}_i)) - \sum_{m=1}^M p_Y(m) \lg(p_Y(m)) . \quad (\text{B.9})$$

For systems simulated using perturbation and proximity techniques, the modified conditional $p_{Y_\epsilon|X}(\cdot)$ in (B.7) and $p'_{Y|X}(m | \mathbf{x})$ in (B.8) and unchanged marginal on Y is used to calculate the ground truth MI.

Algorithm 3 Generate Proximity MVN \mathcal{D} for given \mathbf{g}_r , M , d , ϵ and r

- 1: Define $\mathcal{D} = \{\}$, $N = 1000 \cdot M$
- 2: Calculate $\mathbf{n}_M^{\mathbf{g}_r} = (n_1, \dots, n_M)$ using (B.2)
- 3: Sample positive semi-definite matrix for the MVN distribution

$$\mathbf{Q} \sim \text{OrthogonalMatrix}_{d \times d} = \begin{pmatrix} q_{1,1} & \dots & q_{1,d} \\ \vdots & \ddots & \vdots \\ q_{d,1} & \dots & q_{d,d} \end{pmatrix}, q_{i,j} \in [-1, 1), \forall (i, j) \in [d] \times [d]$$

$$\mathbf{S} \sim \text{Diagonal}(\text{RandomMatrix}_{d \times d}) = \begin{pmatrix} s_{1,1} & \dots & 0 \\ 0 & \dots & 0 \\ 0 & \dots & s_{d,d} \end{pmatrix}, s_{i,i} \in [0, 1), \forall i \in [d]$$

$$\Sigma = (\mathbf{Q} \cdot \mathbf{S}) \cdot \mathbf{Q}^T$$

- 4: **for** $m \in [M]$ **do**
 - 5: Define $\boldsymbol{\mu}_m = (1.5 \cdot m(1 - \epsilon), \dots, 1.5 \cdot m(1 - \epsilon)) \in \mathbb{R}^d$ ▷ Distance $1.5(1 - \epsilon)$
 - 6: **for** $i \in [n_m]$ **do**
 - 7: Sample $\mathbf{x}_i \sim \text{MVN}(\boldsymbol{\mu}_m, \Sigma)$
 - 8: $\mathcal{D} = \mathcal{D} \cup \{(\mathbf{x}_i, m)\}$ ▷ Add instances
 - 9: **end for**
 - 10: **end for**
 - 11: **return** \mathcal{D}
-

Appendix B.3. Implementation Details

This section describes the implementation details, including parameters for performing HPO and the Python packages used for running the experiments.

Hyperparameter Optimization. We outline various models and learning algorithms with their respective hyperparameters and range values in the AutoGluon tool in Table B.4. The objective functions for HPO include balanced error rate (BER) for PC-SOFTMAX, AutoGluon, and TabPFN, Akaike information criterion (AIC) for GMM, and mean squared error (MSE) for MINE. The AutoGluon search space includes tree-based ensemble models like RF, XT, GBM algorithms (LightGBM, CatBoost, XGBoost), and MLP implemented using PyTorch and fastai [4, 45]. We employed dimensionality reduction techniques for high-dimensional datasets ($d > 100$) for TabPFN and GMM. The hyperparameters and range values for TabPFN, AutoGluon models, and baseline MI estimators are detailed in Table B.4.

Python Package. To generate synthetic datasets using the MVN distribution, including ground truth MI calculation, we implemented a script using `multivariate_normal` and `ortho_group` functions from `scipy` [68]. For MI estimation, we used TabPFN and AutoGluon, detailed in Appendix B.1, to induce the Bayes predictor. We incorporated five calibration techniques for estimating MI using the LOG-LOSS approach from `netcal` [40]. The GMM approach was implemented using the `InfoSelect` implementation, extended to include various covariance matrices⁵ [57]. The MINE and PC-SOFTMAX approach were implemented using `PyTorch` [52], provided by the corresponding authors Belghazi et al. [2] and Qin and Kim [59], respectively. For HPO, we used BO implemented by `BayesSearchCV` in `scikit-optimize` [32]. MI-based information leakage detection (ILD) approaches employ one-sample t-test (OTT) statistical tests on estimated MI, as discussed in Section 4.1.1. To implement state-of-the-art classification-based ILD approaches (PTT-MAJORITY, FET-MEAN, and FET-MEDIAN), we induced the Bayes predictor using TabPFN and AutoGluon. Subsequent statistical tests (Fisher’s exact test (FET), paired t-test (PTT), OTT, and Holm-Bonferroni correction) were implemented using `scipy` [68]. The generated 10 IL-Datasets for each time delay were converted into a multi-class classification dataset with 11 padding classes and uploaded on OpenML⁶. [66]. Detailed documented code for all MI estimation approaches, ILD approaches, synthetic dataset generation, and OpenML dataset parser are available on our GitHub repository⁴.

Appendix C. Generalization Capability

This section examines the generalization capabilities of our ILD and MI estimation approaches compared to state-of-the-art methods. We use heatmaps to depict key performance metrics such as Accuracy, FPR, and FNR apropos the time delay of the system (LAS), detailed in Appendix C.1. The time delay indicates the computation time difference between correctly and incorrectly padded messages sent to the OpenSSL TLS server. Additionally, we present heatmaps showing normalized mean absolute error (NMAE) performance results of MI estimation approaches on synthetic datasets generated

⁵<https://github.com/felipemaiapolo/infoselect/issues/5>

⁶https://www.openml.org/search?type=study&sort=tasks_included&study_type=task&id=383

using the MVN distribution. We select the best-performing calibrated LOG-LOSS approach for both AutoGluon and TabPFN. These heatmaps provide insights into generalization capabilities across various scenarios, considering factors like the number of classes (M), input dimensions (d), class imbalance (r), and noise level (ϵ) (flip percentage for MVN perturbation datasets), detailed in Appendix C.2.

Appendix C.1. ILD Approaches

We evaluated the generalization capability of various ILD approaches for detecting timing side-channels aimed at mitigating the Bleichenbacher attack, focusing on detection accuracy, FPR, and FNR. Using heatmaps with a fixed rejection threshold ($\tau = 5$), Figure C.10 shows performance for time delays in linear steps of $5 \mu\text{s}$, while Figure C.11 presents performance for time delays in logarithmic steps of $2 \mu\text{s}$.

Appendix C.1.1. TabPFN

This section analyzes MI and classification-based ILD approaches using TabPFN, generally detecting more ILs in systems generating balanced datasets than imbalanced ones. Notably, TabPFN IR CAL LOG-LOSS excels in generalization, detecting over 60% of ILs with a minimal time delays under $20 \mu\text{s}$.

Classification-based Approaches. The PTT-MAJORITY approach stands out in detecting ILs in systems generating *balanced* datasets, while FET-MEDIAN proves to be more adept in detecting ILs for imbalanced ones. For systems generating *imbalanced dataset*, all approaches can detect ILs when its time delay exceeds $35 \mu\text{s}$: otherwise failing, resulting in a 100% FNR, with FET-MEDIAN showcasing the best performance. In the case of systems generating *balanced* datasets, all approaches detect ILs when it has a minimum time delay of $15 \mu\text{s}$ and below this threshold, detection fails, resulting in a 100% FNR. PTT-MAJORITY performs best, occasionally detecting over 60% of ILs for systems with delays beyond $15 \mu\text{s}$.

MI-based Approaches. Overall, IR CAL LOG-LOSS is the most proficient in detecting ILs for systems generating balanced and imbalanced datasets. For systems generating *imbalanced* datasets, most approaches, except IR CAL LOG-LOSS and HB CAL LOG-LOSS, overfit and overestimate MI, detecting non-existent ILs and resulting in a 100% FPR. Both IR CAL LOG-LOSS

and HB CAL LOG-LOSS detect over 80 % of ILs in systems with time delays above 32 μs , with IR CAL LOG-LOSS occasionally detecting over 55 % ILs in systems with minimal delays under 20 μs . For systems generating *balanced* datasets, these approaches reliably detect ILs even in ones with short delays of 15 μs , with IR CAL LOG-LOSS occasionally detecting more than 80 % of ILs. However, they fail with delays below this threshold, resulting in a 100 % FNR. This highlights the enhancement IR CAL LOG-LOSS brings to LOG-LOSS, with HB CAL LOG-LOSS also contributing positively.

Appendix C.1.2. AutoGluon

This section analyzes MI and classification-based ILD approaches using AutoGluon. Generally, they detect non-existent ILs in systems generating imbalanced datasets, especially with time delays under 20 μs . However, in systems generating balanced datasets, they occasionally detect over 70 % of ILs with similar short delays.

Classification-based Approaches. Overall, FET based approaches show almost comparable detection performance in systems generating balanced and imbalanced datasets, while PTT-MAJORITY performs better in the case of balanced systems datasets. For systems generating *imbalanced* datasets, all approaches reliably detect ILs in ones with time delays exceeding 30 μs : otherwise missing ILs, resulting in around 100 % FNR, with FET-MEDIAN outperforming others. When considering systems generating *balanced* datasets, all approaches reliably detect ILs even in ones with a brief time delay of 15 μs , occasionally detecting over 60 % of them.

MI-based Approaches. Overall, MID-POINT approach outperforms in detecting ILs in systems generating balanced datasets, whereas LOG-LOSS is exceptionally proficient for ones generating imbalanced datasets, implying the failure of calibration (CAL LOG-LOSS) to enhance log-loss MI estimation, with IR CAL LOG-LOSS and HB CAL LOG-LOSS deteriorating it. These approaches overfit and overestimate MI, detecting non-existent ILs, leading to a 100 % FPR, which is consistent with our findings in Sections 3.3.1 and 4.3. Within systems generating *imbalanced* datasets, all approaches consistently detect ILs for time delays beyond 25 μs , with LOG-LOSS variant emerging as the front runner: otherwise failing to detect any ILs, resulting in a 100 % FNR. As expected, the MID-POINT approach also mistakenly detects non-existent ILs, leading to a 100 % FPR. For systems generating *balanced* datasets, all approaches showed enhanced performance, with most methods

ILD with Rejection Threshold = 5, $\tau \geq 5$
Class Imbalance $r = 0.1$

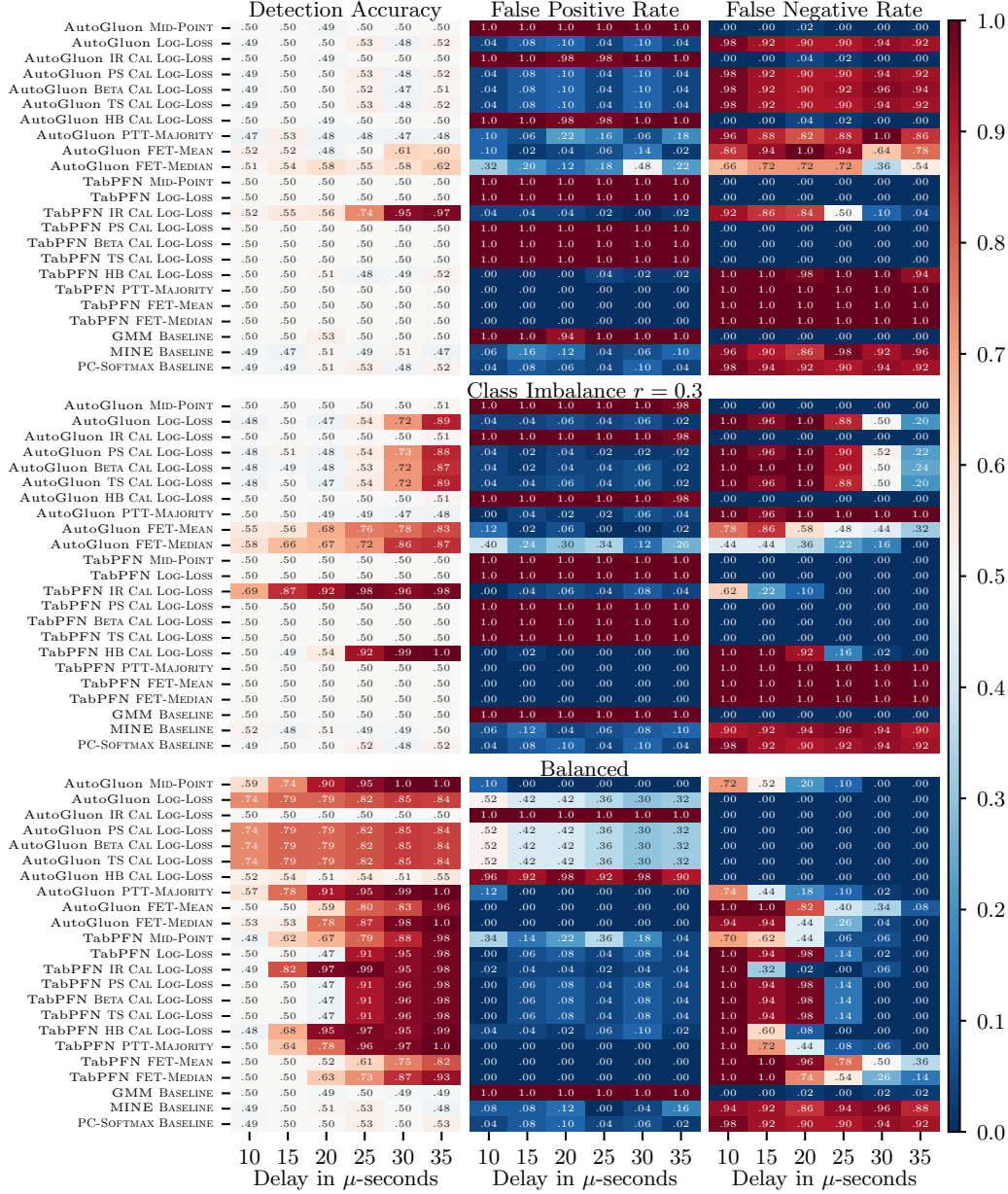


Figure C.10: Performance of ILD approaches versus time delay with 5 μ s step

detecting approximately 74% ILs in ones with time delays over 10 μ s, with

ILD with Rejection Threshold = 5, $\tau \geq 5$
 Class Imbalance $r = 0.1$

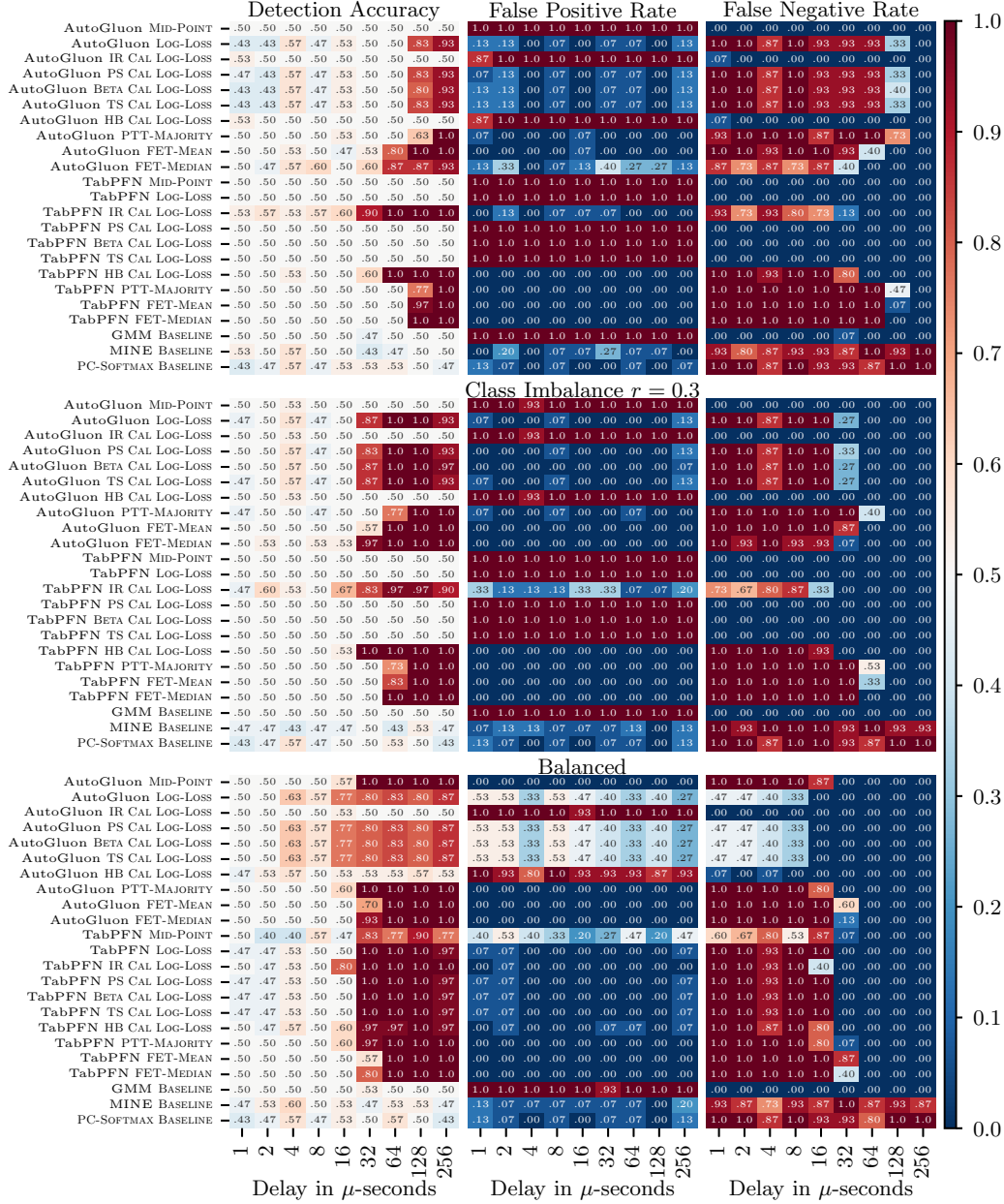


Figure C.11: Performance of ILD approaches versus time delay with 2 μ s logarithmic step

the MID-POINT approach emerging as the front runner.

Appendix C.1.3. Baselines

The ILD baselines consistently achieve a detection accuracy of approximately 50% on systems generating *balanced* or *imbalanced* datasets. MINE and PC-SOFTMAX often miss ILs, while occasionally detecting up to 60% of ILs. GMM overestimates MI and detects non-existent ILs, leading to a 100% FPR due to overfitting in high-dimensional datasets. These results highlight the need for specialized approaches in ILD.

Appendix C.1.4. Summary

Calibration techniques (CAL LOG-LOSS) have varied impacts on the performance of the LOG-LOSS approach using TabPFN and AutoGluon. Specifically, IR CAL LOG-LOSS and HB CAL LOG-LOSS often deteriorate AutoGluon’s performance due to overfitting while enhancing TabPFN’s performance. This is consistent with our findings in Sections 3.3 and 4.2, indicating the necessity and choice of calibration techniques depending on the underlying datasets. TabPFN IR CAL LOG-LOSS consistently demonstrates superior detection accuracy across systems generating both balanced and imbalanced datasets. In contrast, when using AutoGluon, the FET-MEDIAN excels in detecting IL in systems generating imbalanced datasets, while MID-POINT and PTT-MAJORITY strategies perform best for systems generating balanced dataset. The baseline ILD approaches remain subpar, detecting only 50% of the ILs across all systems, with high FPR or FNR around 100%.

Appendix C.2. MI Estimation Approaches

We assessed the generalization capability of our MI estimation approaches using AutoGluon and TabPFN against baseline methods, using the NMAE metric defined in Appendix Appendix B.2.3. For balanced, binary-class, and multi-class imbalanced datasets, we determined the NMAE for each configuration of the number of classes (M), input dimensions (d), class imbalance (r), and noise level (ϵ). We selected the top-performing calibration technique (CAL LOG-LOSS) to enhance the LOG-LOSS approach for MI estimation. Our comprehensive assessment used heatmaps to illustrate generalization capabilities concerning the number of classes (M) and input dimensions (d) in balanced datasets in Appendix C.2.1 and class imbalance (r) and noise level (ϵ) in binary-class and multi-class imbalanced datasets in Appendix C.2.2.

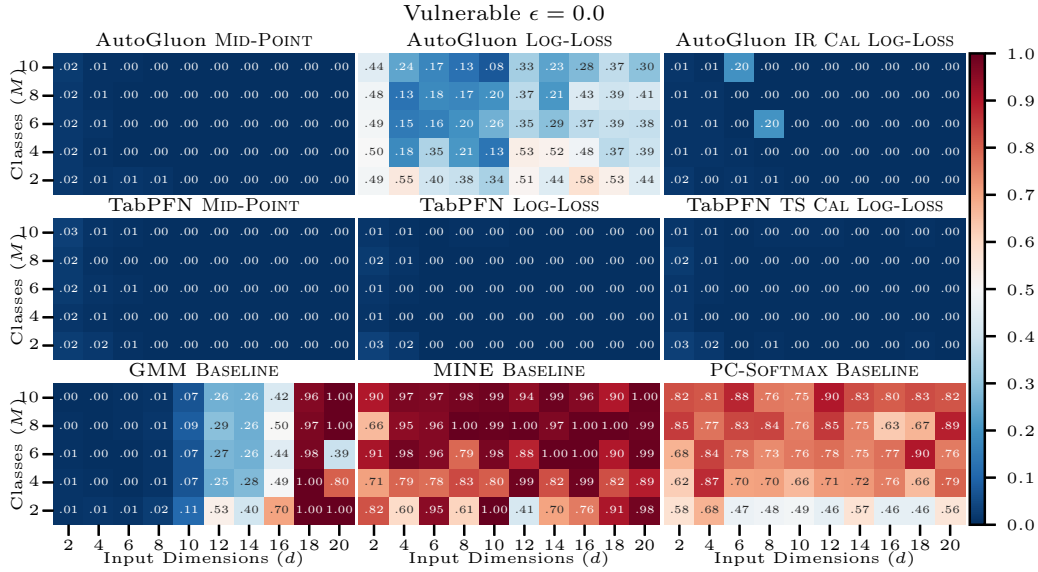
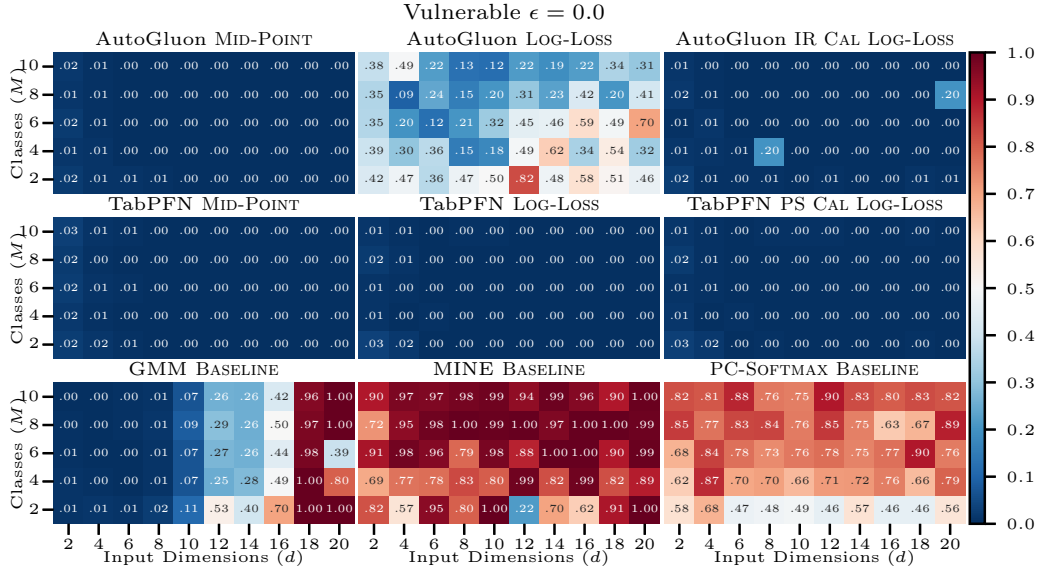


Figure C.12: Generalizability of MI estimation approaches on noise-free vulnerable systems

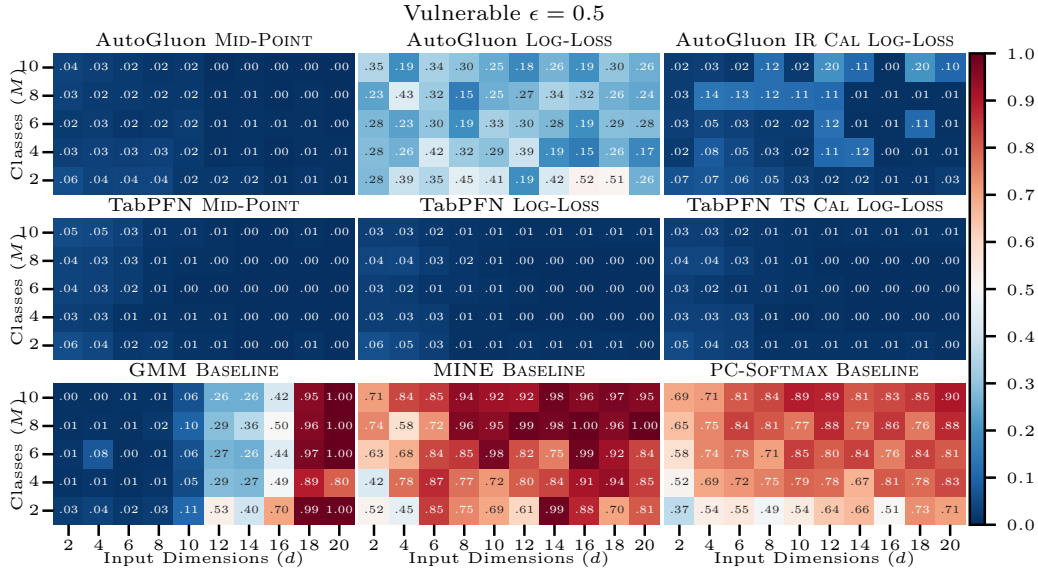
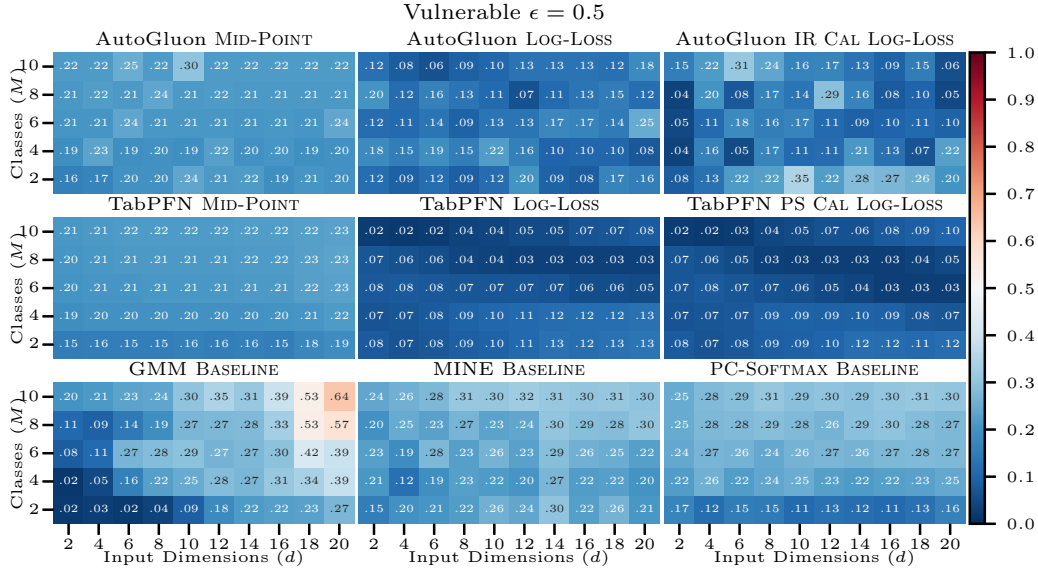


Figure C.13: Generalizability of MI estimation approaches on noisy vulnerable systems

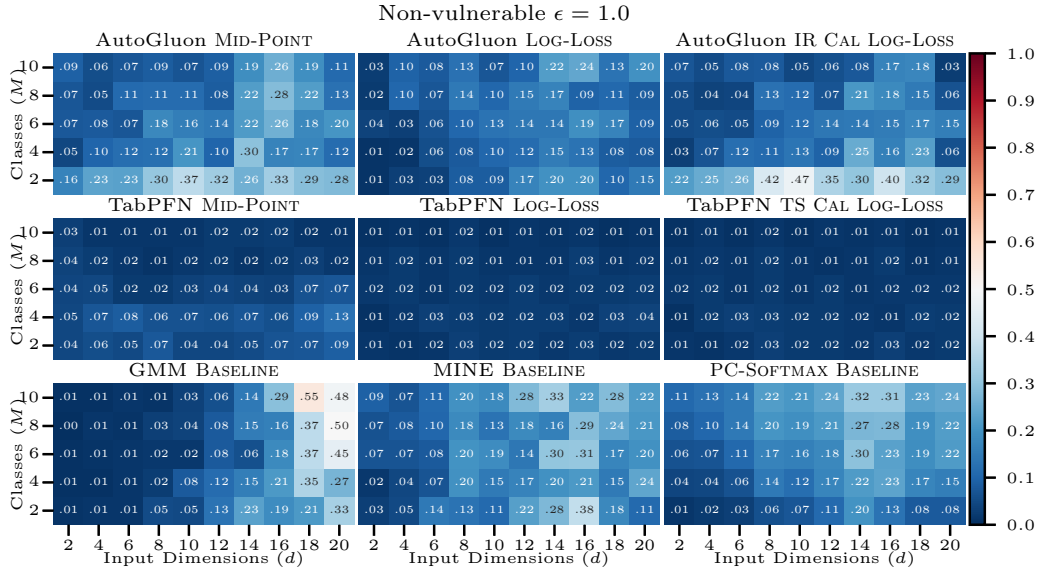
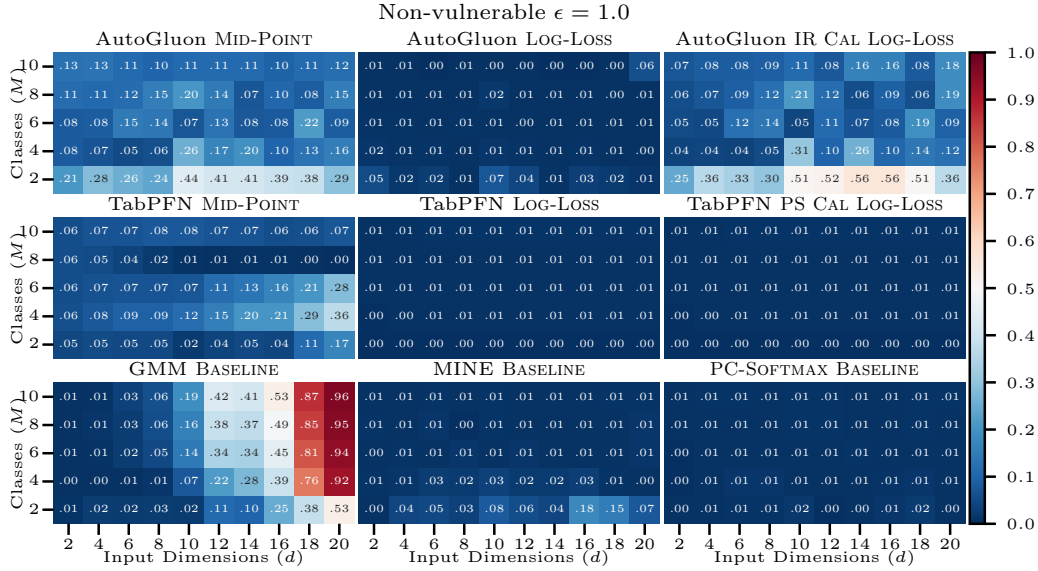


Figure C.14: Generalizability of MI estimation approaches on non-vulnerable systems

Appendix C.2.1. Number of Classes (M) and Input Dimensions (d)

We analyze the NMAE of different MI estimation approaches for balanced datasets to understand their generalization capabilities concerning the number of classes (M) and input dimensions (d). We evaluate their performance on *vulnerable* systems at 0% and 50% noise levels in Figures C.12 and C.13, respectively, and on *non-vulnerable* synthetic systems at 100% noise level in Figure C.14. In the heatmaps, the Y-axis represents the number of classes (2 to 10), and the X-axis represents the input dimensions (2 to 20).

TabPFN. Overall, MI estimation approaches using TabPFN show strong generalization capabilities across the number of classes (M) and input dimensions (d). However, MID-POINT performs poorly for high-dimensional datasets ($d \geq 14$) in vulnerable systems ($\epsilon = 1.0$), with a maximum NMAE of 0.20, especially for MVN perturbation technique. TabPFN LOG-LOSS and TabPFN CAL LOG-LOSS approaches achieve an NMAE around 0.01 in most cases, except for vulnerable systems with 50% noise in MVN perturbation datasets, indicating that their estimation precision is generally independent of the number of classes and input dimensions. Additionally, calibration (CAL LOG-LOSS) does not enhance TabPFN LOG-LOSS precision, consistent with previous findings in Section 3.3.1.

AutoGluon. Overall, MI estimation approaches using AutoGluon generally perform well regarding the number of classes (M) and input dimensions (d), with some exceptions noted in Section 3.3.2. Notably, MID-POINT and CAL LOG-LOSS with AutoGluon overestimate MI due to overfitting in non-vulnerable systems with binary-class datasets ($M = 2$). The performance of AutoGluon CAL LOG-LOSS sometimes deteriorates with the increasing number of classes and input dimensions of the vulnerable synthetic dataset. As also observed in Section 3.3.1, the usage of calibration techniques by AutoGluon LOG-LOSS approach mostly leads to overfitting and overestimating MI in **non-vulnerable systems**. In contrast, the **vulnerable systems** mostly improves the precision of estimated MI. This leads to supporting the observation that these ILD approaches detect non-existent ILs and produce false positives, as confirmed in Section 4.3.

Baselines. All baseline approaches exhibit diminished generalization capability for both **vulnerable** and **non-vulnerable systems**, with performance consistently deteriorating as the number of classes (M) and input dimensions (d) increase. The GMM faces significant challenges with high-dimensional

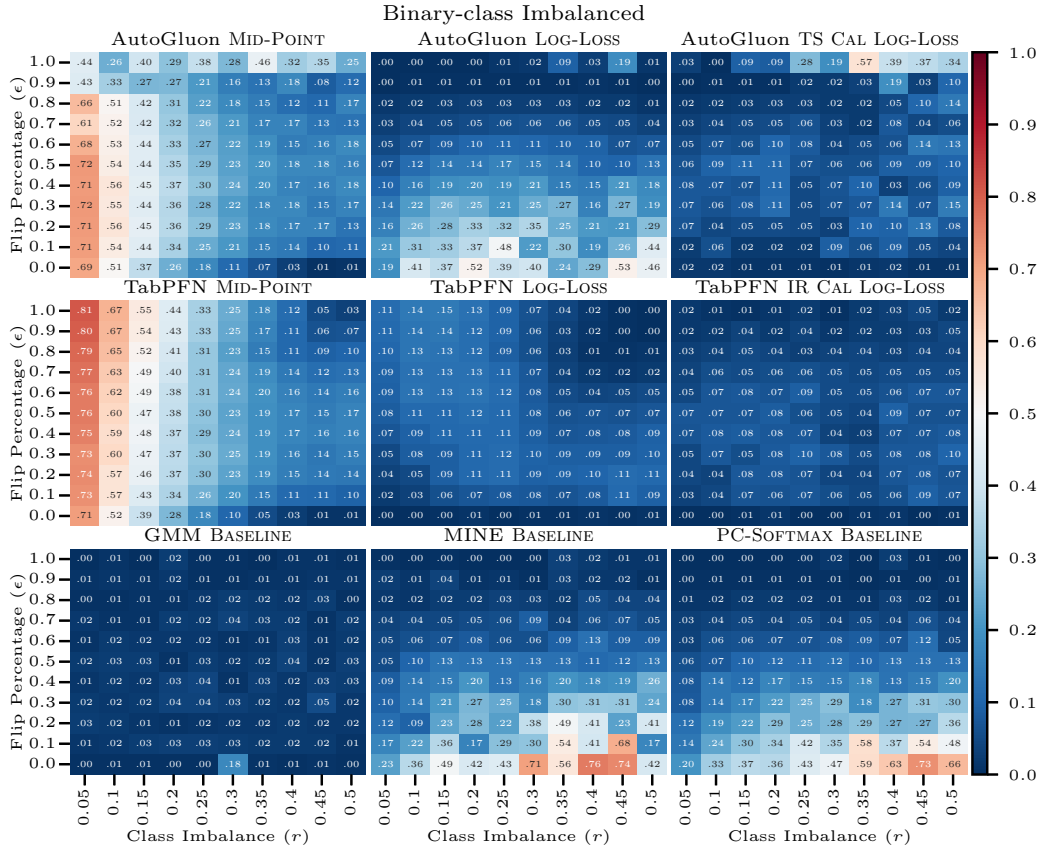


Figure C.15: Generalizability on MVN perturbation binary-class imbalanced datasets

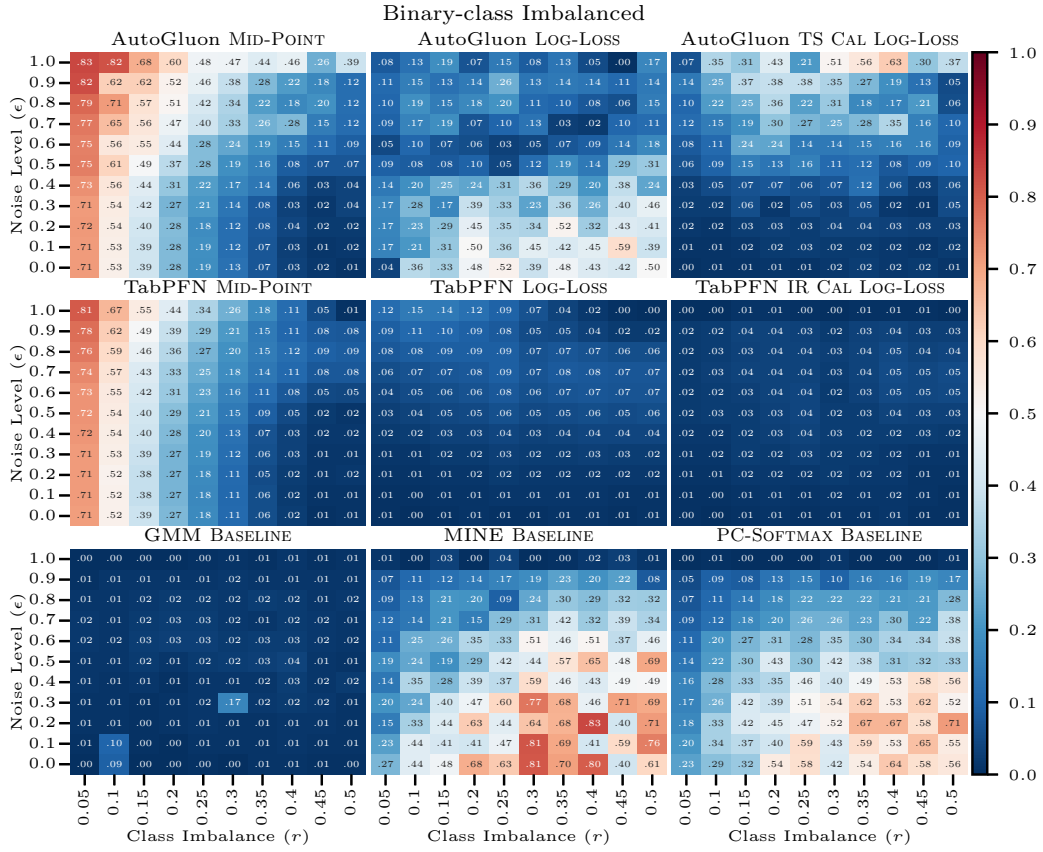


Figure C.16: Generalizability on MVN proximity binary-class imbalanced datasets

datasets, showing substantial performance degradation beyond 10 input dimensions, aligning with its known limitations in high-dimensional spaces. Overall, the GMM performs better than PC-SOFTMAX and MINE, except

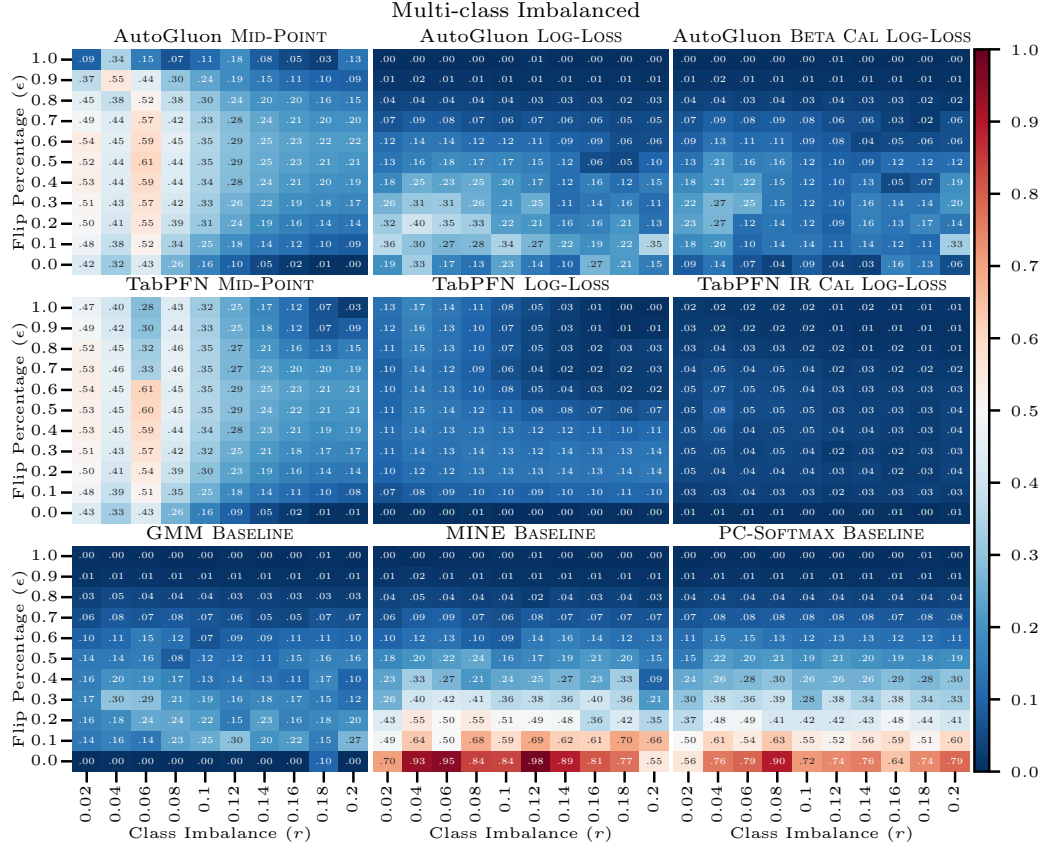


Figure C.17: Generalizability on MVN perturbation multi-class imbalanced datasets

in non-vulnerable synthetic systems using the MVN perturbation technique, as also observed in Section 3.3.1.

Appendix C.2.2. Class Imbalance (r) And Noise Level (ϵ)

To understand the generalization capabilities of MI estimation approaches concerning class imbalance (r) and noise level (ϵ), we analyze their performance using NMAE on binary-class imbalanced datasets generated by MVN perturbation and the MVN proximity technique, illustrated via heatmaps in Figures C.15 and C.16, respectively. Similarly, we assess the performance

on multi-class imbalanced datasets generated by MVN perturbation and the MVN proximity technique, illustrated via heatmaps in Figures C.17 and C.18, respectively. The Y-axis represents noise levels (ϵ) from 0.0 to 1.0, while the X-axis represents class imbalance, ranging from 0.05 to 0.5 for binary-class datasets and 0.02 to 0.2 for multi-class datasets.

TabPFN. Overall, LOG-LOSS and CAL LOG-LOSS approaches using TabPFN exhibit strong generalization capabilities regarding class imbalance and noise levels, demonstrating resilience to variations in these factors in both binary-class and multi-class imbalanced synthetic datasets. The TabPFN MID-POINT approach performs well concerning noise levels. Still, it underperforms in highly imbalanced datasets since the MID-POINT strategy tends to overestimate MI in imbalanced datasets, as elaborated in Section 3.1.1. Using calibration techniques (CAL LOG-LOSS) with the TabPFN LOG-LOSS approach significantly improves MI estimation precision, particularly in multi-class systems simulated using the perturbation technique.

AutoGluon. Overall, the generalization capabilities of MI estimation approaches using AutoGluon for class imbalances and noise levels in imbalanced datasets display varied results. Among these methods, the AutoGluon MID-POINT approach performs the worst, particularly with highly imbalanced datasets ($r \leq 0.2$ for binary-class systems and $r \leq 0.08$ for multi-class systems) and increased noise levels, confirming that the MID-POINT strategy tends to overestimate MI in imbalanced datasets, as elaborated in Section 3.1.1. AutoGluon LOG-LOSS and CAL LOG-LOSS approaches often overestimate MI, indicating a tendency to overfit in cases of certain class imbalances and low noise levels, particularly in datasets generated using the MVN proximity technique. This issue is less pronounced in multi-class scenarios but still evident in specific configurations. A notable observation with AutoGluon is its sensitivity to changing noise levels. As noise increases, CAL LOG-LOSS’s performance fluctuates, suggesting potential noise sensitivity in imbalanced datasets. The AutoGluon CAL LOG-LOSS often excels with average noise levels, highlighting the benefits of calibration, especially for multi-class datasets, while it deteriorates MI estimation precision in non-vulnerable, imbalanced datasets.

Baselines. The MINE and PC-SOFTMAX baselines struggle with imbalanced datasets, whether binary or multi-class, with generalization capabilities deteriorating as class imbalance and noise levels decrease. Interestingly, MINE and PC-SOFTMAX estimate MI precisely in both binary-class and multi-class

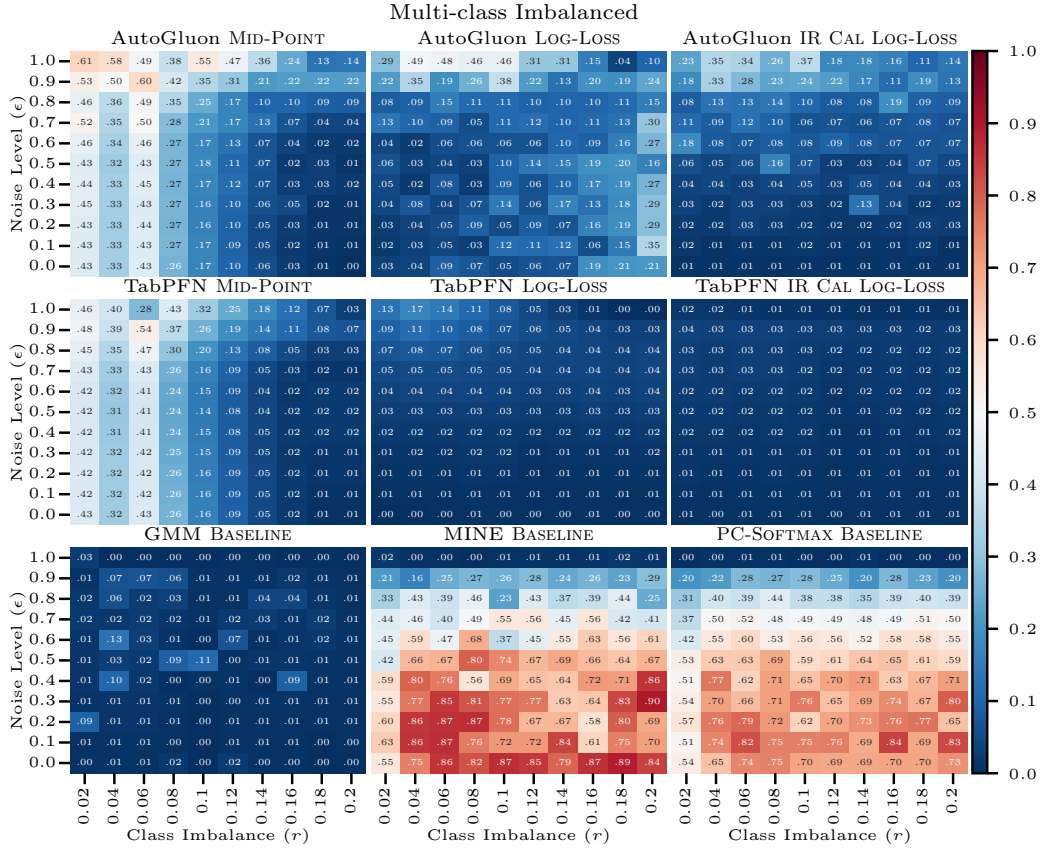


Figure C.18: Generalizability on MVN proximity multi-class imbalanced datasets

non-vulnerable synthetic datasets, as also observed in Appendix C.2.1 and Section 3.3. The GMM generally adapts well to class imbalance and noise levels, especially in multi-class synthetic systems simulated using the MVN perturbation technique. It tends to slightly outperform the TabPFN approaches, particularly in imbalanced binary-class synthetic datasets generated by MVN perturbation. The strong generalization capability of GMM can be attributed to the low dimensionality ($d = 5$) of the imbalanced datasets, suggesting its primary challenges lie in estimating MI for high-dimensional synthetic datasets, with minimal impact from noise and class imbalance.

Appendix C.2.3. Summary

In conclusion, TabPFN CAL LOG-LOSS consistently demonstrates strong generalization capabilities in estimating MI across various factors for both

MVN perturbation and proximity datasets, with CAL LOG-LOSS sometimes enhancing MI estimation using LOG-LOSS. Calibration techniques (CAL LOG-LOSS) significantly enhance MI estimation using LOG-LOSS with AutoGluon for vulnerable datasets but reduce it for non-vulnerable ones, which is the reason that AutoGluon CAL LOG-LOSS ILD often detects non-existent ILs, leading to false positives. In contrast, TabPFN CAL LOG-LOSS ILD outperforms other approaches, as seen in Section 4.3.3 and Appendix C.1.4. The baselines struggle with high-dimensional, imbalanced noisy datasets, emphasizing their limitations, as confirmed in Section 3.3.

References

- [1] Barlow, R.E., Brunk, H.D., 1972. The isotonic regression problem and its dual. *Journal of the American Statistical Association* 67, 140–147. doi:10.2307/2284712.
- [2] Belghazi, M.I., Baratin, A., Rajeshwar, S., Ozair, S., Bengio, Y., Courville, A., Hjelm, D., 2018. Mutual information neural estimation, in: *Proceedings of the 35th International Conference on Machine Learning, Proceedings of Machine Learning Research, Stockholmsmässan, Stockholm, Sweden*. pp. 531–540.
- [3] Bhattacharya, B., Habtzghi, D., 2002. Median of the p -Value under the alternative hypothesis. *The American Statistician* 56, 202–206. doi:10.1198/000313002146.
- [4] Biau, G., Devroye, L., Lugosi, G., 2008. Consistency of random forests and other averaging classifiers. *Journal of Machine Learning Research* 9, 2015–2033.
- [5] Bishop, C.M., 2006. *Probability Distributions*. Springer New York, NY, Springer New York, NY. doi:10.5555/1162264.
- [6] Bleichenbacher, D., 1998. Chosen ciphertext attacks against protocols based on the rsa encryption standard pkcs #1, in: *Advances in Cryptology — CRYPTO '98*, Springer Berlin Heidelberg, Berlin, Heidelberg. pp. 1–12.
- [7] Camilli, G., 1995. The relationship between fisher’s exact test and Pearson’s chi-square test: A bayesian perspective. *Psychometrika* 60, 305–312. doi:10.1007/bf02301418.

- [8] Chatzikokolakis, K., Chothia, T., Guha, A., 2010. Statistical measurement of information leakage, in: *Tools and Algorithms for the Construction and Analysis of Systems*, Springer Berlin Heidelberg, Berlin, Heidelberg. pp. 390–404.
- [9] Chicco, D., Tötsch, N., Jurman, G., 2021. The matthews correlation coefficient (mcc) is more reliable than balanced accuracy, bookmaker informedness, and markedness in two-class confusion matrix evaluation. *BioData Mining* 14, 13. doi:10.1186/s13040-021-00244-z.
- [10] Cover, T.M., Thomas, J.A., 2005. *Elements of Information Theory*. Wiley. chapter 2. pp. 13–55. doi:10.1002/047174882x.ch2.
- [11] Cristiani, V., Lecomte, M., Maurine, P., 2020. Leakage assessment through neural estimation of the mutual information, in: *Lecture Notes in Computer Science*. Springer International Publishing, Berlin, Heidelberg, pp. 144–162. doi:10.1007/978-3-030-61638-0_9.
- [12] Daley, D.J., Vere-Jones, D., 2004. Scoring probability forecasts for point processes: the entropy score and information gain. *Journal of Applied Probability* 41, 297–312. doi:10.1239/jap/1082552206. full publication date: 2004.
- [13] Demšar, J., 2006. Statistical comparisons of classifiers over multiple data sets. *Journal of Machine Learning Research* 7, 1–30.
- [14] Devroye, L., Györfi, L., Lugosi, G., 1996. *The Bayes Error*. Springer New York, Springer New York, NY. volume 31. chapter 2. doi:10.1007/978-1-4612-0711-5.
- [15] Domingos, P., Pazzani, M., 1997. On the optimality of the simple Bayesian classifier under zero-one loss. *Machine Learning* 29, 103–130. doi:10.1023/a:1007413511361.
- [16] Erickson, N., Mueller, J., Shirkov, A., Zhang, H., Larroy, P., Li, M., Smola, A., 2020. AutoGluon-tabular: Robust and accurate AutoML for structured data. arXiv preprint arXiv:2003.06505 .
- [17] Erickson, N., Shi, X., Sharpnack, J., Smola, A., 2022. Multimodal AutoML for image, text and tabular data, in: *Proceedings of the 28th ACM SIGKDD International Conference on Knowledge Discovery and Data*

Mining, Association for Computing Machinery, New York, NY, USA. pp. 4786–4787. doi:10.1145/3534678.3542616.

- [18] Faezi, S., Yasaei, R., Barua, A., Faruque, M.A.A., 2021. Brain-inspired golden chip free hardware trojan detection. *IEEE Transactions on Information Forensics and Security* 16, 2697–2708. doi:10.1109/TIFS.2021.3062989.
- [19] Falkner, S., Klein, A., Hutter, F., 2018. BOHB: robust and efficient hyperparameter optimization at scale, in: *Proceedings of the 35th International Conference on Machine Learning, (ICML), Proceedings of Machine Learning Research, Stockholmsmässan, Stockholm, Sweden*. pp. 1436–1445.
- [20] Fano, R.M., 1961. *Transmission of Information: A Statistical Theory of Communications*. The MIT Press, Cambridge, MA.
- [21] Feuerverger, A., Rahman, S., 1992. Some aspects of probability forecasting. *Communications in Statistics - Theory and Methods* 21, 1615–1632. doi:10.1080/03610929208830868.
- [22] Feurer, M., Klein, A., Eggenberger, K., Springenberg, J.T., Blum, M., Hutter, F., 2019. Auto-sklearn: Efficient and robust automated machine learning, in: *Automated Machine Learning*. Springer International Publishing, Cham, pp. 113–134. doi:10.1007/978-3-030-05318-5_6.
- [23] Fisher, R.A., 1922. On the interpretation of χ^2 from contingency tables, and the calculation of p. *Journal of the Royal Statistical Society* 85, 87. doi:10.2307/2340521.
- [24] Frazier, P.I., 2012. Optimization via simulation with bayesian statistics and dynamic programming, in: *Proceedings of the 2012 Winter Simulation Conference (WSC), IEEE. WSC, Berlin, Germany*. pp. 1–16. doi:10.1109/WSC.2012.6465237.
- [25] Funke, D., 2022. Pushing the AutoSCA tool to picosecond precision: Improving timing side channel detection. doi:10.13140/RG.2.2.33070.08005.
- [26] Gao, S., Ver Steeg, G., Galstyan, A., 2015. Efficient Estimation of Mutual Information for Strongly Dependent Variables, in: *Proceedings*

of the Eighteenth International Conference on Artificial Intelligence and Statistics, PMLR, San Diego, California, USA. pp. 277–286.

- [27] Gijbbers, P., Bueno, M.L.P., Coors, S., LeDell, E., Poirier, S., Thomas, J., Bischl, B., Vanschoren, J., 2024. Amlb: an automl benchmark. *Journal of Machine Learning Research* 25, 1–65.
- [28] Gneiting, T., Raftery, A.E., 2007. Strictly proper scoring rules, prediction, and estimation. *Journal of the American Statistical Association* 102, 359–378. doi:10.1198/016214506000001437.
- [29] Good, I.J., 1992. *Rational Decisions*. Springer New York, New York, NY. pp. 365–377. doi:10.1007/978-1-4612-0919-5_24.
- [30] Guo, C., Pleiss, G., Sun, Y., Weinberger, K.Q., 2017. On calibration of modern neural networks, in: *Proceedings of the 34th International Conference on Machine Learning*, (ICML), JMLR.org. p. 1321–1330.
- [31] Gupta, P., Ramaswamy, A., Drees, J., Hüllermeier, E., Priesterjahn, C., Jager, T., 2022. Automated information leakage detection: A new method combining machine learning and hypothesis testing with an application to side-channel detection in cryptographic protocols, in: *Proceedings of the 14th International Conference on Agents and Artificial Intelligence, INSTICC. SCITEPRESS - Science and Technology Publications, Virtual Event*. pp. 152–163. doi:10.5220/0010793000003116.
- [32] Head, T., Kumar, M., Nahrstaedt, H., Louppe, G., Shcherbatyi, I., 2021. *scikit-optimize/scikit-optimize*. doi:10.5281/zenodo.5565057.
- [33] Hellman, M., Raviv, J., 1970. Probability of error, equivocation, and the chernoff bound. *IEEE Transactions on Information Theory* 16, 368–372. doi:10.1109/tit.1970.1054466.
- [34] Hettwer, B., Gehrler, S., Güneysu, T., 2019. Applications of machine learning techniques in side-channel attacks: A survey. *Journal of Cryptographic Engineering* 10, 135–162. doi:10.1007/s13389-019-00212-8.
- [35] Hollmann, N., Müller, S., Eggenberger, K., Hutter, F., 2023. TabPFN: A transformer that solves small tabular classification problems in a second, in: *The Eleventh International Conference on Learning Representations*. URL: https://openreview.net/forum?id=cp5PvcI6w8_.

- [36] Holm, S., 1979. A simple sequentially rejective multiple test procedure. *Scandinavian Journal of Statistics* 6, 65–70.
- [37] Kelsey, J., 2002. Compression and information leakage of plaintext, in: *Fast Software Encryption*, Springer Berlin Heidelberg, Berlin, Heidelberg. pp. 263–276.
- [38] Koyejo, O., Ravikumar, P., Natarajan, N., Dhillon, I.S., 2015. Consistent multilabel classification, in: *Proceedings of the 28th International Conference on Neural Information Processing Systems - Volume 2*, MIT Press, Cambridge, MA, USA. pp. 3321–3329. doi:10.5555/2969442.2969610.
- [39] Kull, M., Filho, T.S., Flach, P., 2017. Beta calibration: a well-founded and easily implemented improvement on logistic calibration for binary classifiers, in: *Proceedings of the 20th International Conference on Artificial Intelligence and Statistics, Proceedings of Machine Learning Research*. pp. 623–631.
- [40] Küppers, F., Kronenberger, J., Shantia, A., Haselhoff, A., 2020. Multivariate confidence calibration for object detection, in: *The IEEE/CVF Conference on Computer Vision and Pattern Recognition (CVPR) Workshops*, IEEE, Los Alamitos, CA, USA. pp. 1322–1330. doi:10.1109/cvprw50498.2020.00171.
- [41] Li, L., Jamieson, K.G., DeSalvo, G., Rostamizadeh, A., Talwalkar, A., 2017. Hyperband: A novel bandit-based approach to hyperparameter optimization. *J. Mach. Learn. Res.* 18, 185:1–185:52.
- [42] Li, L., Jamieson, K.G., Rostamizadeh, A., Gonina, E., Ben-tzur, J., Hardt, M., Recht, B., Talwalkar, A., 2020. A system for massively parallel hyperparameter tuning, in: *Proceedings of Machine Learning and Systems 2020, MLSys 2020, March 2-4, 2020, mlsys.org, Austin, TX, USA*.
- [43] Maia Polo, F., Vicente, R., 2022. Effective sample size, dimensionality, and generalization in covariate shift adaptation. *Neural Computing and Applications* 35, 18187–18199. doi:10.1007/s00521-021-06615-1.
- [44] Meyer, C., Somorovsky, J., Weiss, E., Schwenk, J., Schinzel, S., Tews, E., 2014. Revisiting SSL/TLS implementations: New bleichenbacher side

- channels and attacks, in: 23rd USENIX Security Symposium (USENIX Security 14), USENIX Association, San Diego, CA. pp. 733–748.
- [45] Mielniczuk, J., Tyrcha, J., 1993. Consistency of multilayer perceptron regression estimators. *Neural Networks* 6, 1019–1022. doi:10.1016/s0893-6080(09)80011-7.
- [46] Mohr, F., Wever, M., Hüllermeier, E., 2018. ML-plan: Automated machine learning via hierarchical planning. *Machine Learning* 107, 1495–1515. doi:10.1007/s10994-018-5735-z.
- [47] Moon, K.R., Sricharan, K., Hero, A.O., 2021. Ensemble estimation of generalized mutual information with applications to genomics. *IEEE Transactions on Information Theory* 67, 5963–5996. doi:10.1109/TIT.2021.3100108.
- [48] Moos, T., Wegener, F., Moradi, A., 2021. DL-LA: Deep learning leakage assessment. *IACR Transactions on Cryptographic Hardware and Embedded Systems* 2021, 552–598. doi:10.46586/tches.v2021.i3.552-598.
- [49] Mushtaq, M., Akram, A., Bhatti, M.K., Chaudhry, M., Lapotre, V., Gogniat, G., 2018. NIGHTS-WATCH: A cache-based side-channel intrusion detector using hardware performance counters, in: *Proceedings of the 7th International Workshop on Hardware and Architectural Support for Security and Privacy*, Association for Computing Machinery, New York, NY, USA. doi:10.1145/3214292.3214293.
- [50] Nadeau, C., 2003. Inference for the generalization error. *Machine Learning* 52, 239–281. doi:10.1023/a:1024068626366.
- [51] Olson, R.S., Bartley, N., Urbanowicz, R.J., Moore, J.H., 2016. Evaluation of a tree-based pipeline optimization tool for automating data science, in: *Proceedings of the Genetic and Evolutionary Computation Conference 2016*, Association for Computing Machinery, New York, NY, USA. pp. 485–492. doi:10.1145/2908812.2908918.
- [52] Paszke, A., Gross, S., Massa, F., Lerer, A., Bradbury, J., Chanan, G., Killeen, T., Lin, Z., Gimelshein, N., Antiga, L., Desmaison, A., Köpf, A., Yang, E., DeVito, Z., Raison, M., Tejani, A., Chilamkurthy, S., Steiner, B., Fang, L., Bai, J., Chintala, S., 2019. PyTorch: An Imperative Style,

High-Performance Deep Learning Library. Curran Associates Inc., Red Hook, NY, USA.

- [53] Perianin, T., Carré, S., Dyseryn, V., Facon, A., Guilley, S., 2020. End-to-end automated cache-timing attack driven by machine learning. *Journal of Cryptographic Engineering* 11, 135–146. doi:10.1007/s13389-020-00228-5.
- [54] Picek, S., Heuser, A., Jovic, A., Bhasin, S., Regazzoni, F., 2018. The curse of class imbalance and conflicting metrics with machine learning for side-channel evaluations. *IACR Transactions on Cryptographic Hardware and Embedded Systems* 2019, 209–237. doi:10.13154/tches.v2019.i1.209-237.
- [55] Picek, S., Perin, G., Mariot, L., Wu, L., Batina, L., 2023. Sok: Deep learning-based physical side-channel analysis. *ACM Computing Surveys* 55. doi:10.1145/3569577.
- [56] Platt, J.C., 2000. *Probabilities for SV Machines*. Cambridge: MIT Press. pp. 61–73. doi:10.7551/mitpress/1113.001.0001.
- [57] Polo, F.M., Da Silva, F.L., 2020. InfoSelect - mutual information based feature selection in python.
- [58] Powers, D.M., 2011. Evaluation: From precision, recall and f-measure to roc., informedness, markedness & correlation. *Journal of Machine Learning Technologies* 2, 37–63.
- [59] Qin, Z., Kim, D., 2019. Rethinking softmax with cross-entropy: Neural network classifier as mutual information estimator. *CoRR* abs/1911.10688. arXiv:1911.10688.
- [60] Roulston, M.S., Smith, L.A., 2002. Evaluating probabilistic forecasts using information theory. *Monthly Weather Review* 130, 1653–1660.
- [61] Shabtai, A., Elovici, Y., Rokach, L., 2012. *A Survey of Data Leakage Detection and Prevention Solutions*. 1 ed., Springer US, New York, NY. doi:10.1007/978-1-4614-2053-8.
- [62] Silva Filho, T., Song, H., Perello-Nieto, M., Santos-Rodriguez, R., Kull, M., Flach, P., 2023. Classifier calibration: A survey on how to assess and

- improve predicted class probabilities. *Machine Learning* 112, 3211–3260. doi:10.1007/s10994-023-06336-7.
- [63] Szegedy, C., Vanhoucke, V., Ioffe, S., Shlens, J., Wojna, Z., 2016. Rethinking the Inception architecture for computer vision, in: *Proceedings of the IEEE Conference on Computer Vision and Pattern Recognition, CVPR, Las Vegas, NV, USA, June 27-30, IEEE Computer Society*. pp. 2818–2826.
- [64] Tebbe, D., Dwyer, S., 1968. Uncertainty and the probability of error (Corresp.). *IEEE Transactions on Information Theory* 14, 516–518. doi:10.1109/tit.1968.1054135.
- [65] Thornton, C., Hutter, F., Hoos, H.H., Leyton-Brown, K., 2013. Autoweka: Combined selection and hyperparameter optimization of classification algorithms, in: *Proceedings of the 19th ACM SIGKDD International Conference on Knowledge Discovery and Data Mining, Association for Computing Machinery, New York, NY, USA*. pp. 847–855. doi:10.1145/2487575.2487629.
- [66] Vanschoren, J., van Rijn, J.N., Bischl, B., Torgo, L., 2014. Openml: Networked science in machine learning. *SIGKDD explorations newsletter* 15, 49–60. doi:10.1145/2641190.2641198.
- [67] Vapnik, V., 1991. Principles of risk minimization for learning theory, in: *Proceedings of the 4th International Conference on Neural Information Processing Systems, Morgan Kaufmann Publishers Inc., San Francisco, CA, USA*. pp. 831–838.
- [68] Virtanen, P., Gommers, R., Oliphant, T.E., Haberland, M., Reddy, T., Cournapeau, D., Burovski, E., Peterson, P., Weckesser, W., Bright, J., van der Walt, S.J., Brett, M., Wilson, J., Millman, K.J., Mayorov, N., Nelson, A.R.J., Jones, E., Kern, R., Larson, E., Carey, C.J., Polat, İ., Feng, Y., Moore, E.W., VanderPlas, J., Laxalde, D., Perktold, J., Cimrman, R., Henriksen, I., Quintero, E.A., Harris, C.R., Archibald, A.M., Ribeiro, A.H., Pedregosa, F., van Mulbregt, P., SciPy 1.0 Contributors, 2020. *Scipy 1.0: fundamental algorithms for scientific computing in python*. *Nature Methods* 17, 261–272. doi:10.1038/s41592-019-0686-2.

- [69] Zadrozny, B., Elkan, C., 2001. Obtaining calibrated probability estimates from decision trees and naive bayesian classifiers, in: Proceedings of the 18th International Conference on Machine Learning , (ICML), Morgan Kaufmann Publishers Inc., San Francisco, CA, USA. p. 609–616.
- [70] Zhang, J., Zheng, M., Nan, J., Hu, H., Yu, N., 2020. A novel evaluation metric for deep learning-based side channel analysis and its extended application to imbalanced data. IACR Transactions on Cryptographic Hardware and Embedded Systems 2020, 73–96. doi:10.46586/tches.v2020.i3.73-96.
- [71] Zhao, M.J., Edakunni, N., Pocock, A., Brown, G., 2013. Beyond fano’s inequality: Bounds on the optimal f-score, ber, and cost-sensitive risk and their implications. Journal of Machine Learning Research 14, 1033–1090.
- [72] Zöllner, M., Huber, M.F., 2021. Benchmark and survey of automated machine learning frameworks. Journal of Artificial Intelligence Research 70, 409–472. doi:10.1613/jair.1.11854.